IPPJ-AM-64

FUTURE PROSPECTS OF RESEARCH AND DATA ACTIVITIES ON PLASMA-WALL INTERACTION IN FUSION DEVICES

MEMOIRS OF THE COOPERATIVE WORKSHOP IN INSTITUTE OF PLASMA PHYSICS, NAGOYA UNIVERSITY

EDITED BY
N. ITOH AND T. KAWAMURA

INSTITUTE OF PLASMA PHYSICS
NAGOYA UNIVERSITY

NAGOYA, JAPAN

IPPJ-AM-64

FUTURE PROSPECTS OF RESEARCH AND DATA ACTIVITIES ON PLASMA-WALL INTERACTION IN FUSION DEVICES

Memoirs of the Cooperative Workshop
in Institute of Plasma Physics, Nagoya University

Edited by
Noriaki Itoh and Takaichi Kawamura

Institute of Plasma Physics, Nagoya University
Chikusa-ku, Nagoya 464-01, Japan

May 1989

Preface

Knowledge on plasma-wall interactions is one of the indispensable informations for the research and development of nuclear fusion devices. In the Research Information Center (RIC) in Institute of Plasma Physics, Nagoya University, the Working Group on Plasma-Wall Interaction has been active on data evaluation and compilation relevant to plasma-wall interactions. Some evaluated numerical data have already been filed as databases in computer, and they can be accessed and retrieved on computer terminals. Up to now, physical sputtering yields of monatomic solids by ions (SPUTY) and particle and energy backscattering coefficients of light ions from solids (BACKS) are available. Semi-empirical formulas reproducing evaluated data are also derived and can be displayed together with the numerical data. Other results related to data assessment on plasma-wall interactions have successively been published in IPPJ-AM report series.

Recently the problem of control of plasma-wall interactions has been more seriously recognized as a key issue for achieving better confinements of the core plasma in a large tokamak. And, since the studies of boundary plasmas have been known important for control of particle and energy balances in toroidal devices, the data of interactions in low energy particle irradiation become the center of interest, however, there exist few reliable experimental data in the low energy region. Therefore the interest of the Working Group expanded from basic processes to synergistic effects and device-oriented phenomena. In order to get reliable data under complex conditions and ones in low energy particle incidence, computer simulations seem to be appropriate. For developing computer codes a comprehensive survey on basic processes and realistic experimental conditions which would be expected in the present-day devices and in future reactors is needed.

This is a report of the Workshop which was held on Dec. 16-17, 1988 at Institute of Plasma Physics under the cooperative research program mainly with the intention of obtaining future prospects of data activities relevant to plasma-wall interactions. We would like to express our sincere thanks to all contributors of the Workshop.

Noriaki Itoh
Takaichi Kawamura

Contents

Preface

Part I : Near Term Problems

Part II : Long Term Problems

List of participants of the Workshop

Akaishi, Kenya	IPP, Nagoya Univ.
Atsumi, Hisao	Kinki Univ.
Doyama, Masao	Nagoya Univ.
Funato, Yasuyuki	Tohoku Univ.
Furuyama, Yuichi	Kobe Univ. of Marcantile Marine
Hasebe, Yuji	Nagoya Univ.
Horino, Yuji	Nagoya Univ.
Hosogane, Nobuyuki	JAERI, Naka
Itoh, Noriaki	Nagoya Univ.
Kawamura, Takaichi	IPP, Nagoya Univ.
Kinoshita, Chiken	Kyushu Univ.
Koshikawa, Takanori	Osaka Electro-Communication Univ.
Maruyama, Tadashi	Tokyo Inst. of Tech.
Morita, Kenji	Nagoya Univ.
Muroga, Takeo	Kyushu Univ.
Nakajima, Tadashi	Kobe Univ. of Marcantile Marine
Noda, Nobuaki	IPP, Nagoya Univ.
Nunogaki, Masanobu	Osaka Univ.
Obayashi, Haruo	IPP, Nagoya Univ.
Ohno, Hideo	JAERI, Tokai
Sagara, Akio	IPP, Nagoya Univ.
Seki, Masahiro	JAERI, Naka
Sugai, Hideo	Nagoya Univ.
Tabata, Tatsuo	Osaka Pref. Rad. Res. Lab.
Takamura, Shuichi	Nagoya Univ.
Takatsu, Hideyuki	JAERI, Naka
Tanabe, Tetsuo	Osaka Univ.

Tomita, Michio	Kyoto Univ.
Toyoda, Hirotaka	Nagoya Univ.
Tuchimoto, Masanori	Tokyo Univ., Tokai
Yagi, Yasuyuki	Electrotechnical Lab.
Yamada, Reiji	JAERI, Tokai
Yamamura, Yasunori	Okayama Univ. of Science
Yoshida, Shinji	Nagoya Univ.

An Overview on Data Compilation of Plasma-Materials Interaction

Noriaki Itoh
Department of Physics, Faculty of Science, Nagoya University,
Furocho, Nagoya 464-01, Japan

I. Introduction

Plasma-materials interaction is one of the most crucial problems for the development of nuclear fusion machines. Extensive works have been carried out in these two decades, since the importance of the problem has been recognized. The objectives of these studies are (1) to clarify the phenomena that may occur while a plasma is fired in a machine by interaction with materials and (2) to obtain the basis for the design of future machines. In science, understanding of a process leads to establishment of it physical basis. When development of understanding of a specific series of processes reaches at this stage, phenomena that may occur under specific conditions can be anticipated. It is often the case, however, that the needs for information are too urgent to carry out detailed analysis of the relevant processes. In such a case tests of materials under the practical conditions of fusion machines are carried out.

Studies of the plasma-materials interaction can be divided broadly into two categories: for the near term development of fusion machines and for the long term development of the nuclear fusion reactors. The near term studies should respond to the experimental data having been and being obtained using the current machines and to the design of near future machines. The long term studies should be more fundamental and should be intended to develop basic physics, so that the phenomena that occur under the operating conditions of nuclear fusion reactors can be anticipated. The accuracy of the anticipation needed depends on the situation, but often need not be very high. There are of course a variety of research problems that lie between these two extremities. At the early stages of development of a field of science, fragmental data are needed and to be analyzed to derive fundamental rules. These fragmental data should be integrated to a science, so that existing results are subjected to extrapolation.

Because of the diversity of scientific references regarding the fusion reactors, data compilation is an important task for developments of fusion machines. The data needs for fusion reactors now extend to a variety of fields, depending on near-term and long-term necessities. The data compilation for plasma-material interaction were started already twenty years ago and having been carried out actively by several groups in the world1-5). It is of interest to survey the data needs and data compilation in the past and discuss those in future. Each paper presented in this symposium is intended to answer the above problem for each topic. A brief survey on the trends of data needs and compilation in the past and future is given in this paper.

II. Trends of data compilation in the past

Several of review articles on plasma-surface interaction in 1970's describes the importance of a few basic processes that may occur in fusion devices[6)]. These fundamental processes includes reflection of ions, ion-induced sputtering, evaporation, arcing, hydrogen retention and re-emission, and adsorption and desorption. Several efforts have been carried out to compile data for these phenomena.

In the preliminary stage the data compilation is simply the collection of fragmental data, after a certain evaluation. These data will be of use for design purpose, only when the data are obtained with the materials and on the conditions the same as that used for fusion machines. If not, as is often the case, the data are of use as offhand data for obtaining order-of-magnitude information. Ideally the data compiled should have been analyzed, so that extrapolation and interpolation are capable by means of either empirical or theoretical formula.

Many of the data of atomic processes compiled so far are well organized and satisfies the requirement described above[5)]. Most of the processes, which are of interest for plasma-materials interaction, however, are not simple but involve several collisional and material processes. Furthermore often a small amount of impurities, defects and microstructures in materials influence the results. Therefore data compilation for plasma-materials interaction should involve sophisticated procedures in order that they are of wider use.

An example of well organized data compilation in the area of the plasma-materials interaction is that of the physical sputtering of monatomic solids7). The physical sputtering is essentially a collisional phenomenon and is little influenced by properties of solids, particularly for monatomic solids. An empirical formula has been derived to predict the sputtering yield for normal incidence as a function of energy for a given combination of the incident particle and target. Further refinement for the dependence on the incident angle and for the angular distribution has been derived8). The empirical equation is simple, includes only a few parameters: vaporization energy and a factor depending on the group in the periodic table.

The sputtering of alloys and compounds is no more so simple as that of monatomic solids, because of the change in the surface composition under bombardment9,10). At sufficiently low temperatures, a steady state is established forming so-called depleted zone of (a) specific component(s) at the surface due to preferential ejection, surface segregation and diffusion. Under the steady state, because of the mass balance, the composition of sputtered atoms is the same as that of the composition of the material. The situation will be complicated if temperature is high and if radiation field is mixed11). Therefore the data of the sputtering yield of an alloy, for example, obtained by laboratory experiments would be regarded as a measure of sputtering yield at a certain limited conditions but not always. To understand the behaviors of metals under mixed conditions, each of microscopic processes that influence the sputtering should be made clear.

III. Data compilation in future

We described already the complexity of the phenomena of plasma-surface interaction in which material processes are involved. The complexity is further enhanced by the situation where the materials are placed in a complex conditions; high temperatures, temperature cycles, mixed irradiation, complex ambient, redeposition and so on. The possibility of synergistic effects should be fully analyzed[12).

For near-term data compilation, we should grasp the first-order approximation on the behaviors of the materials under the conditions in which the materials may be placed. For this purpose, any compiled data for material properties will be useful[13,14). For the design of fusion devices, however, the conditions under which materials are placed should be fully characterized and the material behaviors under the conditions should be analyzed. For this purpose series of materials tests does not help, unless the results are analyzed to derive the general rules governing the materials behaviors. Thus for long term, the basic behaviors of the materials under the conditions of the fusion rectors should be made clear.

As an example, we describe hydrogen re-emission and retention. The kinetics of hydrogen re-emission and retention have been developed[15). It describes many of the laboratory experimental data. In real systems, however, hydrogen re-emission is influenced by hydrogen content, sputtering, impurity deposition, rapid temperature change, continuing implantation, neutron radiation damage and so on[16]. We need "data compilation" which is capable to predict the materials behavior under these complex conditions.

If we divide the data needs into those for near term and long term, the requirements for the short term are easier to specify. The short term needs are entirely depends upon the requirement coming from the design teams[17,18]. Of course the distinction is not often clear; data for short-term needs are often useful for long term purpose and vice versa. It is clear that the motivation for short term data production and compilation should come from the design teams but not from materials scientists.

The data needs for long term should be fully discussed among materials scientists, plasma scientists, who are involved in the current machine experiments, and the design teams. The material scientists could tell the direction of the future developments of materials science based on the requirements presented by the other partners. They know the difficulty of predicting materials behaviors and could tell how much studies are needed to attain the goal. The directions of the studies taken by the materials scientists should be advised by plasma scientists. The collaboration is essential.

Here importance of computer simulation of the response of materials to the plasma is emphasized. Because of the complex conditions under which materials are placed, it is advisable to construct computer codes for materials behavior under complex conditions. The codes should treat various processes at the same time: radiation damage, hydrogen re-emission, sputtering, chemical reaction and so on[19)]. In order to construct such codes, we should know every microscopic processes involved. One may argue that it is still too early to construct such computer codes; the understanding of the microscopic processes is not sufficient. I emphasize, however, that such codes will help to prompt the understanding, specification of the data needs and then in turn improvement of the codes. I am strongly tempted to consider that construction of such computer codes, with careful comparison with laboratory and machine experimental data, is urgent. Here data compilation is needed for the parameters for the computer codes. Ideally such codes should be combined with the codes for the plasma-edge simulation. But this will occur further in future.

Another important area in future is radiation damage of plasma facing materials[20)]. The fragmental data have been accumulated, but still it is not yet possible to evaluate the extent of radiation damage in given conditions.

IV. Conclusions

I have surveyed the data compilation on plasma-materials interaction in the past and then discussed the future direction. Emphasis is given particularly on the importance for future studies purposed to establish science needed for completing fusion reactors. The choice of the problems should be made carefully made under discussions among scientist of various fields.

One of the objectives of holding the present symposium is to carry out critical discussions on the present situation and future direction of data compilation. The programme is divided into near term and long term, rather arbitrary, and each presentation is given by the scientists most actively participating in the researches of each subject.

Reference

1) R. A. Langley, J. Bohdansky, W. Eckstein, P. Mioduszewski, J. Roth, E. Taglauer, E. W. Thomas, H. Verbeek, K. L. Wilson, Nuclear Fusion, Special issue (1984).

2) See relevant volumes of Max-Planck-Institute for Plasmaphysik Reort IPP-Series.

3) See relevant volumes of Oak Ridge National Laboratory Report ORNL Seriies.

4) See relevant volumes of Japan Atomic Energy Research Institute Report JAERI-memo-Series.

5) See relevant volumes of Nagoya University, Institute of Plasma Physics Report IPPJ-AM-Series.

6) See relevant volumes of Oak Ridge National Laboratory Report ORNL Seriies.

7) IPPJ-AM 14, 32. See also N. Matsunami, Y. Yamakura, Y. Itikawa, N. Itoh, Y. Kazumata, S. Miyagawa, K. Morita, R. shimizu, and H. Tawara, Atomic Data and Nuclear Data Tables 31, 1 (1984).

8) IPPJ-AM 34, 52, 60.

9) K. Koshikawa, paper in this issue.

10) N. Itoh and K. Morita, Rad. Effects 80, 163 (1984).

11) K. Morita, M. Hayashibara, H. Ohno and N. Itoh, J. Nucl. Mat. 122/123, 629 (1984).

12) N. Itoh and K. Kamada (eds), Proceedings of the Workshop on Synergistic Effects in Surface Phenomena Related to Plasma-Wall Interaction (Radiation Effects vol. 89 (1985)).

13) T. Tanabe, paper in this issue.
14) H. Atsumi, paper in this issue.
15) B. L. Doyle and D. K. Brice, reference 11, p. 21.
16) R. Yamada, paper in this issue.
17) H. Takatsu, paper in this issue.
18) N. Hosogane, paper in this issue.
19) Y. Yamamura, paper in this issue.
20) C. Kinoshita, paper in this issue.

ENGINEERING FEATURES OF PLASMA WALL INTERACTIONS IN LARGE TOKAMAK DEVICES

Hideyuki TAKATSU

Naka Fusion Research Establishment
Japan Atomic Energy Research Institute

1. INTRODUCTION

A variety of materials have been used for first wall and high heat flux components in tokamak devices. Initially operating with metalic limiters and walls, such as TiC-coated molybdenum limiters in JT-60, Inconel wall protection in JET and Inconel bellows cover plates in TFTR, the inner surface of the vessel is now covered in graphite tiles in most of the currently operating tokamaks. Several grades of fine grain isotropic graphites and C/C composites are used. Carbonisation technique is also employed in a few machines.

Behavior of graphite tiles has been widely examined in large tokamaks from the viewpoint of plasma wall interactions and been understood to some extent. However, there still remain a number of issues to be solved for further advancement of both main plasma parameters and graphite wall characteristics [1].

This section reviews engineering features of plasma wall interactions in three large tokamak devices, JET, TFTR and JT-60, laying emphases on conditioning, recycling, erosion and thermal shock characteristics of graphite.

2. CONDITIONING

A typical procedure of wall conditioning in JT-60 is 3 d bake-out at a temperature of up to 300 °C, followed by 20 h Taylor-type discharge cleaning (TDC) keeping the vessel temperature around 300°C [2][3]. Reduction rates of carbon hydrides are comparable to those of TiC-coated first walls [4], and very rapid start-up of discharge conditioning can be obtained. Figure 1 shows a time history of the main plasma discharges just after above-mentioned conditioning in June '87. The first five shots terminated in the start-up phase due to the rapid density build-up, but a stable 0.5 MA plasma was obtained at the 6th trial [2].

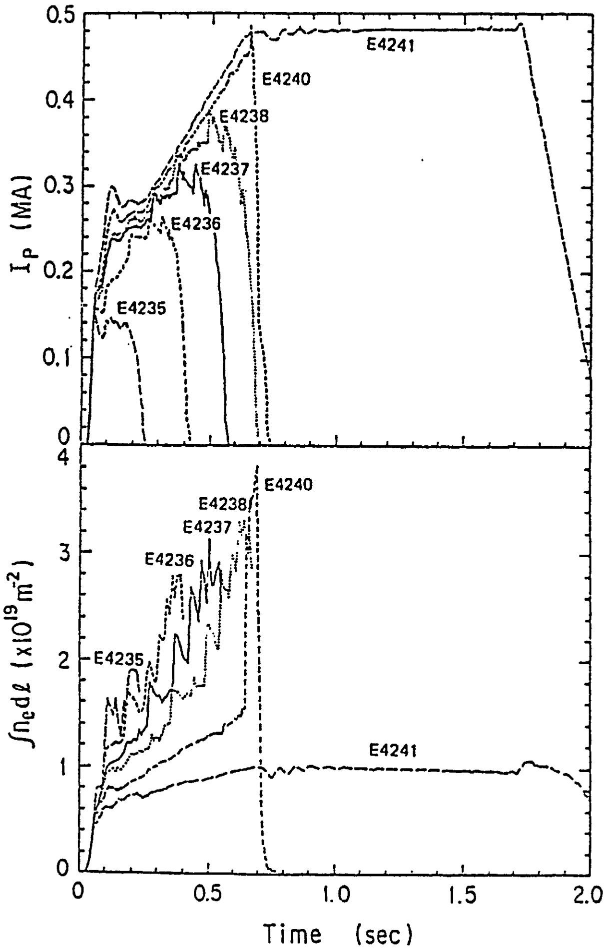

Fig. 1

Time history of main plasma discharges just after 7d conditioning in June '87. Shot number E4253 corresponds to the first trial and a stable 0.5 MA plasma was attained at the 6th trial [2].

In JET a typical procedure after opening of the vessel to air is first to bake-out the vessel for 24 h at a temperature of 300 °C. Then an RF-assisted glow discharge cleaning (GDC) in hydrogen is executed for about 70 h. To reduce the metal contamination carbonisation is used and the vessel is covered by carbon films of thickness up to ~1 μm [5][6].

The initial conditioning of the TFTR vacuum vessel after opening to air involves a 6 week bake-out at a temperature of 150°C. During this time 130 h of GDC and 175 h pulse discharge cleaning (PDC) are applied [7]. However, such standard vessel conditioning procedures were found insufficient after introduction of a significant amount of graphite, bumper limiter and protective plate in '85. Intentional exposure to a series of disruptive discharges at increasing current levels, dubbed "disruptive discharge cleaning (DDC)" was found necessary to heat and degass the bumper limiter [8].

Figure 2 shows temperature dependence of water release rates for several grades of graphite [8]. Strong peaks are shown at the temperature of around 350° C for porous graphites. As the primary desorption temperature for H_2O is in the range of 300-350°C, TFTR 150 °C vessel bake-out temperature is ineffective in desorbingthe H_2O from graphite tiles, and DDC is needed for limiter degassing.

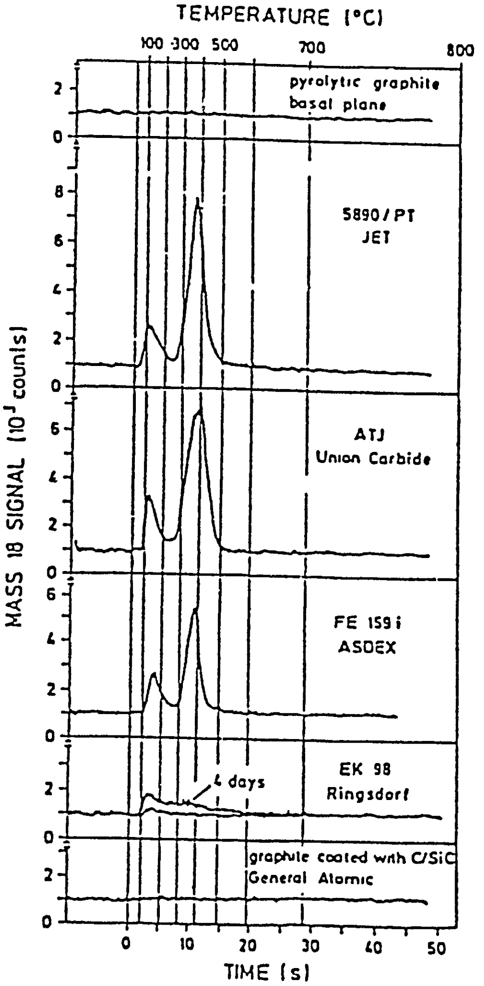

Fig. 2

Temperature dependence of water release rates for several grades of graphites. Strong peaks are shown at the temperature of around 350°C for porous graphites [8].

3. RECYCLING

With the introduction of the graphites as first wall material density pump-out has been observed during discharges in many tokamaks.

In JET this phenomenon has been used to terminate beam-heated discharges with densities above the ohmic density limit. An example of wall pumping is shown in Fig. 3, where the average electron density during a discharge is shown as a function of time. The plasma is shifted from the outboard limiter to the inner wall at the end of neutral beam injection, and strong density pump-out effect is observed [9]. Helium conditioning (He-conditioning) of the inner wall increases the pumping capability and makes it possible to operate at low densities and high heating power in the hot ion mode [10].

In JT-60 particle recycling rate less than unity has been obtained with graphite first walls in the same manner as TiC-coated walls, which makes density control relatively easy [11]. Figure 4 shows density evolutions of two Joule-heated divertor discharges. Density decay is observed just after stopping the gas feeding, showing typical examples of recycling rates less than unity. As density control deeply depends on the wall conditions, a series of conditioning shots or helium-fueled TDC (He-TDC) has been applied to drive out hydrogen gases from the graphite walls.

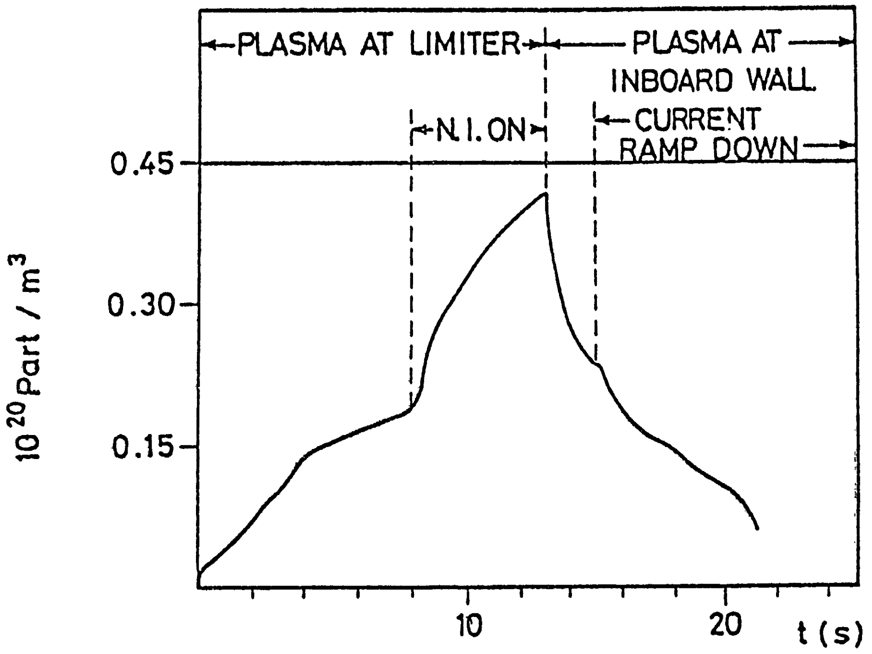

Fig. 3 Example of wall pumping in JET. The plasma is shifted from the outboard limiter to the inner wall at the end of neutral beam injection. The pumping rates of the inner wall of about 50 mbar•ℓ/s can be estimated [9].

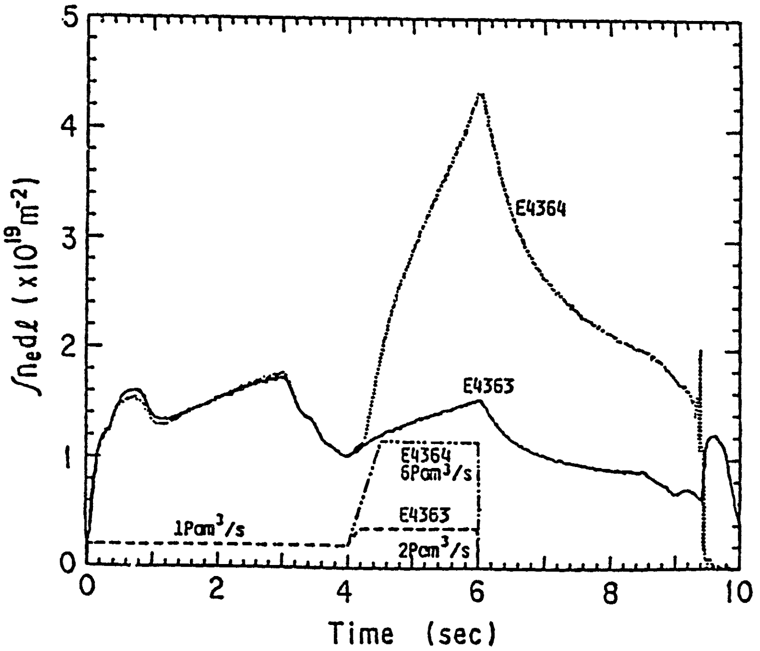

Fig. 4 Example of wall pumping in JT-60. Density decay is observed just after stopping the gas feeding, showing the particle recycling rate of the wall less than unity [11].

A strong pumping effect has been also observed in TFTR with plasma operation on the toroidal graphite bumper limiter [8] [12]. The pumping effect is induced by conditioning the limiter with a short series (10-20) of low density deuterium or helium initiated discharges (He-conditioning). Gas fueling and plasma density waveforms for three representative cases are shown in Fig. 5, (a) typical gas fueling with ohmic discharges on the moveable limiter, (b) bumper limiter and (c)bumper limiter after He-conditioning. The decay constant (τ_p*) for gas fueled Ohmic discharges is reduced from τ_p*> 10 s before conditioning to a minimum of τ_p* = 0.15 s after conditioning, which corresponds to a reduction in the global recycling coefficient from about 100% to less than 50%.

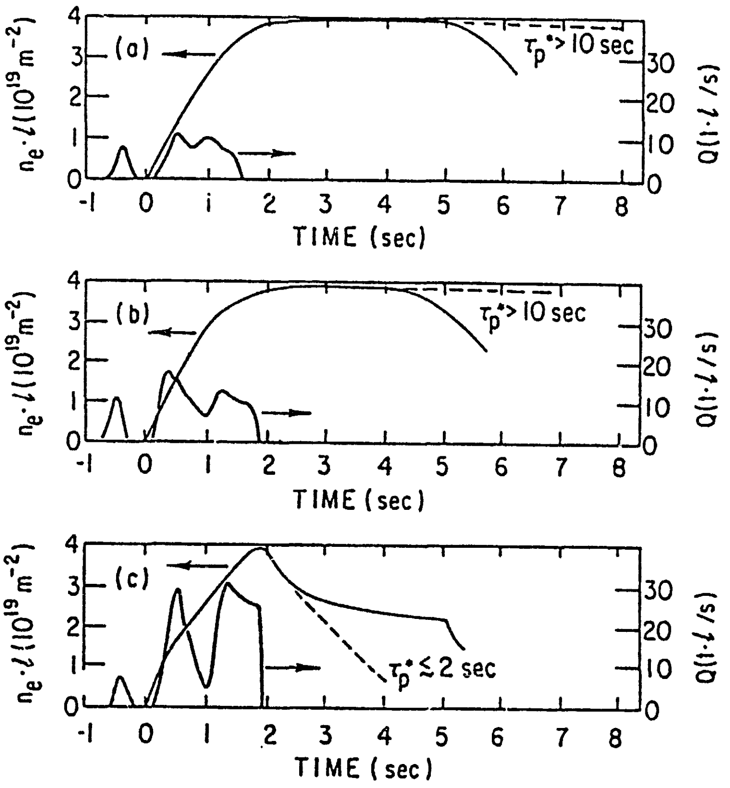

Fig. 5 Gas fueling and plasma density waveforms for three representative cases in TFTR [8].

(a) typical gas fueling with ohmic discharges on the moveable limiter
(b) typical gas fueling with ohmic discharges on the bumper limiter
(c) special case of fueling on the bumper limiter after He-conditioning, which shows density pump-out effect

The mechanisms governing the wall pumping are not yet fully understood. There exist a variety of models. They range from assuming transient effects similar to the hydrogen pumping by metal walls [13][14] to the co-deposition of hydrogen and graphite in form of surface H-C films [15][16]. To date it cannot be decided which process is dominant.

4. EROSION AND THERMAL SHOCK CHARACTERISTICS

In JT-60 graphite tiles have been used for limiters of main chamber and for divertor plates from June '87. The graphite tiles of the main chamber performed admirably, and maintained their integrity with only one exception. This may be due to the graphite tile alignment with a flattened surface level, rather than protruding ones like TiC-coated limiters, which increases the contact area of the first wall with the plasma.

Figure 6 shows the inboard of #8 rigid sector after the operation period from June to Oct. '87. Only one heavy damage is observed on the tiles located at the midplane and on the electron side. This damage might be caused by runaway electron bombardment during disruptions due to a level difference [17].

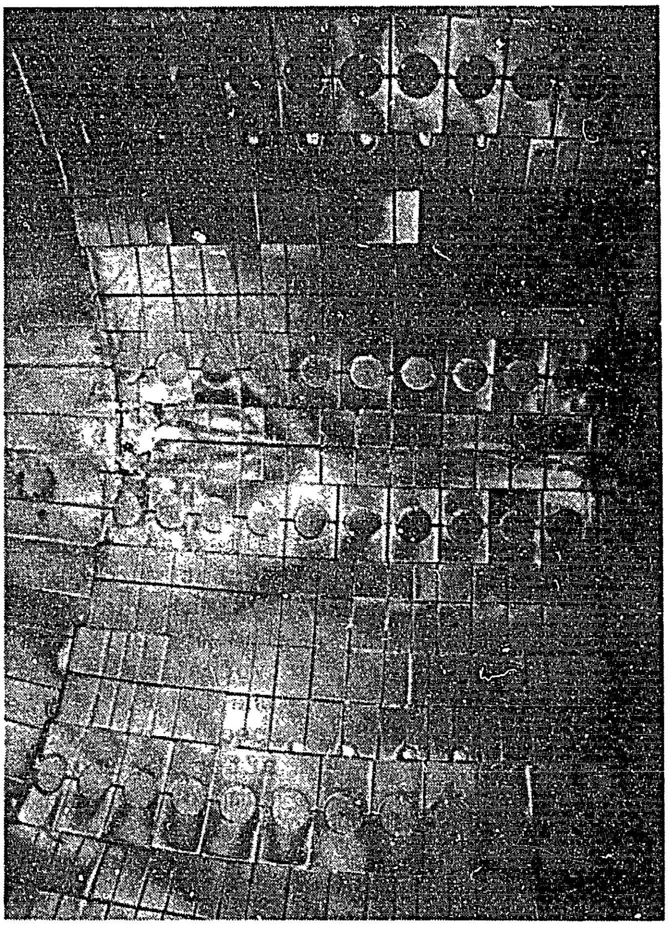

Fig. 6

Inboardof #8 rigid sector aftertheoperation period from June to Oct. '87. Heavydamageis evident on the left-side tiles at the midplane [17].

Substantial erosion was observed on the tiles located on the edge of each rigid sector because of heat concentration due to a toroidal gap. Deposition of eroded graphite was also seen on every kind of an in-vessel component. Figure 7 shows carbon flakes collected in the vacuum vessel after 4-month operation in '87 [17].

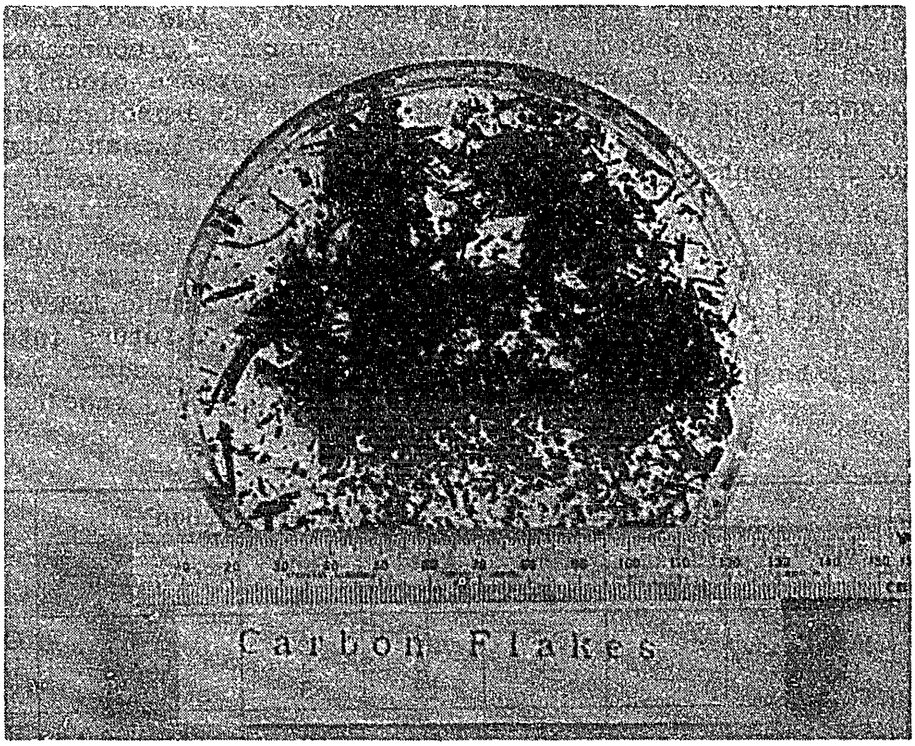

Fig. 7 Carbon flakes collected in the JT-60 vacuum vessel after 4-month operation with graphite first wall [18].

The number of damaged divertor plates was much larger than that expected during operation period in '87. One of the reasons of the unexpected failure is selection of the grade of graphite. Grade of high density and high mechanical strength, used for divertor plates, is not preferable from the thermo-mechanical viewpoint, and that of low thermal expansion coefficient and well-balanced characteristics, used for limiters of the main chamber, is preferable.

In JET, fine grain isotropic graphite was chosen for areas where during the flat top time of the discharge (typically 10 s), the power loads do not exceed 5 MW/m^2, and C/C composite was selected for areas where loads above 20 MW/m^2 can be expected.

Damage to the graphite tile was minimal but was concentrated at the midplane and octant joint areas during operation period in '86 and '87. As the inner wall in the region of all the octant joints protrude slightly into the vessel, all the octant joint tiles at the midplane suffered damage to some degree. Damage observed on the inner wall tiles is caused primarily by runaway electrons which are generated during disruptions. All of the tiles located at the midplane were replaced with C/C composite tiles. Although C/C composite tiles showed evidence of substantial erosion, they are clearly intact and capable of still fulfilling its role as a protection ofthe vessel. Operation experiences of JET first walls and high heat flux components are summarized in Table 1 [18].

Table 1 Data for various materials used in the JET vacuum vessel, and for others of possible future interest [18].

	Material	Design Limits		Normal Operation			Disruptions
		Load MWm^{-2}	Time S	Load MWm^{-2}	Time S	Comment	Comment
Discrete Limiters	Fine Grain Graphite	5	10	3 6 12	7 5 3	O.K.	One Single Event Local Damage Surface Cracking
Wall Protection	Fine Grain Graphite	5	10	5.5	2	Erosion at Edges	Runaway Damage at Protruding Edges
Wall Protection	Carbon Fibre Composite	35	≥ 3.5	<2	3	Erosion at Edges	500 MJm^{-2} on 3.5 x $10^{-3} m^2$ 2 x $10^{-3} m$ Erosion No Failure
Belt Limiter	Fine Grain Graphite	3.5	10	<1	≤ 2	O.K.	No Events Observed
X-point Plates	Fine Grain Graphite	5	10	20	≤ 2	Strong Erosion Failure	No Events Observed
X-point Plates	Carbon Fibre Composite	5	10	Not yet installed			Not yet installed

Disruption heat load has been examined in TFTR [20]. Typical time behaviors of plasma current and the temperature of the bumper limiter are shown in Fig. 8. A standard disruption is assumed to take place in two stages: the thermal quench portion in which the plasma thermal stored energy is deposited on the limiter over a 0.2-2 ms time scale at power fluxes up to 1000 MW/m^2 and the plasma current decay portion in which the current decays linearly at 1 MA/ms.

Cracking of the graphite tiles of moveable limiter were observed during the operation in '85 and '86 [21], which was resulted from excessive heat load, up to 2.5 times greater than the design value.

The bumper limiter has performed admirably. The only observable damage is several spalled, ablated areas located on the midplane. It is believed that the damaged areas are high spots on the limiter which are subject to runaway electron bombardment or enhanced thermal loading during a disruption. These high spots exist even though the bumper limiter was aligned to the toroidal field to better than ± 1 mm accuracy [20].

C/C composites have been introduced for the guard limiters of RF antenna [22].

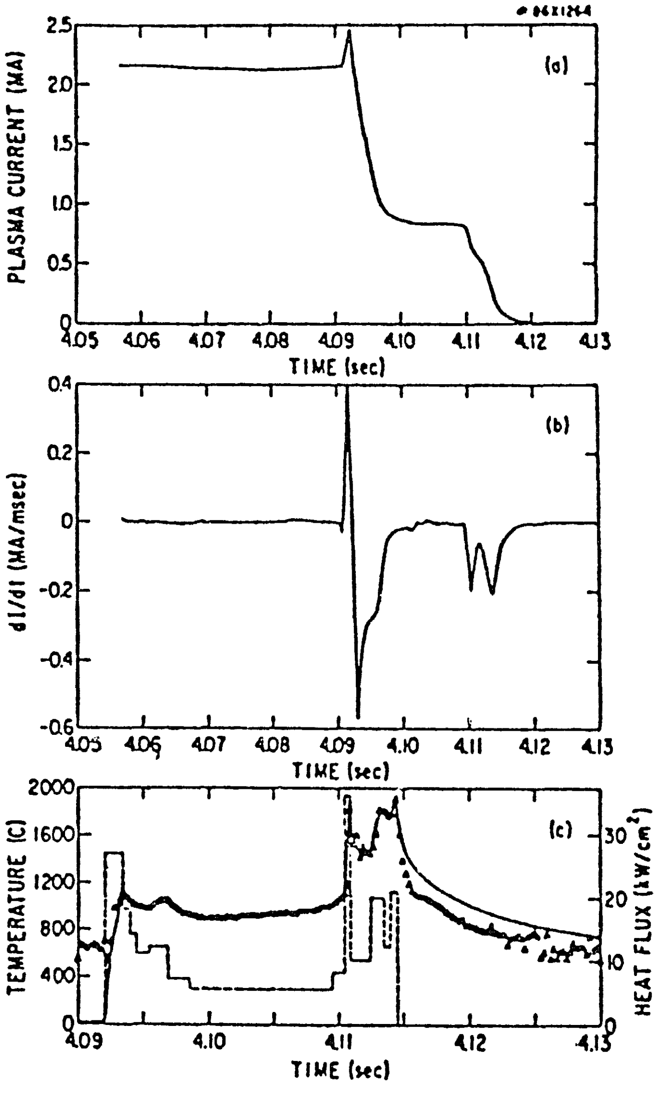

Fig. 8

Fast disruption on TFTR.
(a) plasma current
(b) time derivation of the plasma current
(c) surface temperature and inferred heat fluxto the bumper limiter at the max. of the deposition pattern [20].

Most of the damages of the graphite tiles observed in the large tokamaks are caused by runaway electrons generated during a disruption. Good alignment to the magnetic field configuration is important to suppress an excessive heat concentration on the edge of the graphite tile and its damage. Grades of graphite of low thermal coefficient and well-balanced characteristics are preferable from the thermo-mechanical viewpoint.

C/C composites have been introduced for high heat flux components of the large tokamaks [2][18][22]. They have shown superior thermal shock resistance and good compatibility with plasma so far, and erosion due to sublimation is considered to be a critical issue in application to high heat load conditions [23][24][25]. A few grades of newly developed C/C composites, which have very high thermal conductivity over 300 W/mK at room temperature, have a possibility to overcome the sublimation problem [26] and are now planned to be employed in upgraded program of JT-60 and JET [27][18].

5. SUMMARY

Protection of vacuum vessel is necessary and graphite tiles have shown to be a good material. This is partly because of the good thermal shock resistance and partly because of the natural spreading of the heat load caused by runaway electrons [28].

The mechanism of recycling is not yet fully understood, but a number of operational techniques of wall conditioning have been established both for initial conditioning and for degassing of graphite tiles.

From the viewpoint of erosion and thermal shock characteristics surface area of the graphite tiles is required to be large so as to increase the contact area with plasma and to suppress too high surface temperature. And good alignment of the graphite tiles is needed to prevent excessive heat concentration on the edge of the graphite tile.

C/C composites have been introduced for high heat flux components in the large tokamaks and shown superior thermal shock characteristic. Though erosion due to sublimation is a critical issue for conventional C/C composites, newly developed ones of very high thermal conductivity over 300 W/mK have possibilities to overcome this problem. "The introduction of C/C composites marks the end of a road. Further improvement of materials to handle even more power seems to be unlikely at least in the short time." [18]

On the other hand, there still remain a number of tough problems in application of isotropic graphites or C/C composites to the next step machines such as ITER, FER and NET. Critical issues to be solved are erosion due to sputtering, radiation induced sublimation, neutron damage (especially degradation of thermal conductivity), tritium absorption and steady state recycling control. Further research on plasma wall interaction is needed both in the large tokamak device and in the laboratories.

REFERENCES

[1] H. Takatsu and T. Oku, Tanso 135 (1988) 286 (in Japanese).
[2] H. Takatsu et al.,J. Nucl. Mater. 155-157 (1988) 27.
[3] T. Arai et al., presented at the 8th Symp. on Plasma Surface Interaction, Julich (1988) and to appear in J. Nucl. Mater.
[4] T. Arai et al., J. Nucl. Mater. 145-147 (1987) 686.
[5] L. de Kock et al., J. Nucl. Mater. 145-147 (1987) 26.
[6] P.H. Rebut et al., JET-P(88)21 (1988).
[7] H.F. Dylla et al., J. Nucl. Mater. 128-129 (1984) 861.
[8] H.F. Dylla et al., J. Nucl. Mater. 145-147 (1987) 48.
[9] K. Sonnenberg et al., Proc. 14th Symp. on Fusion Technol., Avignon (1986) 273.
[10] R.J. Bickerton, Plasma Physics and Contr. Fusion, Vol. 29-10A (1987) 1219.
[11] JT-60 Team, JAERI-M 88-063 (1988).
[12] H.F. Dylla et al., J. Nucl. Fusion 27 (1987) 1221.
[13] F. Waelbroeck et al., J. Nucl. Mater. 85-86 (1979) 345.
[14] M.A. Pick and K. Sonnenberg, J. Nucl. Mater. 131 (1985) 208.
[15] J. Winter, J. Vac. Sci. Technol. A, 5 (1987).
[16] W.L. Hsu and R.A. Causey, J. Vac. Sci. Technol. A, 5 (1987).
[17] H. Takatsu et al., presented at Internat. Symp. on Fusion Nucl. Technol., Tokyo (1988) and to appear in J. Fusion Eng. Des.
[18] K.J. Dietz, J. Nucl. Mater. 155-157 (1988) 8.
[19] M.A. Pick et al., Proc. 12th Symp. on Fusion Eng., Monterey (1987) 137.
[20] D.K. Owens et al., Proc. 14th Symp. on Fusion Technol., Avignon (1986) 1873.
[21] S.S. Medley et al., Rev. Sci. Instrum. 56 (1985) 1873.
[22] G.W. Labik et al.,Proc. 12th Symp. on Fusion Eng., Monterey (1987) 125.
[23] J. Bohdansky et al., Proc. 14th Symp. on Fusion Technol., Avignon (1986) 1063.
[24] H. Bolt et al., IPPJ-AM-51 (1987).
[25] M.Seki et al., presented Internat. Symp. on Fusion Nucl. Technol., Tokyo (1988) and to appear in J. Fusion Eng. Des.
[26] H. Takatsu et al., to be presented in J. Fusion Eng. Des.
[27] M. Kikuchi et al., presented 15th Symp. on Fusion Technol., Utrecht (1988).
[28] L. de Kock et al., JET-P(88)22 (1988).

Study of the first wall in JT-60 and its recent plan
———————— from plasma-wall interaction

N. Hosogane
Japan Atomic Energy Research Institute

Recent PWI studies in JT-60 are presented on wall conditioning, impurity behavior and radiation loss,characteristics of IDC (Improved Divertor Confinement) discharges and effects of Zeff on LHCD efficiency.

1. Conditioning of graphite wall

The combination of high temperature vessel operation (200-300 ° C) and conditioning discharges of 1 MA without gas puff is employed as a wall conditioning in JT-60.[1,2) One or two conditioning discharges are conducted after a high current and high density tokamak discharge to desorp hydrogen gas which is retained in the graphite wall after the discharge. As shown in Fig.1, high vessel temperature increases the proportion of hydrogen gas exhausted after a high current and high density discharge ($Q_{exhaust}/Q_{IN}$) and the amount of hydrogen gas exhausted by a conditioning discharge($Q_{exhaust}$). To maintain the graphite wall condition unchanged and to obtain reproducible discharges (To keep hydrogen gas retained in the graphite wall constant), high vessel temperature is quite favorable. In case of 150° C operation, conditioning discharges are not so effective that disruptions occur in several high density discharges.

The He-TDC is also effective to disorb hydrogen gas in the graphite wall. After the He-TDC of 15 min. following about 1 hour H-TDC, a tokamak discharge of 0.7 MA and 9 sec was successively produced at the first shot. Without the He-TDC, 14 shots were conducted to obtain a stable tokamak discharge of 0.7 MA and 9 sec.

2. Impurity behavior

2.1 Effective charge and radiation loss

The characteristic of effective charge (Z_{eff}) and radiation loss in JT-60 is summarized as follows.[1)

(1) divertor with TiC-Mo wall; $Z_{eff} \sim 1.5$-2 at $n_e > 3 \times 10^{19}\ m^{-3}$.
$P_{rad}/P_{abs} \sim 10\ \%$

(2) outer X-point divertor with graphite wall ; $Z_{eff} \sim 3$-4 at $n_e \sim 2 \times 10^{19}\ m^{-3}$ and ~ 2 at $n_e > 5 \times 10^{19}\ m^{-3}$.
$P_{rad}/P_{abs} \sim 20\ \%$

(3) limiter with graphite wall; $Z_{eff} \sim 4$-5.5 at $n_e \sim 2 \times 10^{19}\ m^{-3}$,~ 3 at

n_e =4-7 X 10 ^{19} m^{-3} and $\sim$ 1.8 at 1 x 10^{20} m^{-3}.
P_{rad}/P_{abs} $\sim$ 30 % (5 x 10^{19} m^{-3}) -50 % (10 x 10 ^{19} m^{-3})

In the low density reion, oxygen impurities are responsible for Z_{eff} and radiation loss.

2.2 Behavior of carbon impurity

The carbon impurity production strongly relating with the graphite wall temperature is observed in limiter and divertor discharges with high power NB heating. Fig.2 shows evolutions of CII/Hα at the divertor plates versus temperture of the divertor plates during a discharge for three shot with different NB power of 9.5MW,15MW and 25MW. Here, CII/Hα is used as a quantity proportional to carbon impurity production rate at the graphite divertor plates. The carbon impurity production rate seems to depend only on the graphite temperature, irrespective of NB power. Up to around 550° C, the production rate increases ,but above 550° C it seems saturated. This property strongly suggests chemical sputtering as a cause of carbon impurity producation. To confirm this mechanism furthermore, an experiment with He discharges is planned which has no chemical reaction with carbon.

3. Characteristics of IDC discharges

In recent experiment with lower X-point divertor, favorable discharges (IDC discharge: Improved Divertor Confinement discharge) are observed with good energy confinement and high recycling state in the divertor region (Fig.3).[3]
The main characteristics of IDC discharge are:

(1) The stored energy increases up to 1.2-1.5 X (L-mode level of limiter plasmas) during NB heating, accompanying electron density increase.
(2) The hydrogen recycling in the divertor region increases and is kept at high level, which causes large radiation loss of 20-60 % of the absorbed heating power.
(3) Oxygen impurity begins to decrease just before or at the same time as the electron density begins to increase, and decreases to low level. Carbon impurity increases corresponding to the decrease in oxygen impurity, but its concentration does not change so much because of increase in electron density.
(4) IDC discharge is obtained in the high power region of > 15 MW. At the same absorbed heating power, the q-value of discharge is higher,IDC is obtained at lower electron density.

When IDC mode starts, the divertor radiation increases. This results in lowering the heat flux to the divertor plates (remote radiative cooling.

Fig.4). This property is essential for next generation tokamaks.

The detailed IDC mechanism is now under investigation.

4. Effects of Zeff on LHCD efficiency

Figure 5 shows the effect of Z_{eff} on LHCD (Lower Hybrid Current Drive) efficiency.[4)] The LHCD efficiency is in proportion to $1/(Z_{ef}f + 5)$ in accordance with the theoretical analysis. This experiment is carried out in the range of $n_e \sim 1.3 \times 10^{19}$ m^{-3} and RF power of 1.5 MW. In next generation tokamaks, higher RF power is required. It is, hence, important to study the interaction between fast electron induced by LHRF and the first wall.

5. Summary and recent plan on PWI in JT-60

The high temperature vaccum vessel opeartion, conditioning discharge wihtout gas puff and He-TDC are effective to conditioning graphite walls. The chemical sputtering is strongly suggested as a cause of production of carbon impurity during NB heating. IDC discharge with good confinement and high recycling state are obtained in lower X-point divertor with high power NB heating. The LHCD efficiency decreases in proportion to $1/(Z_{eff}+5)$. To maintain high LHCD efficiency in high power regime, it is important to study the interaction between fast electron and the first wall,and to control it.

The following PWI studies are planned:

(1) detailed study of IDC.
(2) divertor characteristics for LHCD plasmas and investigation on fast electron-wall interaction.
(3) Test of several graphite materials by using PWI in lower X-point divertor experiment. This test is carried out to select a suitable graphite material for JT-60 Up-grade (JT-60U).

Reference

1) N. Hosogane and JT-60 Team, Proc. of 8th PSI ,julich,1988,to be published in J.Nucl.Mater.
2) R.Yoshino et al. ibid.
3) S.Tsuji et al., in Plasma Physics and Controlled Nuclear Fusion Research, Niece, 1988
4) K.Ushigusa et al.,ibid.

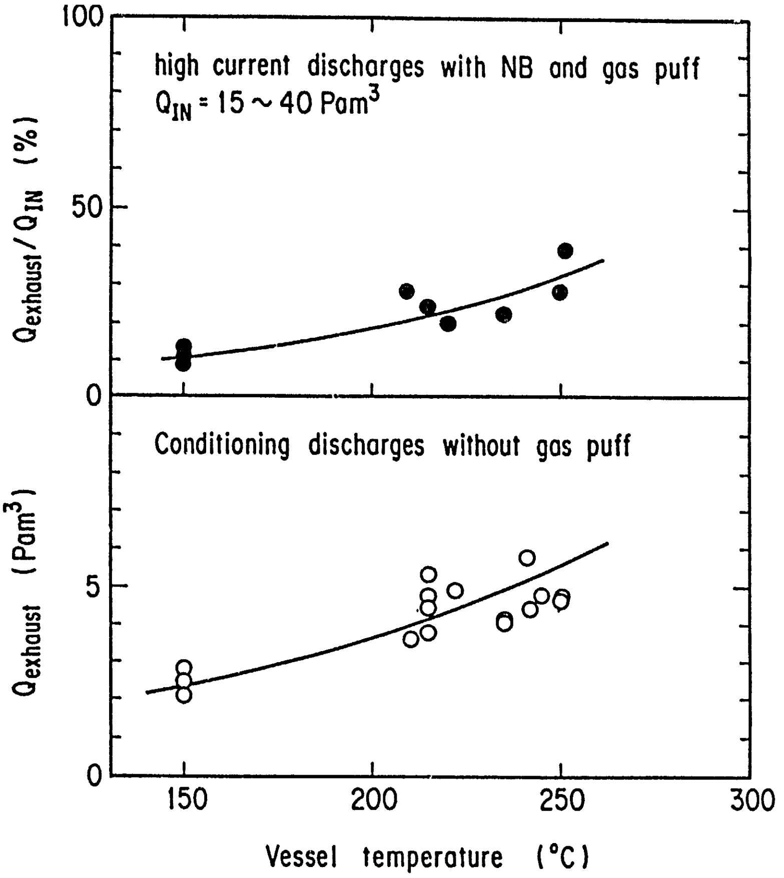

Fig.1 Dependence on the vessel temperature of hydrogen exhaust after high current and high density discharges and by conditioning discharges. $Q_{exhaust}/Q_{IN}$ is proportion of hydrogen gas exhausted for 16-19 min. after a discharge and hydrogen gas fuelled during the discharge. $Q_{exhaust}$ for conditioning discharges is the amount of hydrogen gas exhausted for 11-14 min. after the discharge.

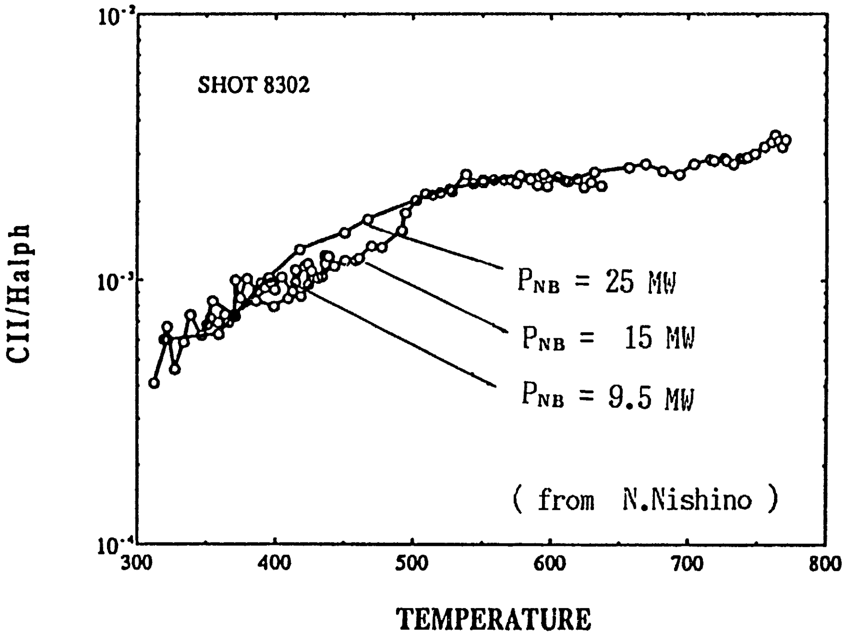

Fig.2 Dependence on the graphite wall temperature of the carbon production during discharges with different NBI heating power. The carbon production rate is expressed by the ratio of intensity of CII line and intensity of Hα in the divertor region.

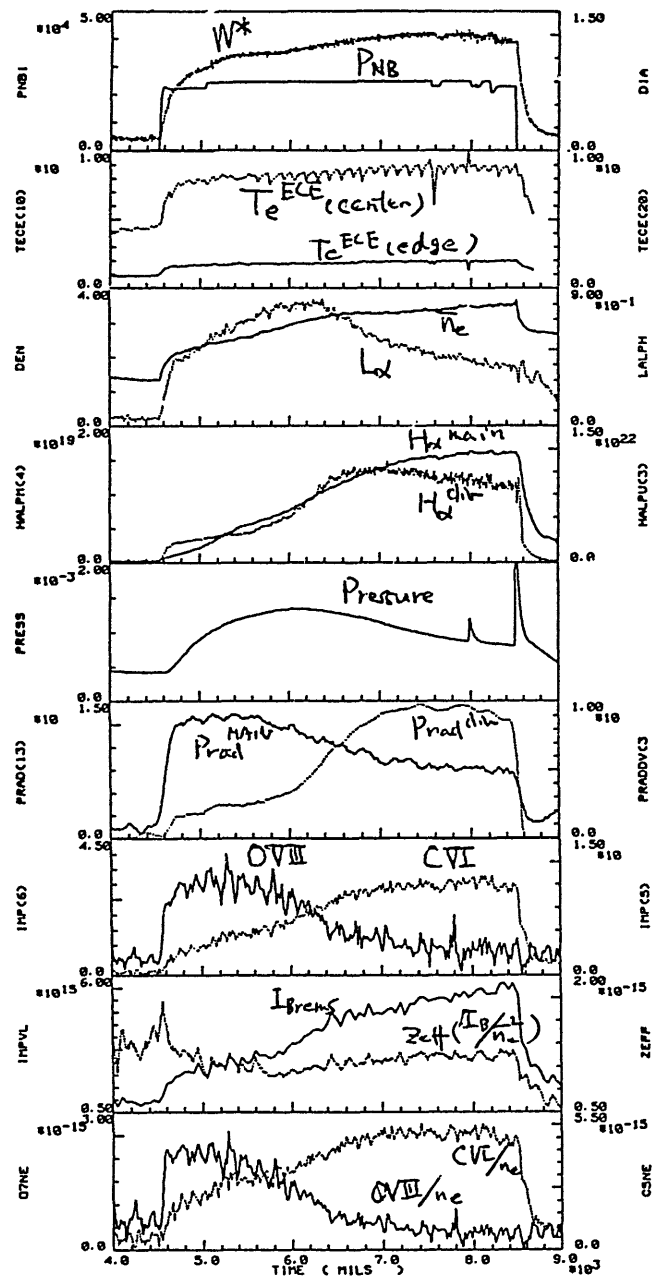

Fig.3 Typical waveforms of the IDC (Improved Divertor Confinement) I_P = 1MA, B_T =4.5T

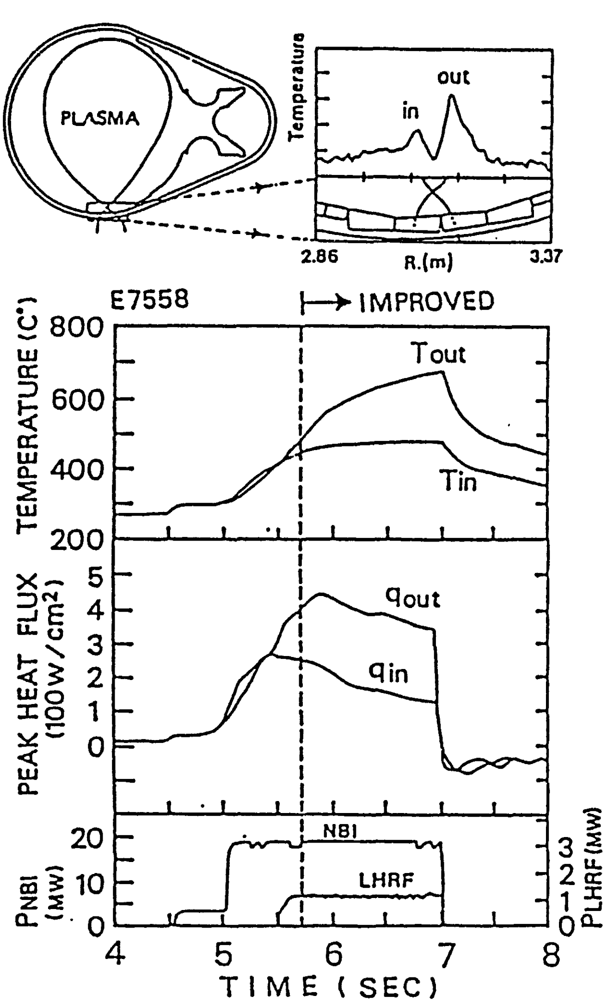

Fig.4 Time evolution of divertor plates during an IDC discharge

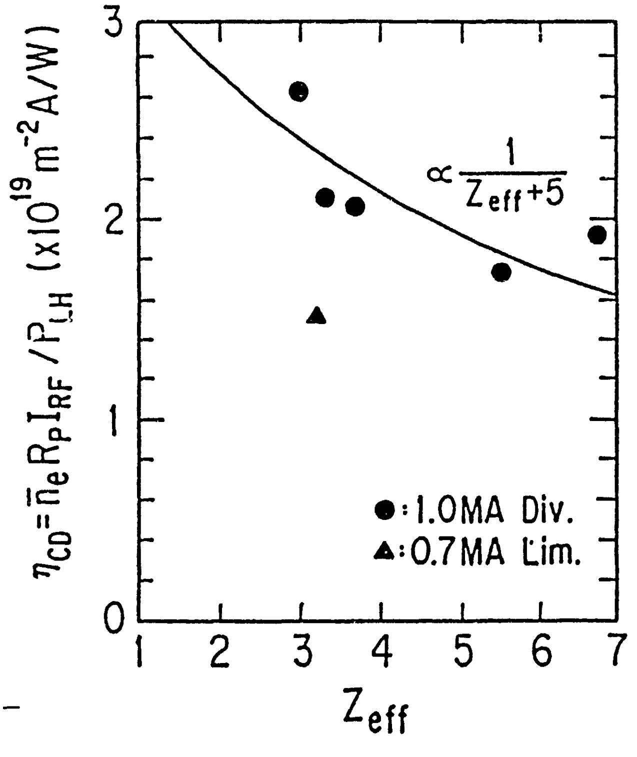

Fig.5 Effect of Z_{eff} on the LHRF current drive efficiency

Design of Plasma Facing Components in ITER

JAERI Naka Fusion Research Establishment
Plasma Heating Laboratory I M. Seki

1. Main operating conditions for plasma facing components

Operating parameters are listed in Table 1. Average heat flux on the first wall is predicted to be around 0.1-0.2 MW/m2. The peak heat flux due to neutral beam shine through and alpha ripple loss is rather uncertain. The heat flux on the divertor plate has a sharp peak which reaches as high as 17 MW/m2.

The assumed disruption energy deposition is also summarized in Table 1.

2. Typical design of the first wall

Figure 1 shows an example of the first wall design, where the metal surface is protected with the radiation cooled CFC tiles. Results of thermal and stress analyses are shown in Fig. 2. In the radiation cooled tiles, heat flux through the back surface of the tile is so small that heat flow is concentrated through the washer to the metal substrate. The use of ceramics with low thermal conductivity is required to suppress high thermal stress in the metal structure. The allowable heat flux on the radiative tiles are determined by the thermal stress in the metal structure and the maximum temperature of the tile surface.

3. Typical design of the divertor plate

Figure 3 shows an example of the divertor plate. CFC tiles with high thermal conductivity are metallurgically bonded to the heat sink material, preferably copper or copper alloys.

Critical issues in designing the divertor plate include thermal stress and fatigue of armor tiles, heat sink materials, and their interfaces, and high heat flux heat removal. Separatrix sweeping with an intention to reduce heat flux on the divertor plate is seriously examined.

Life time of the divertor plate is limited by loss of surface material due to sputtering and disruption. Use of high Z materials such as tungsten as a surface material should be examined in more detail, which can significantly reduce sputtering erosion, provided that plasma temperature in front of the divertor plate is sufficiently low.

MAIN OPERATING REQUIREMENTS FOR PLASMA FACING COMPONENTS

OPERATION PHASE		PHYSICS		TECHNOLOGY	
COMPONENTS		FIRST WALL	DIVERTOR PLATES	FIRST WALL	DIVERTOR PLATES
1. NOMINAL OPERATION					
- AVER.NEUTRON WALL LOAD	MW/m^2	1.0	0.6	1.0	0.6
- HEAT FLUX •AVERAGE	MW/m^2	0.1-0.2		0.1-0.2	
•PEAK	MW/m^2	0.5-1	up to 15*	0.5- 1	up to 25*
- TOTAL NUMBER OF LOAD PULSES	10^4	1	0.2**	2-5	0.4-1**
- AVERAGE NEUTRON FLUENCE	MWY/m^2	0.02	.004**	1-3	0.1-0.4**
- PEAK IRRADIATION DAMAGE***	DPA	≈0.4	.02**	12-45	0.6-2**
- INCIDENT PEAK PARTICLE					
•FLUX	$10^{20}/m^2s$	1	$5-1\cdot10^3$	1	$5-1\cdot10^3$
•ENERGY	eV	10-200	100	10-200	100-800
2. DISRUPTIONS					
- THERMAL QUENCH					
• TOTAL NUMBER AT FULL LOAD		1000	200**	10-100	2-20**
• TIME	ms	0.1-3		0.1-3	
• PEAK ENERGY DEPOSITION	MJ/m^2	1-2	5-10	1-2	5-10
- CURRENT QUENCH					
• TOTAL NUMBER AT FULL LOAD		2000	400**	10-100	2-20**
• TIME	ms	5-50		5-50	
• RADIATIVE ENERGY DEPOS.	MJ/m^2	2	1-2	1.5	0.5-1
• RUN-AWAY ELECTRONS	MJ/m^2	50-500		50-500	

NOTES

* For double-null plasma on outboard divertor plates with 20° inclination to the separatrix assuming ignited operation in the physics phase and driven operation (Q ~ 10) in the technology phase

** Assuming about 4 divertor plate replacements during each phase.

*** For austenitic steel and carbon based material in the first wall and divertor respectively.

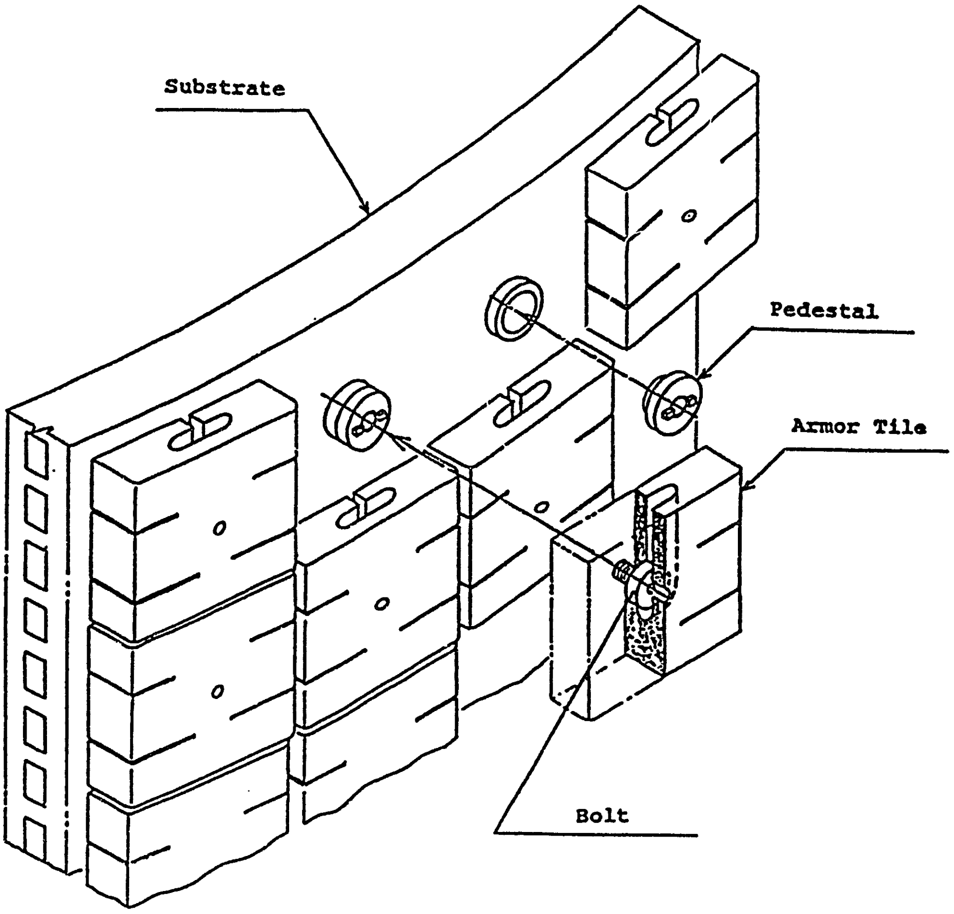

Fig 1 Radiation-cooled Mechanically Attached First Wall (TYPE I)

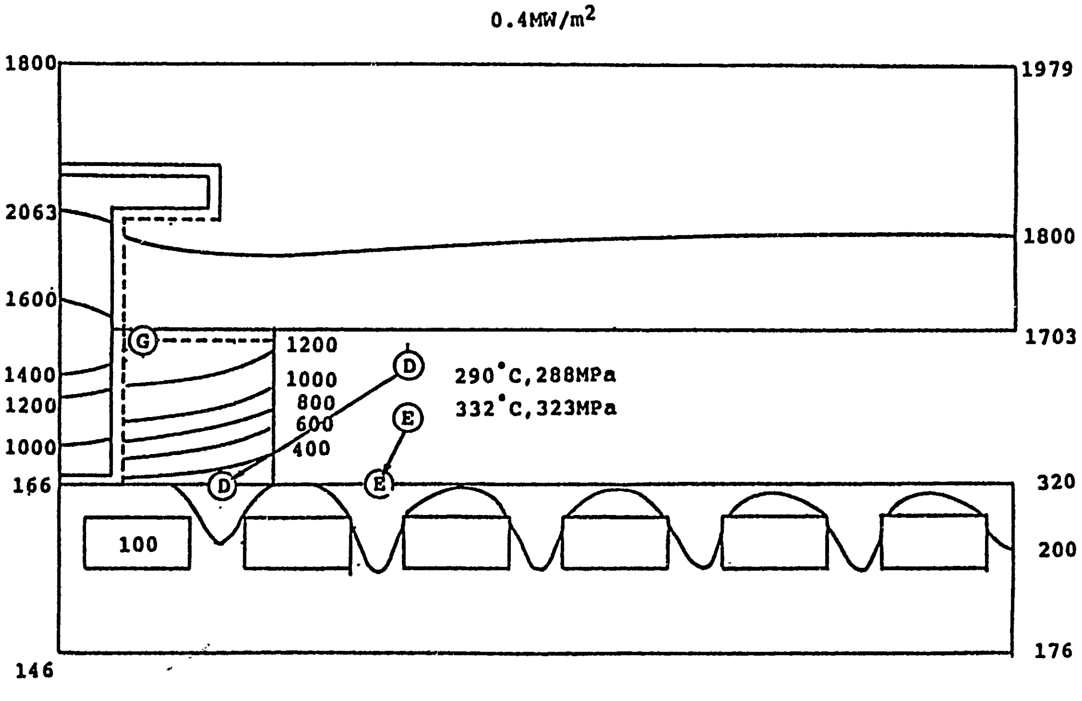

Fig. 2 Temperature profiles and peak stresses in stainless steel substrate of mechanically attached first wall, with ceramic washer and heat flux of 0.4MW/m^2.

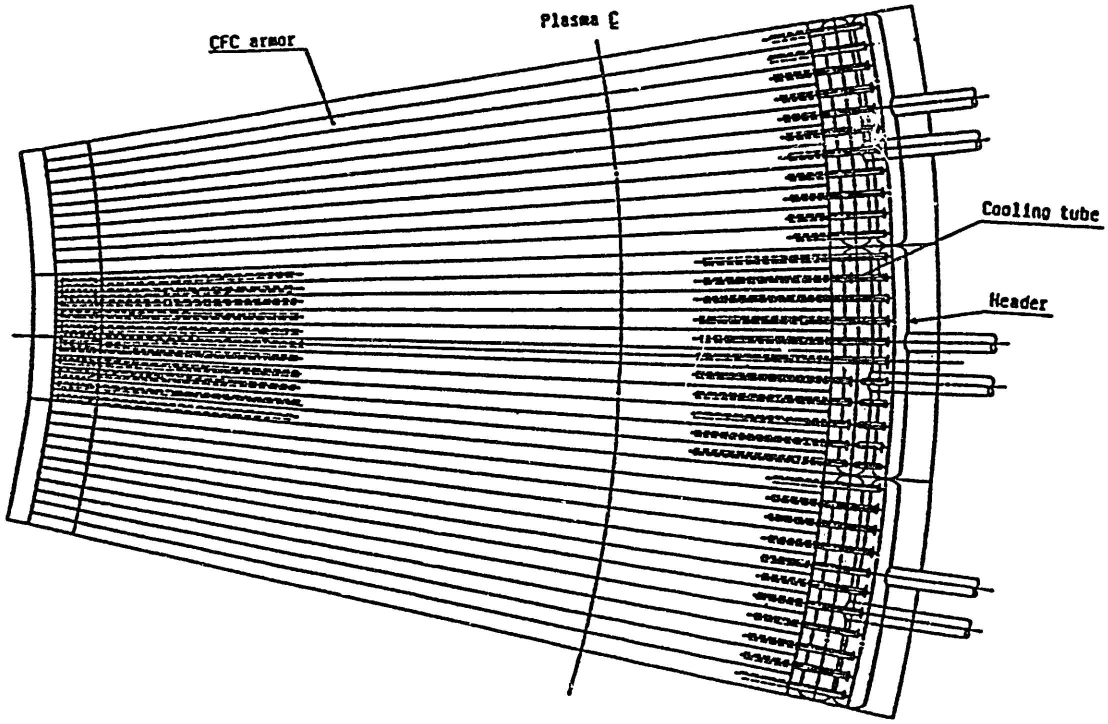

Plan View of Lower Divertor Module
(Physics Phase)

Fig. 3

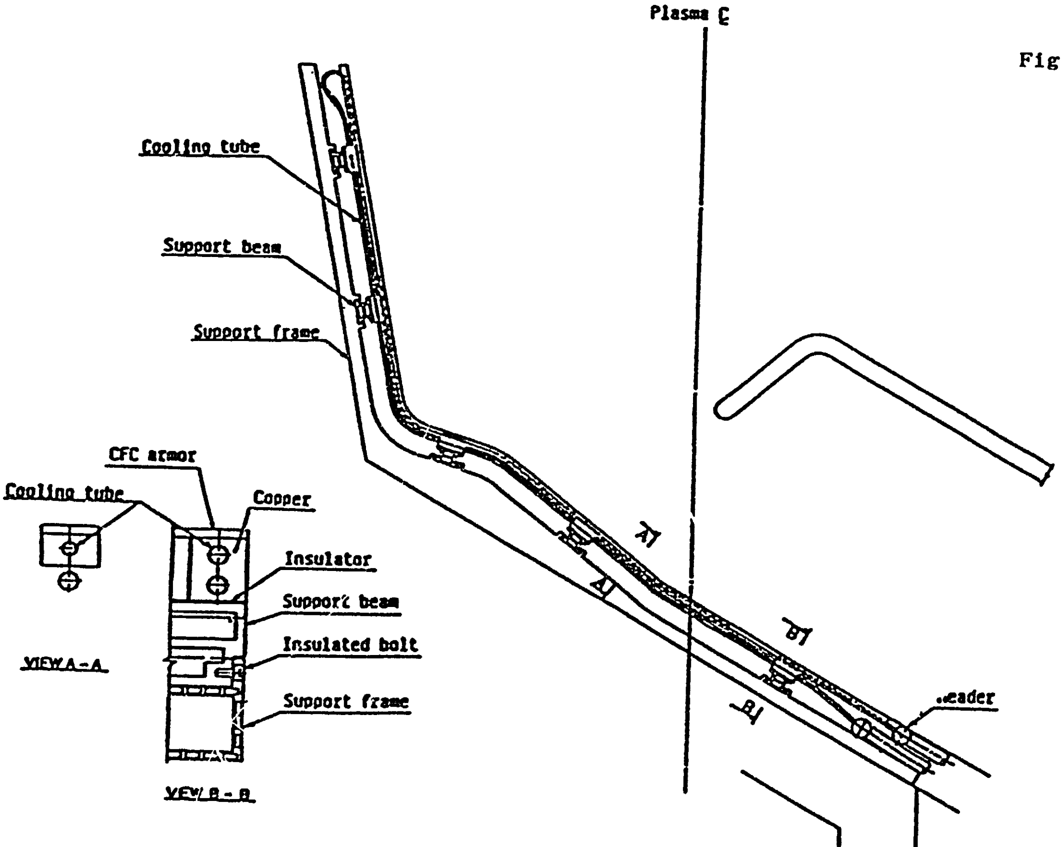

Cross-sectional View of Lower Divertor Module
(Physics Phase)

Ploblems in First Walls of Near Term Devices

Nobuaki Noda
Plasma Physics Laboratory, Kyoto University, Uji 611, Japan*

December 16, 1988

* present address : Institute of Plasma Physics, Nagoya University,
Nagoya 464-01, Japan

– from Experiences on Carbon-Wall Experiments in Heliotron E –

One of the near-term ploblems is to give a first-wall condition which enables a good core parameters in D-T/non D-T plasmas. Carbon is only a candidate material as the first wall at the moment because no other materials have not been proved to provide a metal-free plasmas in present devices. However, there is still two problems in carbon walls to assure a good performance of the core plasmas, namely, (1) to achieve low hydrogen-recycling, (2) to reduce low Z impurities (O,C). In some experiments, high wall temperature is helpful to reduce recycling and oxygen[1]. However, it is expensive and not technologically easy to raise a huge vessel up to temperature as high as 300-400 °C. Carbon-wall experiments in Heliotron E have been reviewed to looking for possibilities of low temerature for carbon wall design of the next generation machines.

In Heliotron E, almost all of the divertor region was covered by graphite tiles to block the ion flow to the metallic wall. In this case, we met a problem on hydrogen recycling control. Helium glow discharge was utilized at room temperature to reduce the recycling. Figure 1 shows hydrogen desorbed by ECH/helium discharges as a function of shot numbers[2]. Partial pressure P_2 of H_2 was measured by quadrupole mass analyzer. Amount of the desorbed hydrogen was obtained from the measured pressure multiplied by pumping speed S_{pump} and integrated with time. As is seen in Fig.1, hydrogen desorption was reduced by an order of magnitude after He glow discharge of 1.5 hours. Increasing rate of density after breakdown was also decreased by He glow discharge. After repetitive use of He glow discharge, density decay was seen even during NBI heating, which meant that the recycling rate was less than 1.

After He glow discharges, oxygen-radiation intensity was also small. After NBI discharges and increase in gas puffing, the intensity of oxygen radiation increased shot by shot. This suggests the successive processes as follows;

1. charge-exchange neutral flux increases by NBI and gas puffing and oxygen is released from metalic surfaces of the wall,
2. oxygen is ionized and transferred to carbon surfaces of the divertor plates,
3. these oxygen atoms contaminates the plasmas from initial phases of the next discharge.

After the contamination by oxygen, He-glow discharge was applied again, which reduced the oxygen level to the original level.

Thus both hydrogen recycling and oxygen contamination were controled by He-glow discharges at room temperature of the carbon wall in Heliotron E. These results suggest a possibility of designing carbon walls at room temperature in future devices. However, quantitative investigation is still necessary to make sure whether the absolute recycling rate or oxygen concentration is sufficiently low for these future experiments.

References

[1] J. Winter, J. Nucl. Mater. 145-147 (1987) 131

[2] N. Noda *et al.*, to be published in J. Nucl. Mater. 163-165 (Proc. 8th PSI Conf. Jülich, 1988)

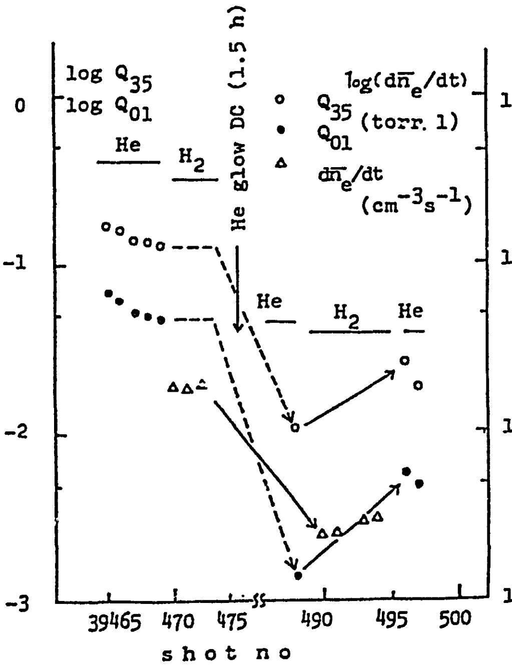

Fig. 1 Hydrogen desorbed by helium/ECH discharges
$Q_{01} = S_{pump} \int_0^1 P_2 dt$
$Q_{35} = S_{pump} \int_0^{35} P_2 dt$
$d\bar{n}_e/dt$: density increasing rate at the start of discharge, see ref[2].
Bars with "He", "H_2" indicate puffed gases.

Graphite as Plasma Facing Material

Osaka Univ. Tanabe, T.

Graphite materials are widely used as plasma facing components for major fusion devices such as TFTR, JET and JT-60, because of their low Z number and good high temperature characteristics. For further application of graphite as plasma facing material(PFM) in near and middle term machines, a comprehensive evaluation has to be undertaken.

According to research and development senario for graphite as PFM shown in fig.1, reviews and discussions on properties and data bases of graphite have been made concerning 8 items and summarized as follows.

1. Outgassing

Outgassing of annealed samples is not serious. Once bake out up to 1700K was performed, most of gas uptake during exposure to air is easily desorbed by heating up to 800K.

2. Conditioning

Because of large capacity for hydrogen occulusion in graphite, conditioning before plasma discharge is one of the most important issue. Although He dischrage cleaning is found to help much to reduce the hydrogen uptake, detailed mechanism of hydrogen release by He discharge is not clear.

3. Sputtering

Most of sputtering data (physical and chemical) show fair agreement in their dependences on temperature, incident energy and flux. Main concern with sputtering is how to reduce the yield and to clarify an effect of impurities.

4, Reflection

Because of difficulty of production of low energy H^o and H^+ source little data is available for low enrgy reflection coefficient (below 100eV). There is also some discrepancy in theories to estimate the reflection coefficent in low energy region.

5. Radiation induced sublimation

Radiation induced sublimation, which, above 1000K, exceeds the chemical sputtering , becomes very important. Although it seems to have collisional origine similar to physical sputtering, more data is needed to confirm this.

6. Tritium retention and recycling

Below 500K, where hydrogen does not seem to diffuse in graphite, saturated level of hydrogen in graphite exposed to plasma is as high as 0.5 in H/C ratio. Such fuge capacity of hydrogen occulusion in graphite makes density controll of plasma very difficult and sofisticated conditioning technique has to be carried out to remove hydrogen in graphite and to get well confined plasma. Above 500K hydrogen behavior in graphite becomes very complex and no adequate model has established yet. Esspecially "dynamic retention", that is, the difference of hydrogen retention with and without plasma exposure, is now on the hot discussion.

7. Thermomechanical properties

Although graphite withstands the heat load in the present machine, an expected heat load in ITER is out of the performance of currently used graphite materials. Though recent development of C/C composite is encouraging, long pulse or steady state operation enforces an employment of the active cooling and brazing to metal substrate is inevitable.

8. Radiation effects

Radiation effect of 14MeV neutron on graphite is the most important problem in DT burning machine. Thermal conductivity, for instance, goes down to 1/3 of the original value with neutron irradiation of several dpa. Not a small data base is established for utilization of graphite material in high temperature gas cooled reactor. However, recent research on radiation damage of metals given by 14MeV neutron clearly shows that radation damage produced by 14MeV neutrons is different from that by fast neutron. In addition, little data is available above 1000^{o}C over which the divertor plate might be operated.

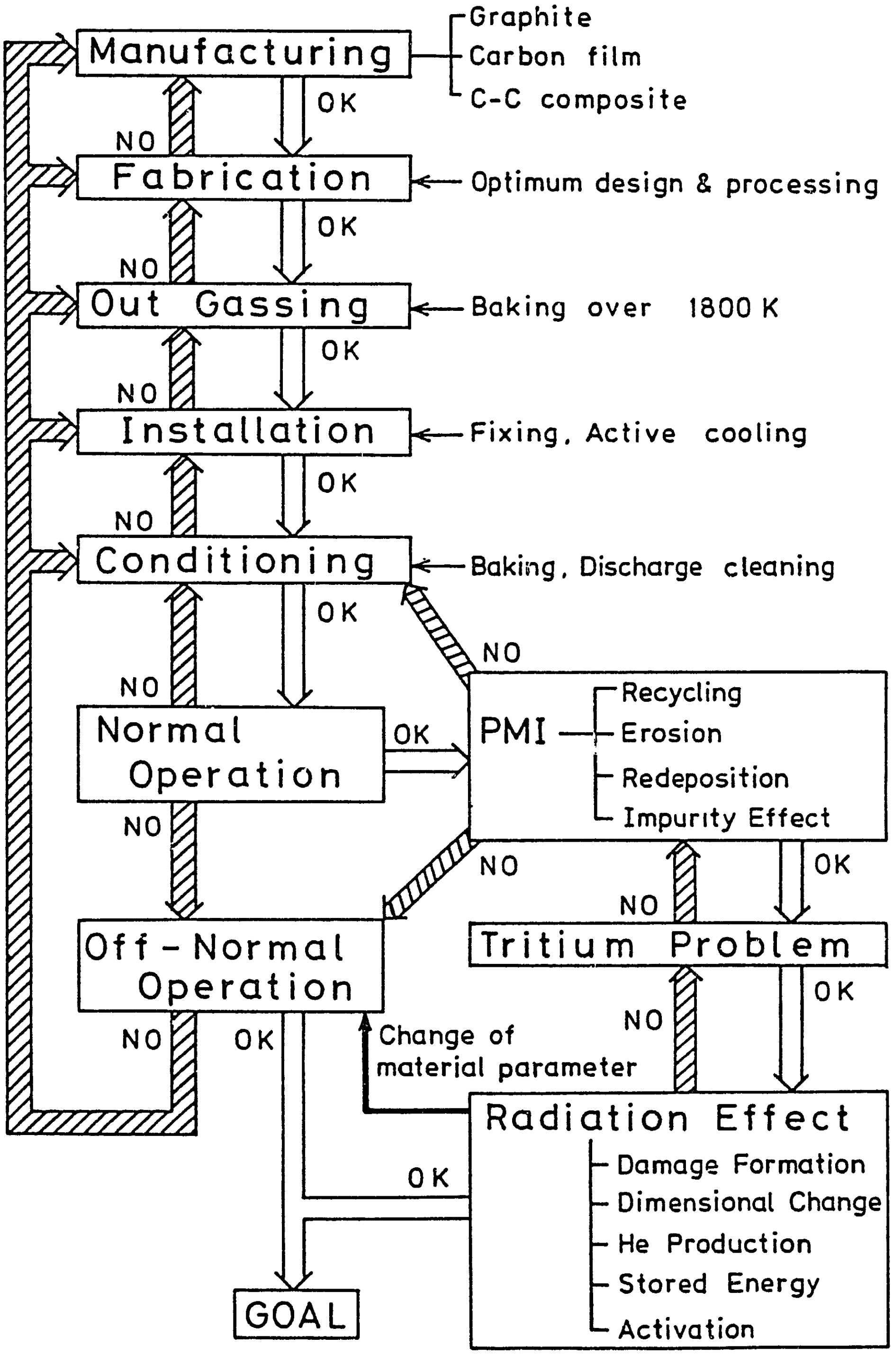

Fig. 1. Research and development scenario for graphite as plasma facing material.

A. Miyahara, T. Tanabe Journal of Nuclear Materials 155–157 (1988) 49–57

DEUTERIUM SOLUBILITY AND DIFFUSIVITY IN GRAPHITE

Hisao ATSUMI
Department of Nuclear Reactor Engineering, Faculty of Science and Technology,
Kinki University, Kowakae 3-4-1, Higashi-Osaka, Osaka 577, Japan

Masanobu MIYAKE
Department of Nuclear Engineering, Faculty of Engineering, Osaka University,
Yamadaoka 2-1, Suita, Osaka 565, Japan

1. Introduction

Graphite is one of the suitable candidate materials for the first walls (limiters, armors) in a fusion reactor. However, graphite will interact with hydrogen isotopes at high temperatures, and it may cause increase in the tritium inventory and produce hydrocarbon species. When using as graphite for the first wall, it is important to obtain broad information on hydrogen recycling and an inventory on graphite. From the viewpoint, this study has been performed with the purpose described as follows.

(1) Data needs on hydrogen absorption and dissolution in graphite
  - Solubility of hydrogen in graphite
  - Chemical form of hydrogen in graphite
  - Influence of the degree of graphitization

(2) Data needs on thermal desorption of hydrogen from graphite
  - Desorption mechanisms (rate-determining step of desorption)
  - Kinetic parameters of thermal desorption
  - Chemical form of hydrogen migrating in graphite

2. Experimental

The samples used in the present study were high density isotropic graphite sheets composed of fine grains (ISOGRAPH-88, Toyo Tanso Co.Ltd.). These graphite samples were degassed at 1100 ℃ for two hours in a vacuum before absorption and desorption experiments.

(1) Deuterium solubility measurement

In the deuterium absorption experiments, the graphite samples in the deuterium atmosphere were heated at the desired temperature of 850-1050 ℃ in a closed constant volume system, and the change in deuterium pressure due to absorption was measured with a Baratron Manometer until the equilibrium pressure was established at each temperature.

(2) Desorption experiment

The treatment procedure for graphite samples used in the thermal desorption experiments is shown in Fig.1. The graphite samples occluding deuterium were prepared by deuterium exposure at a given temperature, T, within 200-900 ℃ under a pressure of 5-95 kPa for 0.1-20 h. After holding these graphite samples for the desired time in deuterium gas atmosphere, they were quenched to room temperature. Thermal desorption measurements of deuterium were made at a constant heating rate of 10 ℃/min in a vacuum below 10^{-5} Pa. In order to determine the desorption mechanisms, step heating tests (reaching a desired temperature within 1 min) at 300-900 ℃ were also performed. Released species were analyzed with a quadrupole mass spectrometer.

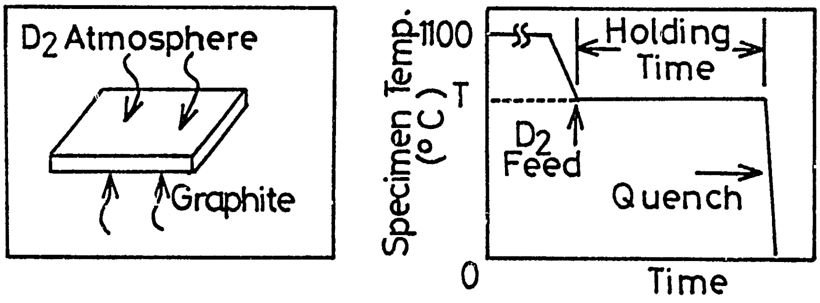

Fig.1 Experimental procedure of D_2 gas exposure.

3. Results and Discussion

3.1 Deuterium solubility in graphite

The solubilty of deuterium in graphite was measured, and it might increase proportionally to the square root of the deuterium gas pressure. From the present data, the solubility, S(STPcm^3/g), can be expressed by the equation:

$$S = 1.9\times10^{-4}\ P^{1/2}(\mathrm{Pa})\ \times\ \exp[4.5(\mathrm{kcal/mol})/RT]\quad (850\text{-}1050℃,\ 2.5\text{-}13\ \mathrm{kPa}).\quad (1)$$

The extrapolated values of the solubility at one atmospheric pressure are shown in Fig.2 with the reported values obtained by Causey et al.[1] for laminar pyrolytic carbon. Both the heat of solution and the solubility are quite low compared with that reported for the temperature range of 1100-1500℃.

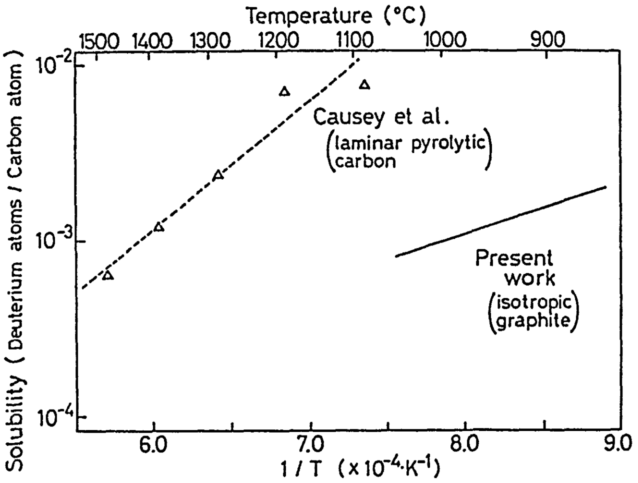

Fig.2 Deuterium solubility at one atmosphere in isotropic graphite (ISOGRAPH-88) and laminar pyrolytic carbon [1] as a function of temperature.

3.2 Thermal desorption of deuterium from graphite

Fig.3 gives deuterium desorption curves`for the graphite exposed at various temperatures for 5 hours under the deuterium gas pressure of 60 kPa. Both shape and peak temperature (apparently seen in Fig.3) considerably change with the exposure temperature. The peak temperature increases with exposure temperature. In Fig.3(b), the total amounts of deuterium from graphite are plotted as a function of exposure temperature. The total amount of released deuterium increases with the exposure temperature up to 700 ℃ and then tends to decrease above this temperature. This behavior can be explained by the deuterium diffusion process into the graphite filler grains as mentioned below. Since it is necessary to have much longer saturation time at lower exposure temperatures, the amount of deuterium uptake during the same exposure time will decrease with decreasing temperature. From eq.(1), the solubility of D_2 in graphite will decrease with increasing temperature. Then, the amount of deuterium uptake should decrease with increasing temperature above 700 ℃ after which the deuterium is almost saturated in the graphite filler grains.

Fig.4 gives deuterium desorption rate in logarithmic scale, which is redrawn of Fig.3(a), as a function of desorption temperature. The deuterium desorption curve on graphite exposed to D_2 gas at 700 ℃ appears to consist of three peaks. Namely,this thermal desorption curve can be explained by the overlap of peaks I , II and III with each maximum at approximately 140 ℃, 480 ℃

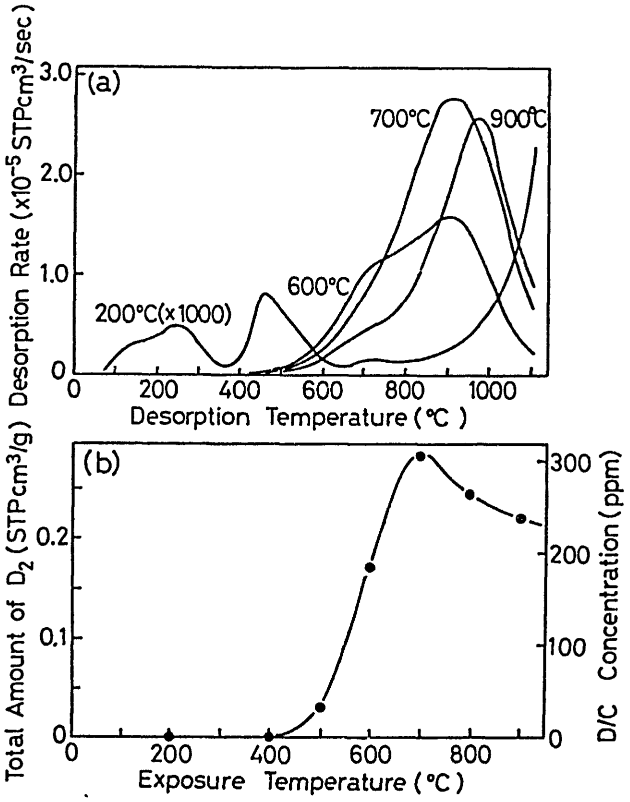

Fig.3 Thermal desorption of D_2 from graphite exposed to D_2at various temperatures (60 kPa, 5 h).

(a) thermal desorption curves for various temperatures

(b) total amount of D_2 released from graphite

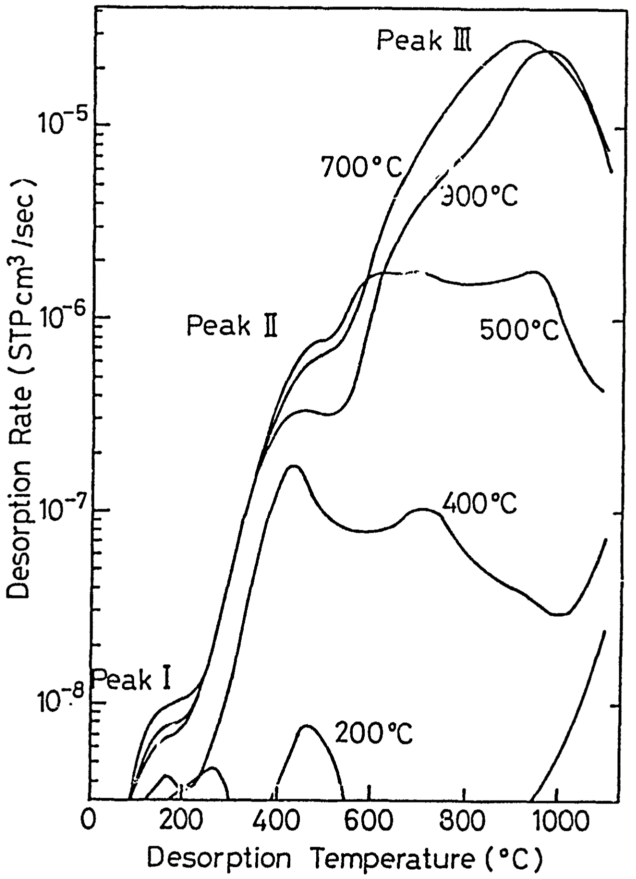

Fig.4 Thermal desorption curves of deuterium for graphite exposed to D_2 at various temperatures (60 kPa, 5 h).

and 930 ℃, respectively.

The change in the amount of deuterium with the exposure pressure has been discussed separately on peaks Ⅱ and Ⅲ. In Figs.5(a) and (b), the amount of released deuterium is plotted for the graphite samples exposed to deuterium gas of various pressures at 700 ℃ for 5 h. From these figures, the deuterium amount for peak Ⅱ appears to be proportional to the deuterium gas pressure during exposure, and that for peak Ⅲ appears to be proportional to the square root of the deuterium gas pressure. In peak Ⅱ, therefore, deuterium in the graphite probably exists as deuterium molecules. On the other hand, the deuterium corresponding to peak Ⅲ probably exists in the form of deuterium atoms.

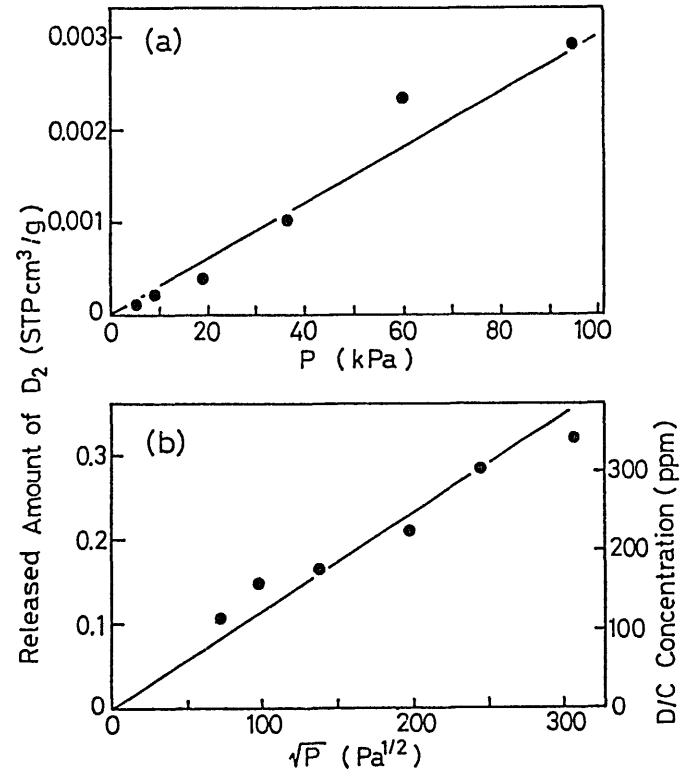

Fig.5 Influence of D_2 gas pressure on the amount of deuterium released from graphite (700 ℃, 5 h).
(a): peak Ⅱ , (b): peak Ⅲ

3.3 Desorption mechanism from graphite

The scheme of the simplified desorption processes of gas atoms is shown in Fig.6. The principal processes of desorption behavior are (a) detrapping (or dissociation), (b) diffusion and (c) recombination at surfaces, and the desorption of gas atoms is controlled by these processes individually or cooperatively. The desorption mechanism and the kinetic parameters can be analyzed for temperature-programmed desorption curves. Heating patterns for the temperature-programmed desorption tests are usually adopted as (1) linear ramp heating ($T=T_0+\beta t$), (2) hyperbolic heating ($1/T = 1/T_0-\alpha t$) and (3) step

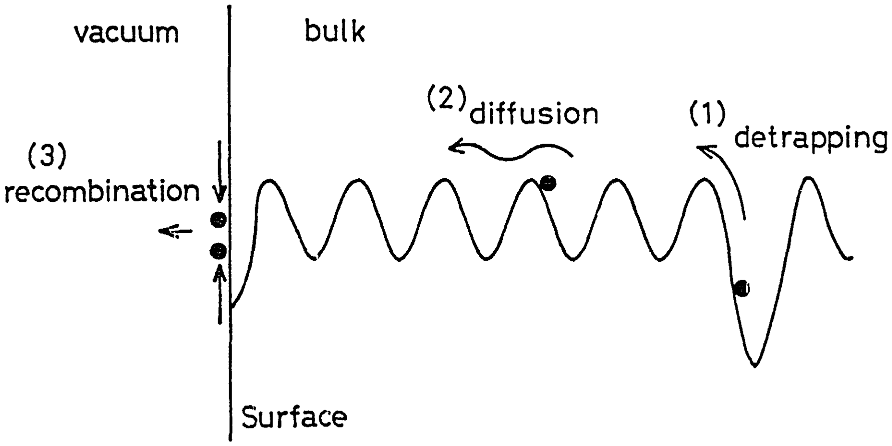

Fig.6 Simplified mechanisms of gas desorption behavior.

heating (isothermal desorption, $T = T_1$ $(t>0)$). In these heating patterns, the desorption curves for step heating tests can be analyzed most easily since the parameters which depend on temperature are constant during desorption. Typical step desorption curves for various mechanisms are shown in Fig.7. Not only the kinetic parameters but also the information to define the release mechanisms can be received from the change of desorption rates for each temperature.

By the discussions on the rate-determining step of desorption [2,3], thermal desorption of deuterium for peaks Ⅱ and Ⅲ may controlled by pore and bulk diffusion, respectively. Theoretically, the desorption rate, R(STPcm^3/sec), at each constant temperature can be given by the following equations [4]:

for the pore diffusion through a graphite sheet (peak Ⅱ),

$$R_{\mathrm{II}}(t) = 4.06 \times 10^{-4}\left[-\frac{d}{dt}\left(\frac{8}{\pi^2}\sum_{n=1}^{\infty}\frac{1}{(2n-1)^2}\exp\left(-\frac{(2n-1)^2\pi^2}{l^2}D_{\mathrm{II}}t\right)\right)\right] , \quad (2)$$

for the bulk diffusion within graphite filler grains (peak Ⅲ),

$$R_{\mathrm{III}}(t) = 4.92 \times 10^{-2}\left[-\frac{d}{dt}\left(\frac{6}{\pi^2}\sum_{g=1}^{17}\left(f_g\sum_{n=1}^{\infty}\frac{1}{n^2}\exp\left(-\frac{n^2\pi^2}{r_g^2}D_{\mathrm{III}}t\right)\right)\right)\right] , \quad (3)$$

where l (cm) is the thickness of the graphite sheet, D(cm^2/sec) is the diffusion coefficient of deuterium in graphite, t(sec) is the desorption time, f_g is the volumetric fraction of grains with each radius, and r_g is the radius of a graphite filler grain. The values of 4.06×10^{-4} and 4.92×10^{-2} were derived

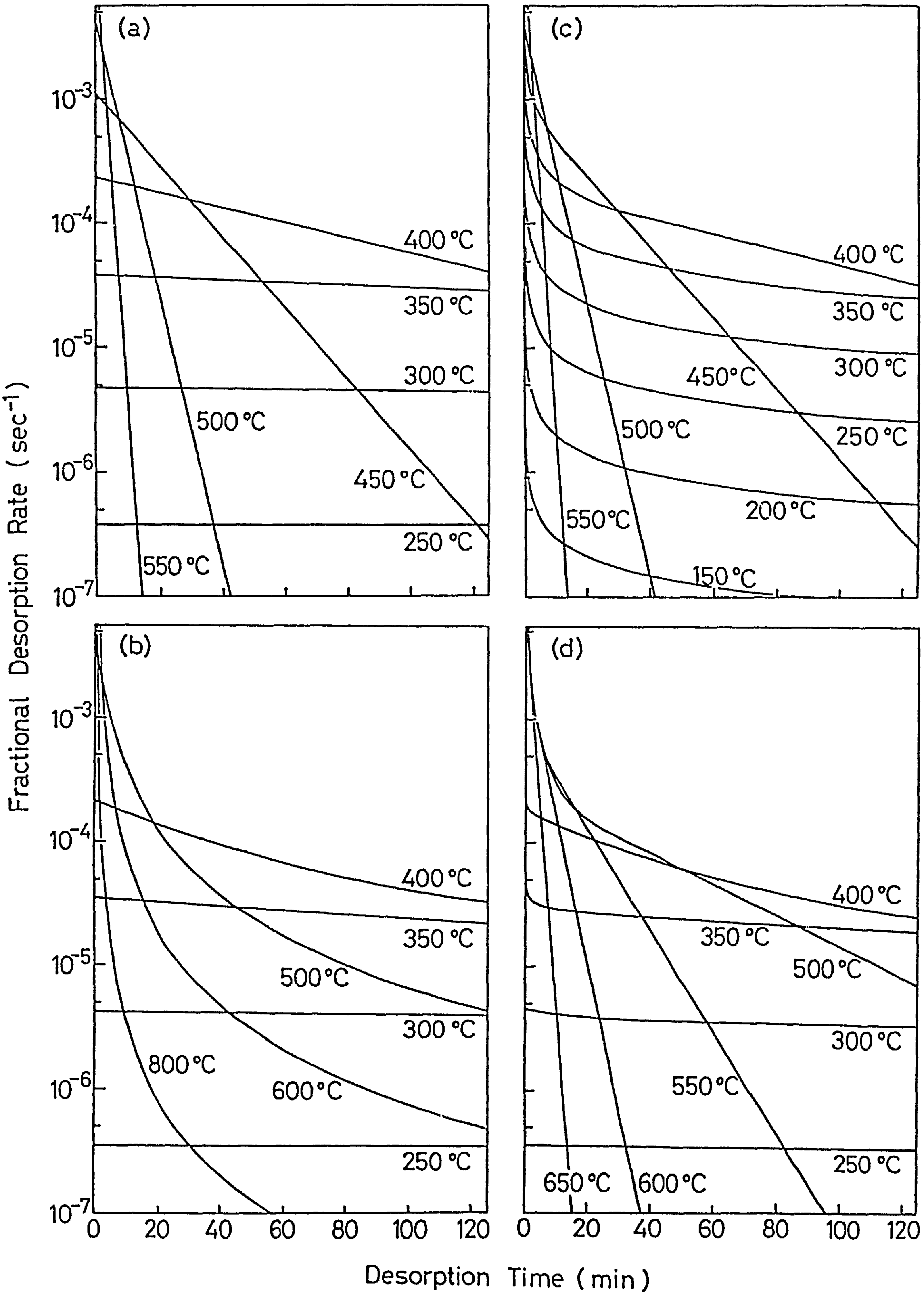

Fig.7 Typical step desorption curves controlled by various mechanisms.
(a) detrapping (b) recombination
(c) diffusion (initial distribution of gas atoms is uniform , a =1 mm)
(d) diffusion (with initial distribution as 20keV He$^+$ ion implantation)

from the deuterium amount given in Fig.5 and the mass of the sample. The theoretical desorption curves have been calculated by eqs.(2) and (3). The results obtained by fitting of theoretical curves to the experimental data are shown in Fig.8. The diffusion coefficients were also determined by fitting. As a result, the pore diffusion coefficient, D_{II}(cm^2/sec), and the bulk diffusion coefficient, D_{III}(cm^2/sec) are expressed by

$$D_{\text{II}} = 1800 \times \exp[-29(\text{kcal/mol})/RT] \quad (300\text{-}500\ ^\circ\text{C}), \qquad (4)$$

$$D_{\text{III}} = 1.69 \times \exp[-60(\text{kcal/mol})/RT] \quad (500\text{-}900\ ^\circ\text{C}). \qquad (5)$$

The thermal desorption curves of deuterium at a heating rate of 10 ℃/min were calculated from eqs.(2), (3), (4) and (5) with temperature extrapolation. The result is given in Fig.9. As shown here, the experimental and theoretical desorption curves correspond well.

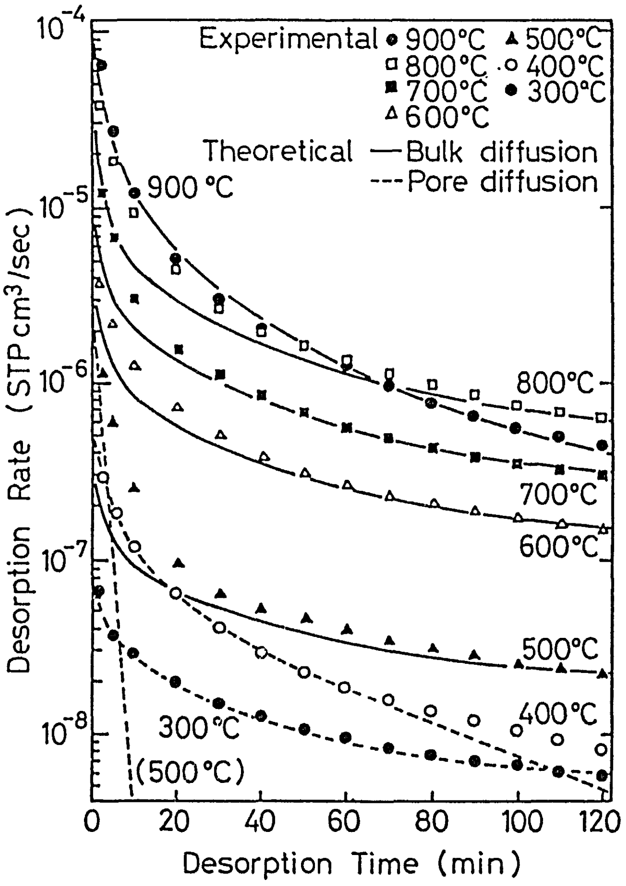

Fig.8 Desorption curves obtained by fitting the theoretical curves to the experimental data.

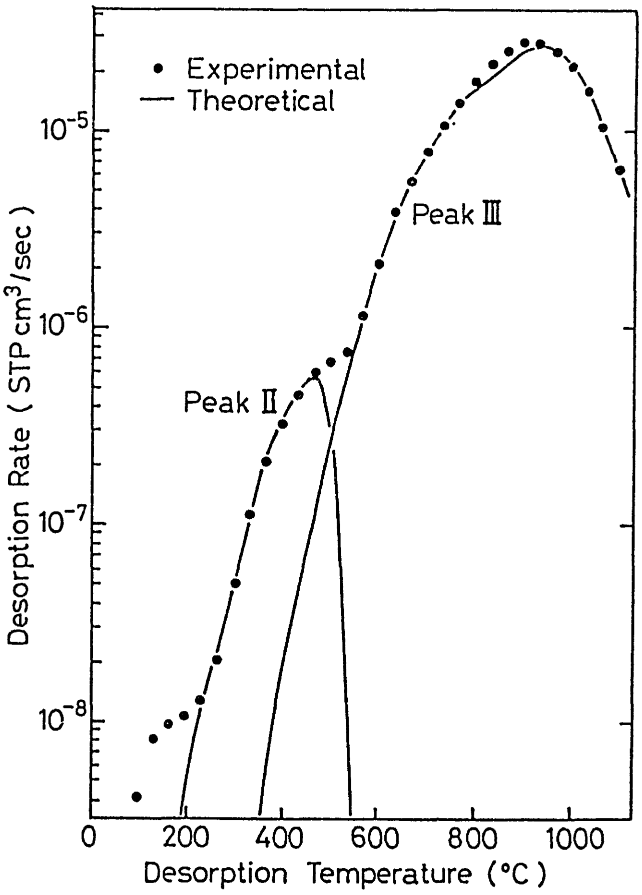

Fig.9 Thermal desorption curve derived from diffusion analysis.

The reported values of bulk diffusion coefficient of hydrogen isotopes in graphite are given in Fig.10. Diffusion coefficients of deuterium obtained in the present work are much larger than those for tritium reported by several authors. This discrepancy may be attributed to the following reasons.

(1) neutron irradiation effect

The reported data were determined almost for tritium diffusion mainly produced by ^{3}He(n,p)^{3}H or ^{6}Li(n,α)^{3}H reaction. Namely, if the neutron irradiation produces many defects as the diffusion barrier, it will cause a low diffusion coefficient and a high activation energy.

(2) isotope effect

Diffusion of deuterium in graphite should be faster than the tritium diffusion due to the isotope effects.

(3) presence of traps with high binding energies (concentration should be low)

The concentration of tritium in graphite would be much lower compared with the deuterium amount studied here. Then the diffusion coefficient of tritium in graphite will be rather small, if a certain amount of traps with high binding energies exists in a graphite sample. It is suggestive and consistent that the retention of deuterium in POCO AXF-5Q graphite did not show the pressure dependence below

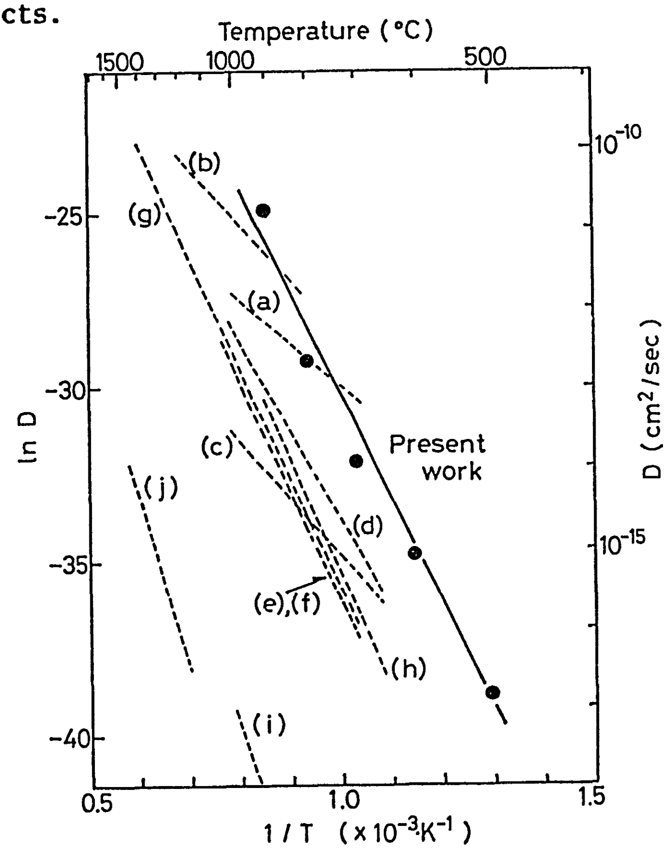

Fig.10 Diffusion coefficients of tritium in various types of graphite as a function of temperature.

(a),(e),(f): Saeki [5], (b),(j): Causey et al.[1]
(c),(d),(h): Saeki [6], (g) : Röhrig et al.[7]
(i) : Malka et al.[8]

66.0 Pa [9]. This pressure range is much lower than that for the present study and saturated concentration of 16 ppm is also significantly low.

By using the diffusion data and eq.(1), deuterium uptaking behavior for various exposure times was estimated as a function of exposure temperature. As shown in Fig.11, a shorter exposure time causes the maximum temperature of deuterium retention to shift toward higher temperature. From this figure, the maximum temperature of deuterium retention with a 5-h exposure time should be approximately 850 ℃, whereas the experimental results show the maximum temperature to be 700 ℃ (Fig.3).

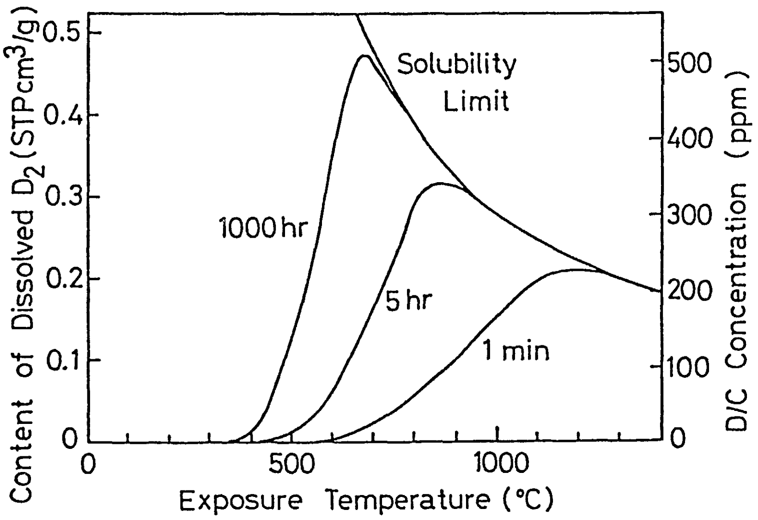

Fig.11 Predicted deuterium retention curves for graphite exposed at various temperatures under D_2 gas pressure of 60 kPa.

4. Future work

Further study will be required for the following items:

(1) Solubility measurements on hydrogen in various types of graphite
  - effects of graphitization
  - effects of grain size, etc.

(2) Migration mechanisms of hydrogen in graphite
  - diffusion path (microscopic)
  - chemical interactions

(3) Chemical state of hydrogen trapping sites
  - trap binding energy

(4) Neutron irradiation effects
   - hydrogen solubility in graphite
   - hydrogen diffusivity in graphite

(5) Simulation of hydrogen recycling on graphite under various conditions

5. Conclusions

The absorption and desorption of deuterium on graphite were studied on isotropic graphite exposed to a deuterium gas atmosphere at elevated temperatures. The results obtained in the present study are summarized as follows:

(1) The solubility of deuterium obeys the Sievert's low which is:
$S(\mathrm{STPcm^3/g}) = 1.9 \times 10^{-4}\ P^{1/2}(\mathrm{Pa})\ \exp[4.5(\mathrm{kcal/mol})/RT]$
(850-1050 ℃, 2.5-13 kPa).

(2) Thermal desorption of deuterium will be controlled by the pore diffusion through the graphite sheet (lower temperatures: ~450℃) and the bulk diffusion within the graphite filler grains (higher temperatures: ~920℃).

(3) Diffusion coefficients of deuterium in graphite can be expressed by the equations:
pore diffusion : $D_{\mathrm{II}}(\mathrm{cm^2/sec}) = 1800\ \exp[-29(\mathrm{kcal/mol})/RT]$ (300-500 ℃),
bulk diffusion : $D_{\mathrm{III}}(\mathrm{cm^2/sec}) = 1.69\ \exp[-60(\mathrm{kcal/mol})/RT]$ (500-900 ℃).

References

[1] R.A.Causey, T.S.Elleman and K.Verghese, Carbon 17 (1979) 323.
[2] H.Atsumi, S.Tokura and M.Miyake, Technol.Rep.Osaka Univ. 37 (1987) 255.
[3] H.Atsumi, S.Tokura and M.Miyake, J.Nucl.Mater. 155-157 (1988) 241.

[4] J.Crank, "The Mathematics of Diffusion, 2nd Edition" (Oxford University Press, Oxford, 1975) p.48,91.

[5] M.Saeki, J.Nucl.Mater. 131 (1985) 32.

[6] M.Saeki, Int.J.Appl.Radiat.Isot. 34 (1983) 739.

[7] H.D.Röhrig, P.G.Fischer and R.Hecker, J.Am.Ceram.Soc. 59 (1976) 316.

[8] V.Malka, H.D.Röhrig and R.Hecker, in: Proc. Tritium Technol. in Fusion, Fission and Isotopic Appl., A.N.S. National Topical Meetings, Ohio, 1980, p.102.

[9] R.A.Causey, M.I.Baskes and K.L.Wilson, J.Vac.Sci.Technol.A 4 (1986) 1189.

A Basic Experiment and Modelling on the Interaction of Hydrogen Plasma with Carbon Films

Hideo Sugai, Shinji Yoshida and Hirotaka Toyoda
Department of Electrical Engineering, Nagoya University
Furo-cho, Chikusa-ku, Nagoya 464-01, Japan

Abstract

H_2 and DH release was investigated in a pulsed deuterium discharge over a carbon-thin-film deposited wall. A large quantity of hydrogen was desorbed from hydrogenated amorphous carbon (a-C:H) deposited by a *hydrogen*-admixed methane discharge. On the other hand, a strong pumping effect was observed in the case of films deposited by a *helium*-admixed discharge. The wall-pumping effect was attributed to the presence of interstitial vacancies rather than dangling bonds in the films. A dynamic model of hydrogen release and retention for a-C:H layers is proposed. Corresponding calculations yield satisfactory agreement with observations when utilizing appropriate rate constants for trapping and detrapping.

Recently, the *in situ* deposition of a-C:H films on the entire inner surface of nuclear fusion devices has been developed as a new method of wall conditioning (carbonization). In a fusion device, however, the first wall is exposed to a high flux of energetic hydrogen ions. As a result, a large quantity of hydrogen is released from a-C:H films, yielding a serious problem of hydrogen recycling. The dynamic behavior of hydrogen in a-C:H layer has not been well understood with respect to hydrogen implantation, trapping, diffusion, recombination to molecules, and release of the molecules. In this paper we present experimental data supporting molecule formation by hydrogen abstraction in a-C:H films. The importance of interstitial trapping and detrapping process in the modeling of ion-induced release and retention of hydrogens will also be shown.

An experiment on the interaction of a hydrogen plasma with a-C:H films was performed in a stainless steel toroidal vessel in order to simulate a nuclear fusion device in a toroidal geometry. The apparatus is equipped with a turbomolecular pump system and a differentially pumped quadrupole mass analyzer (QMA). An a-C:H film of about 500 Å thickness was deposited on the whole inner wall area using a dc glow discharge (voltage V_d= 350 V, current I_d= 1.0 A) in a gas mixture of 10% CH_4 in H_2 or He at 5 mTorr total pressure. After the film was deposited, D_2 gas was introduced at the flow rate Q= 25 ml/min and a pulsed glow discharge (V_d=300 V, I_d= 0.1-1.5 A, 70 sec pulse width) was turned on in order to investigate the hydrogen recycling properties of a-C:H films. The energy of ions impinging the films was about 300 eV.

First, the a-C:H films formed by the *hydrogen*-admixed

(CH_4/H_2) discharge were exposed to a pulsed D_2 discharge. The solid lines in Fig. 1(a) indicate the time evolutions of the DH, H_2, and total pressures after turn-on of the 0.2A-70sec discharge pulse. A similar experiment was performed on a-C:H films formed by the *helium*-admixed (CH_4/He) discharge. The results obtained are shown in Fig. 1(b), where a drastic decrease in the total pressure was observed with the 0.2A-70sec discharge pulse.

The deuterium ion irradiation gives rise to free hydrogen atoms detrapped from the interstitial or bonded sites, in proportion to the discharge current I_d. There are two possible mechanisms of hydrogen molecule formation: (a) a recombination of two free hydrogen atoms and (b) a hydrogen abstraction, where a detrapped free atom or an incident D-atom recombines with a bonded hydrogen or with an interstitially trapped hydrogen. However, the former takes place in proportion to I_d^2 and the latter in proportion to I_d. The observed linear dependence of H_2 and DH desorptions supports molecule formation by the hydrogen abstraction process.

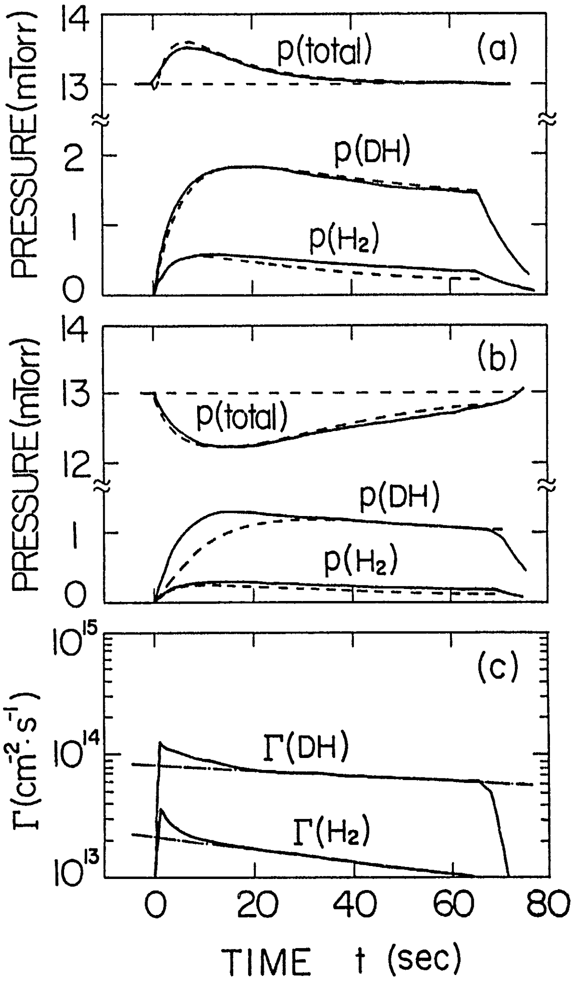

Fig. 1. Time evolution of the H_2, D_2, and total pressures during a D_2 pulsed discharge (a) after *hydrogen*-admixed carbonization and (b) after *helium*-admixed carbonization, together with (c) the DH and H_2 desorption flux from a-C:H films deposited by *helium*-admixed carbonization. Solid lines indicate the measured values and dashed lines the numerical solutions.

In order to model the hydrogen behavior, we define six rate constants of reactions : α and β for chemical abstraction processes, σ and μ for physical detrapping, and γ and ρ for trapping, at carbon-bonded and interstitial sites, respectively. The model is based on bulk molecule formation by hydrogen abstraction followed by rapid molecular diffusion through the a-C:H network, neglecting the depth profile and the diffusion of free hydrogen atoms. Thus, we have eight rate equations governing the densities of the bonded, interstitial, and free H- and D-atoms, together with the densities of interstitial vacancies and dangling bonds. Utilizing this set of equations, an initial value problem for the pulsed deuterium ion incidence flux was solved.

A satisfactory agreement between the experimental data and the model was obtained for the best fit parameters of rate constants, i.e., chemical abstraction rate $\beta=$ $(2.5\text{-}2.8)\times10^{-16}$ cm^2s^{-1}, physical detrapping rate $\mu=$ $(1.3\text{-}2.2)\times10^{-16}cm^2s^{-1}$, interstitial trapping rate $\rho=$ $(3\text{-}40)\times10^{-16}$ cm^2s^{-1}, and with the trapping rate to dangling bonds is rather flexible ($\gamma\simeq$ 15×10^{-16} cm^2s^{-1}). The numerical solutions are indicated by the dashed lines in Fig.1(a) and 1(b). The total H content of 2.4×10^{16} cm^{-2}

for *hydrogen*-admixed carbonization corresponds to the H-atom content within the deuterium-ion-implantation range of ~70 Å estimated in the TRIM code simulation. The films formed by a *helium*-admixed discharge contain a large number of interstitial vacancies, which leads to the pumping effect. The vacancies are considered to arise from the helium-ion induced detrapping of hydrogen during the carbonization process.

EFFECTS OF ENERGETIC IMPURITIES ON THE DIFFUSION OF NITROGEN IN FIRST WALL CANDIDATES

M. Nunogaki, Y. Kuratomi, H.Suezawa and K. Miyazaki

Department of Nuclear Engineering, Osaka University,
2-1 Yamadaoka, Suita, Osaka 565, Japan

The surfaces of first walls are contaminated with various kinds of impurities in relation to walls. Such impurities in the surface layers of walls may give an influence on the adsorption and diffusion of some atoms such as H, N, O, C etc in the wall materials.

We investigated the effects of Ti, N_2, Ar and Mo ions pre-implanted to 316SS and pure aluminium on the diffusion of nitrogen by applying the subsequent surface nitridation[1] to them. The effects were examined by measuring the hardness and thickness of the nitrogen compound layers formed in the implanted surfaces.

The experimental conditions for 316SS and Al were tabulated in Fig.1 and 3, respectively. The variations in the hardness and thickness of nitrogen compound layers were shown in Fig.2 and 4 for 316SS and Al, respectively. The relative change in hardness was plotted as the ratio of the hardness of nitrogen compound to that of the annealed raw material.

It was observed in Fig.2 that the impurity implantation had little effect on the hardness but the thickness increased remarkably from 25um in the un-implanted specimen to about 40um with Ti and N_2 ions implantation.

It was interesting to find in Fig.4 that Mo, Ti and N_2 ions implantation made nitridation of pure Al possible[2]. The kind of ion species and the ion fluence changed the hardness and thickness. The average ratio of the maximum hardness to un-implanted Al was about 2.8 constant. The thickness reached about 1mm or more in maximum with a Mo ion fluence of 2E16 ions/cm^2.

As the results, it was revealed that intermetallic compounds, interstitials and defects created by the bombardment of impurites seemed to enhance the adsorption and diffusion of nitrogen in 316SS and aluminum.

<References>
1) M. Nunogaki et al. Applied Surface Science.33/34(1988)1135.
2) M. Nunogaki et al. in: Proc. Intern. Symp. on Appl. of Ion Beams Produced by Small Accelerators '87, China.

Fig.1

Sample preparation	Ion implantation conditions		Nitridation conditions	
316SS cleaned and annealed at 500°C for 1hr	residual gas pressure	6×10^{-4} Torr	total gas pressure	6×10^{-4} Torr
	temperature	room temperature	$N_2 : H_2$	5 : 2
	energy	25keV	bias voltage	1.0kV
	ion species	fluence (ions/cm^2)	temperature	450°C
	N_2	3×10^{19}	time	3hrs
	Ti	1×10^{16} ~ 1×10^{17}		
	Ar	2×10^{19}		

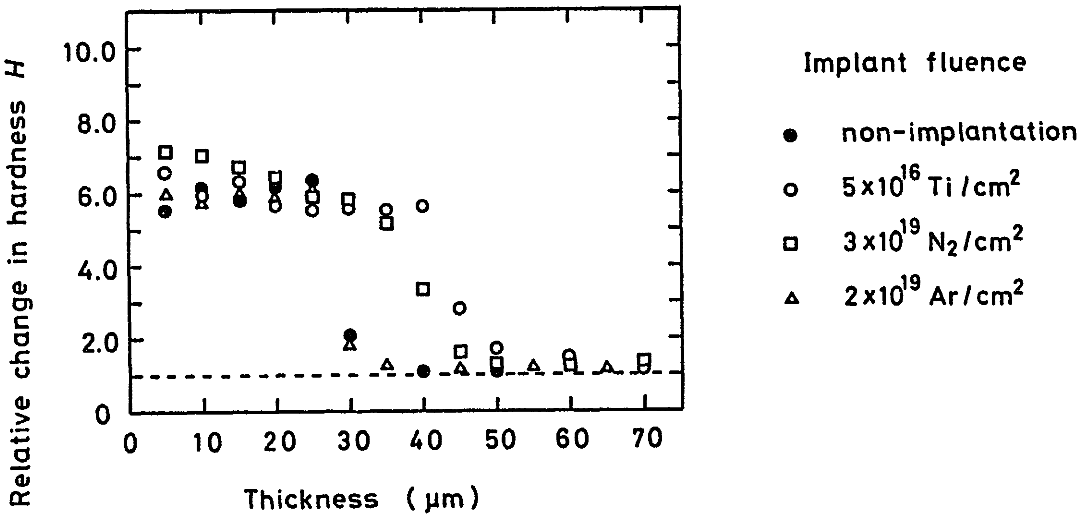

Fig.2
Hardness profile of nitrided 316SS after different ions implantation

Fig. 3

Sample preparation	Ion implantation conditions		Nitridation conditions	
high-purity aluminum (99.999%) cleaned and annealed at 300°C for 1hr	residual gas pressure	6×10^{-4} Torr	total gas pressure	5×10^{-4} Torr
	temperature	room temperature	$N_2 : H_2$	1 : 3
	energy	25keV	bias voltage	1.0 kV
	ion species	fluence (ions/cm^2)	temperature	325°C
	N_2	$1 \times 10^{17} \sim 8 \times 10^{18}$	time	4hrs
	Mo	$1 \times 10^{15} \sim 3 \times 10^{17}$		
	Ti	$1 \times 10^{16} \sim 3 \times 10^{17}$		

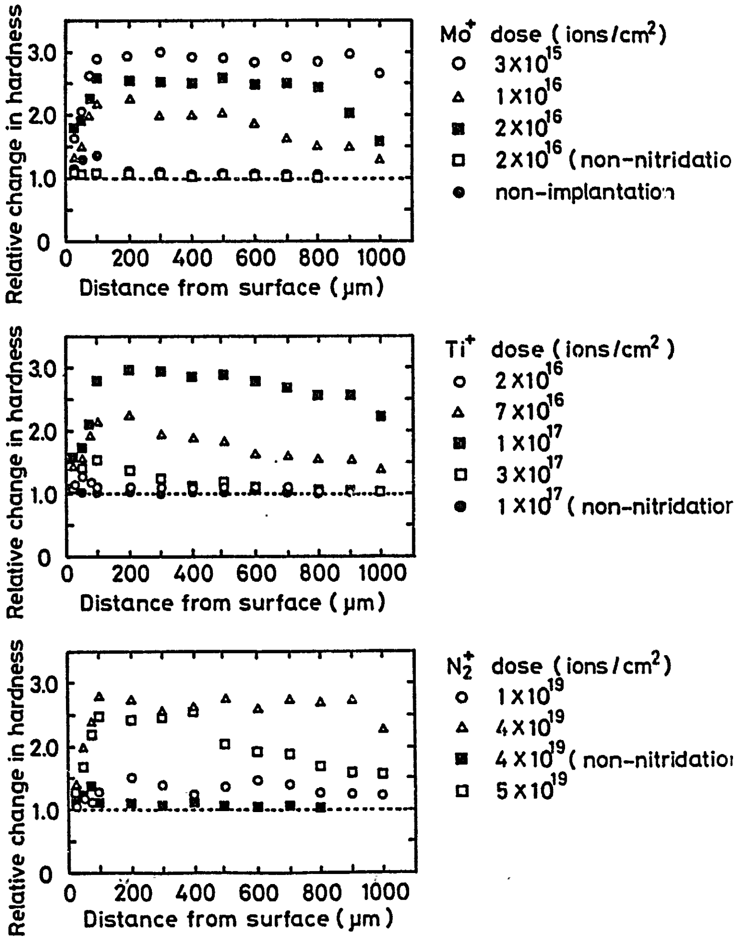

Fig.4

Hardness profiles of plasma source nitrided aluminum after different ions implantation

Design of Boundary Plasmas for Control of Plasma-Wall Interactions

Takaichi Kawamura
Institute of Plasma Physics, Nagoya University, Nagoya 464-01, Japan

The selection of the first wall materials of a fusion device is important not only in view of the reactor engineering but also in view of the core plasma performance in a device. The key issues of the selection criteria of the materials for the control of the core plasma condition are the hydrogen recycling properties of materials and their characteristics as impurities intermingled into the core plasma. As for the latter issue the efficiency of radiation cooling and the reduction of the substantial β-value due to the dilution of a DT plasma are specially significant. From the reactor engineering viewpoint the speed of erosion and the toughness against high particle and heat fluxes should be remarked. In order to match the requests from the above two sides of viewpoints we need to design a desirable boundary plasma for the control of plasma-wall interaction at the first wall surface.

We here describe a simple model analysis to explain the relation between the erosion speed and the steady impurity fraction in the core plasma. The hydrogen ion current from the core plasma to the first wall in the steady state, J_i, is approximately given by

$$J_i \simeq n_i V / \tau_i , \tag{1}$$

where n_i is the average hydrogen ion density in the core plasma,τ_i is the global hydrogen ion confinement time and V is the core plasma volume. Suppose S be an erosion speed (atoms / hydrogen) of the first wall material due to the hydrogen ion bombardment, for example, a sputtering yield, and ε be the screening coefficient due to the boundary plasma. Therefore $\varepsilon S J_i$ becomes the impurity injection current (atoms / sec) into the core plasma. When the impurity fraction also reaches the steady state, the balance relation, $\varepsilon S J_i \simeq n_I V / \tau_I$ holds, where n_I is the average impurity density in the core plasma and τ_I is the impurity particle confinement time. Then, from the above balance relation and Eq. (1) we have

$$\frac{n_I}{n_i} = \varepsilon S \frac{\tau_I}{\tau_i} . \tag{2}$$

If we assume that τ_I is of the order of τ_p, the impurity fraction in the steady state approximately becomes $f_I \equiv n_I / n_i \simeq \varepsilon S$.

The allowable impurity fraction in the core plasma has a maximum value f_I^{max}, which is determined by the power balance between the energy loss mainly due to the radiation loss and the α-particle heating. And this value is a characteristic quantity of the kind of impurities. If we consider an allowable impurity fraction $f_I \equiv n_I / n_i \simeq \varepsilon S$, then we have the inequality,

$$f_I \simeq \varepsilon S \leqq f_I^{max} . \tag{3}$$

From this relation we can have a condition for the screening efficiency of impurities generated from the first wall as

$$\varepsilon \leqq f_I^{max} / S . \tag{4}$$

The value f_I^{max} / S is a quantity referred as the figure of merit of the wall material[1,2], where the erosion rate S and the value f_I^{max} / S itself are functions of the temperature of the boundary plasma near the first wall surface. Therefore, the condition (4) is also rewritten for the condition of the boundary plasma temperature T_B. That is,

$$S(T_B) \leqq f_I^{max} / \varepsilon . \tag{5}$$

For a toroidal device with a divertor or limiter, the screening efficiency depends on the nature of the scrape-off layer plasma. If neutral impurity atoms sputtered from the first wall are ionized inside the scrape-off layer, they go along the magnetic field lines and have probabilities with which they reach the divertor plate or limiter side. In the scrape-off layer ionized impurities also drift across the field lines owing to the anomalous diffusion. From the numerical and statistical analysis on such impurity behavior we can estimate the impurity screening efficiency of the scrape-off layer for the control of the plasma-wall interaction[2,3,4].

References
1) J. Bohdansky et al., Proceedings of the 9th SOFT (1976) 541.
2) T. Kawamura et al., J. Nucl. Mater. 93&94 (1980) 192.
3) T. Kawamura et al., J. Nucl. Mater. 145-147 (1987) 860.
4) T. Kawamura et al., Contrib. Plasma Phys. 28 (1988) 427.

Plasma - First Wall Fuel Dynamics Study at Nuclear Engineering Research Laboratory, University of Tokyo

Masanori Tsuchimoto and Satoru Tanaka

Nuclear Engineering Research Laboratory, Faculty of Engineering, University of Tokyo, 2-22, Shirakata-Shirane, Tokai-mura, Naka-gun, Ibaraki-ken, 319-11, Japan

Recent activities and one of plans for plasma-first wall fuel dynamics research at Nuclear Engineering Research Laboratory are reported.

There are many experimental results and nemerical analyses for plasma-wall interactions [1]. One of the experiments concerning reactor engineering is performed by R. Conn et al. using the PISCES facility in UCLA [2]. They also examined a practical pump limiter module in the TEXTOR reactor and analyze it numerically [3]. Our group has been studying particle transport phenomena near the first wall of a fusion reactor. Both experimental and numerical analyses are planned. Figure 1 shows an apparatus for hydrogen ion bombarding experiments. Ion source used in this study is a Kaufman type as shown in Fig.2 and its particle energy is about 50-100[eV] and current density about 0.1-1.0[mA/cm^2]. We plan to use one port in order to perform exhaust experiments. On the other hand, numerical analyses and boundary plasma modeling are also being conducted by using two dimensional model to study particle transport near a pump limiter or a divertor shown in Fig.3. Effects of many processes, reflection, reconbination, absorption, desorption, plasma seath, sputtering, diffusion, recycling, behavior of impurity and neutral particles, etc, are imposed to boundary conditions. Combinations of both experimental results and numerical analyses are considered to clarify the fuel dynamics.

References

[1] Physics of Plasma-Wall Interactions in Controlled Fusion, ed. by D.E. Post and R. Behrisch, Plenum Press, 1986.

[2] D.M. Goebel et al. : "Plasma Surface Interaction Experimental Facility (PISCES) for Materials and Edge Physics Studies", J. Nucl. Mater. 121,1984,pp.277-282.

[3] R. Conn et al.,UCLA Reports,1987.

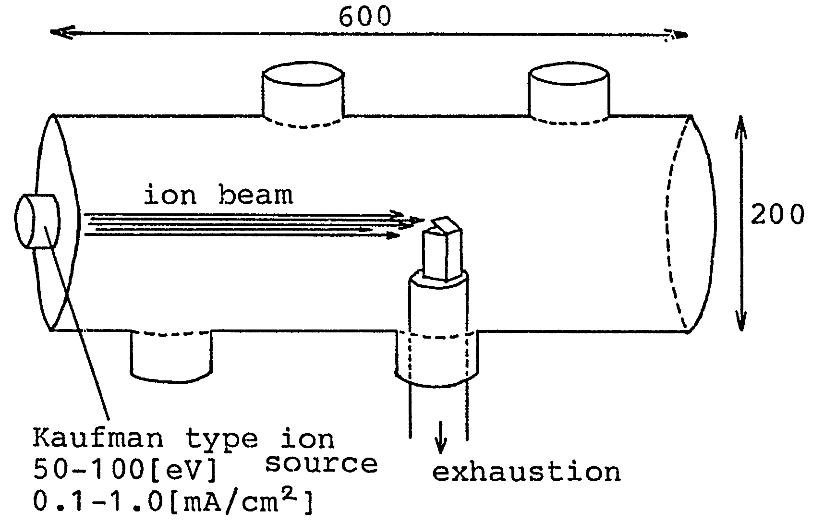

Fig.1 Experimental apparatus

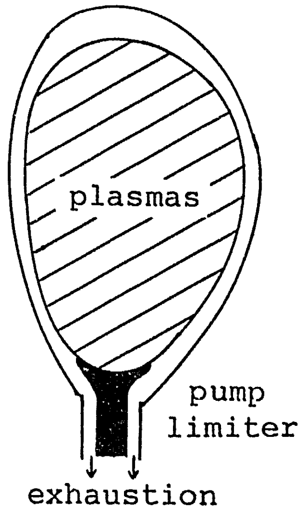

(a) Limiter model

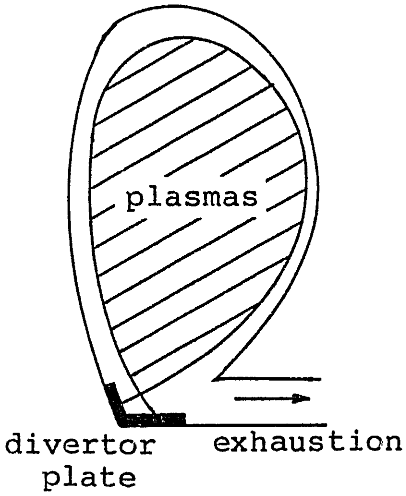

(b) Divertor model

Fig.3 Numerical model

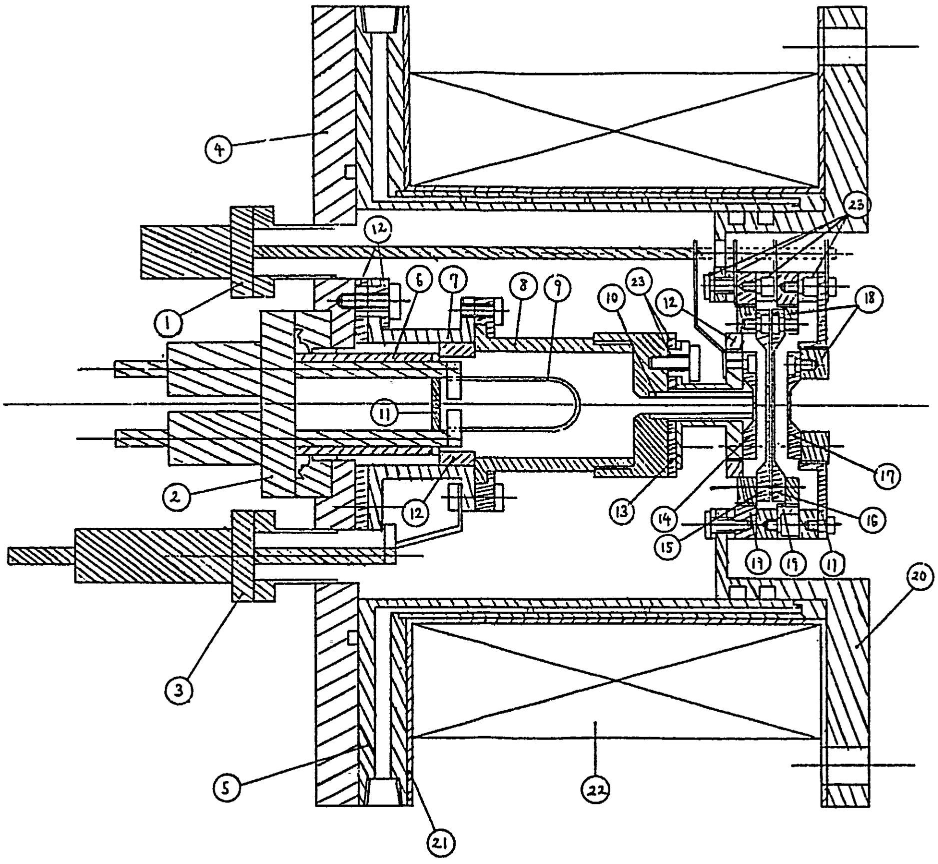

Fig.2 Kaufman type ion source

A Brief Review of the PWI Simulation

Yasunori YAMAMURA*
Institute of Plasma Physics, Nagoya University,
Chikusa-ku, Nagoya 464-01, Japan

The basic physical processes of the PWI simulation problem are the slowing down process of an energetic particle and the thermal (diffusion) process of a thermalized particle. The former slowing down process i[illegible] finished roughly before 1 psec. After the slowing down process the thermal phase begins to start. Then, the existing PWI simulation codes can be classified into two groups, i.e., the simulation code of the slowing down process and the diffusion calculation (see Table 1). Almost all slowing down simulation codes do not include the diffusion process[1-8], while the standard diffusion calculations use the spatial distribution of thermalized particles at the end of the collisional phase as a source term[9,10,11].

From the viewpoint of the method how to follow the trajectories of a slowing down ion and produced recoils, moreover, the slowing-down simul[illegible]tion codes can be classified into two groups, i.e., the space-evolutional treatment and the time-evolutional treatment. The typical codes of the former category are TRIM[1], MARLOWE[2], ACAT[3] and ACOCT[4] which are based on the binary collision approximation. The typical example of the latter category is the molecular dynamics (MD) method such as GRAPE[13], where the simultaneous Newtonian equations are numerically solved.

---

* Permanent address:
Okayama University of Science, Ridai-cho, Okayama 700, Japan.

In order to investigate the non-linear effect in a dense cascade, recently, the DYACAT[15] and DYACOCT[16] codes have been proposed, where the trajectories of slowing down process are followed time-evolutionally within the binary collision approximation. The comparison of the DYACOCT code with the molecular dynamics and the MARLOWE code is shown in Table 2, where M, I, V, and T mean a energetic moving particle, an interstitial, vacancy and a lattice atom at rest, respectively.

As the numerical code of the thermal (diffusion) process, the DIFFUSE[9] code is very famous. This code is successfully applied to the hydrogen recycling problem, where the following equations are numerically solved for the j-th solute $c_j(x,t)$:

$$\frac{\delta\, c_j(x,t)}{\delta\, t} = \nabla\, [D_j \nabla\, c_j(x,t)] + G_j(x,t_0) - \Sigma\, \frac{\delta\, c_{Tj}{}^{i}(x,t)}{\delta\, t} \quad , \qquad (1)$$

which is Fick's law with source and trapping terms. Here, t_0 is the initial starting time. $c_{Tj}{}^{i}(x,t)$ is the concentration of the j-th solute trapped in the i-th trapping site. $G_j(x,\ t_0)$ is the initial spatial distribution of the j-th solute. D_j is the diffusion constant of the j-th solute.

Up-to-now, as the typical PWI simulation codes we have TRIDYN[17], EVOLVE[18] and ACAT-DIFFUSE[19] codes. These codes can treat the high dose effects which bring out the material change during the ion bombardment. The TRIDYN and EVOLVE codes do not include the effect of the diffuison process of thermalized atoms, but the ACAT-DIFFUSE code is a hybrid code of the ACAT code and the DIFFUSE code.

In conclusion, the prospective PWI simulation code should include various physical processes such as slowing down process of an energetic particle, diffusion and segregation process, chemical reaction, and heat transfer. At the same time the diffusion equation should be numerically solved in the three dimension system. Another important feature of the prospective PWI simulation is the hybridization between various existing codes. For example, we should develop a hybrid simulation code which can describe the energy- and particle-balance between the first wall and the scrape-off layer.

REFERENCES

1) J.P. Biersack and L.G. Haggmark, Nucl. Instr. Methods 174 (1980)
J.P. Biersack and W. Eckstein, Appl. Phys. A34 (1984) 73.
2) M.T. Robinson and I.M. Torrens, Phys. Rev. B9 (1974) 5008.
3) Y. Yamamura and Y. Mizuno, IPPJ-AM-40, Institute of Plasma Physics, Nagoya University, 1985.
4) Y. Yamamura and W. Takeuchi, Nucl. Instr. Methods B29 (1987) 461.
5) T. Ishitani and R. Shimizu, Jpn J. Appl. Phys. 11 (1972) 125.
T. Ishitani and R. Shimizu, Appl. Phys. 6 (1975) 241.
6) G. Betz, R. Dobrozemsky and F.G. Viehböck, Int. Mass Spectrom. Ion Phys. 6 (1971) 451.
7) V.I. Shulga, Rad. Eff. 51 (1980) 1.
Rad. Eff. 70 (1983) 65.
8) M. Hautala, Rad. Eff. 51 (1980) 35.
9) K.L. Wilson and M.I. Baskes, J. Nucl. Mater. 76/77 (1978) 291.
10) B.L. Doyle, D.K. Brice and W.R. Wampler, Rad. Eff. Lett. 57 (1980) 81.
11) D.K. Brice, Nucl. Instr. Methodsu B16 (1986) 493.
12) B.L. Doyle, J. Nucl. Mater. 111/112 (1982) 628.
13) J.B. Gibson, A.N. Goland, M. Milgram and G.H. Vineyard, Phys. Rev. 120 (1960) 1229.
14) D.E. Harrison, Jr., J. Appl. Phys. 40 (1969) 3870.
D.E. Harrison, Jr., J. Appl. Phys. 52 (1981) 1499.
D.E. Harrison, Jr., J. Appl. Phys. 52 (1981) 4251.
D.E. Harrison, Jr., W.L. Gay and H.M. Effron, J. Math. Phys. 10 (1969) 1179.
15) Y. Yamamura, Nucl. Instr. Meth. B33 (1988) 493.
16) Y. Yamamura, I. Yamada and T. Takagi, Nucl. Instr. Methods (in press).
17) W. Möller and W. Eckstein, Nucl. Instr. Meth. B2 (1984) 814.
W. Möller and W. Eckstein, Nucl. Instr. Meth. B7/8 (1985) 645.
18) M.L. Roush, O.F. Goktepe, T.D. Andereadis and F. Davarya, Rad. Eff. 55 (1981) 119.
19) Y. Yamamura, Nucl. Instr. Meth. B28 (1987) 17.

Table 1 The PWI simulation codes

SLOWING DOWN PROCESS					DIFFUSION PROCESS
SPACE EVOLUTIONAL CASCADE DEVELOPMENT		TIME EVOLUTIONAL CASCADE DEVELOPMENR			DIFFUSE Local Mixing Model Brice
BIANRY COLLISION APPROXIMATION				MOLECULAR DYNAMICS	
RANDOM TARGET	CRYSTAL	RANDOM TARGET	CRYSTAL	GRAPE Harrison Guinan & Kinney Averback Baskes King & Benedek	
TRIM	MARLOWE				
ACAT	ACOCT	DYACAT	DYACOCT		
Betz	Shulga				
Shimizu	Hautala				

Table 2 Comparison of the DYACOCT code with the MD calculation and the MARLOWE code

	M D	DYACOCT	MARLOWE
CASCADE DEVELOPMENT	time	time	space
COLLISION			
MM	○	○	×
MI	○	○	×
MV	○	○	×
MT	○	○	○
MANY BODY EFFECT	○	△	×
COMPUTING TIME	a lot	mdeium	little
ELECTRONIC STOPPING	○	○	○
DYNAMICAL RECOVERY	○	△	×
THERMAL VIBRATION	○	○	○
DOPPLER EFFECT	○	○	×
PROJECTILE			
MONATOMIC	○	○	○
MOLECULE	○	○	×
CLUSTER	○	○	×

The status and data needs of sputtering for fusion

Reiji Yamada

Japan Atomic Energy Research Institute. Tokai-mura. Ibaraki-ken. Japan

Physical and chemical sputtering relevant to the first wall materials of fusion devices are reviewed. The present status of yield data of low-Z(C, B. Be) and high-Z(Mo. W) materials is briefly described. The data needs of sputtering for fusion are also pointed out. The influence of oxygen that inevitably exists in the devices on sputtering is stressed.

1. Physical sputtering

The data of physical sputtering yields are fairly well accumulated and compiled at least under normal incidence of energetic particles and at ambient target temperature. For compilation we can see. for example. the work of Nagoya group[1] and of Garching group[2].

Empirical formulas for calculating sputtering yields are also developed[1,2]. The calculated values fit fairly well with experimental data. These formulas can thus be used in various calculation codes for estimating sputtering yields. In low energy region(<100 eV). however. some discrepancy still exists: if we focus on candidate plasma facing materials such as B. Be. W, the sputtering yields of Be are smaller than calculated ones for H^+. D^+. He^+ bombardments. and that of W is also smaller for O^+ bombardment[1]. The former results show that the theoretical treatment for low-Z targets bombarded with low energy light ions is still insufficient. The latter one indicates that oxygen has an influence on sputtering. In the case of B the lack of sputtering data in energy region less than 10 keV is severe.

There are data indicating that not only O+ bombardment but also other ion bombardments under oxygen atmosphere have effects on sputtering due to formation of volatile oxide layer, dilution of constituent atoms and change of surface binding energy. In the case of Mo[3.4], for example, oxygen uptake suppresses Ar^+ sputtering yields at room temperature, whereas it enhances the yields at about 500 C due to ion-assisted evaporation of MoO and MoO_2. At higher temperature(1400 C) the ion-assisted evaporation asymptotically increases with increasing oxygen pressure and becomes identical with thermally activated evaporation.

In the tokamak machines the plasma facing materials at high temperature will be bombarded not only with oxygen ions but also with fuel ions and impurity ions under oxygen partial pressure originated from various oxygen sources. Hence, the enhancement of erosion must be possible in a certain condition. In that respect, experimental data are limited.

The data of angular dependence of sputtering yields are compiled and an empirical formula for them is proposed[5]. The agreement between the calculated yields and the experimental data is satisfactory, still the available data are not necessarily enough in comparison with the data of the normal incidence. The compilation of angular distribution of sputtered atoms is now in progress[6]. The above experimental data are also insufficient. The influence of oxygen uptake on the angular dependence of sputtering yields and on the angular distribution of sputtered atoms are yet unclear.

2 Chemical sputtering

Among ion-assisted chemical reactions occurring during ion bombardment the chemical sputtering of carbon has been most intensively studied from impurity problem relevant to fusion. In last 10 years at least the chemical sputtering yield data for $H^+(D^+)$ bombardment have been accumulated and compiled[7-11]. The data are somewhat scattered among investigators. compared with the accuracy of physical sputtering data. With respect to the data of temperature and energy dependence of the $CH_4(CD_4)$ production yield, however, we can say that the agreement is rather good, considering chemical reactions are much more influenced by experimental conditions than physical processes.

Several models were proposed to explain CH_4 formation due to impact of energetic hydrogen ions[12-17]. Every model can explain the experimental temperature dependence and obtain an expression for the temperature(T_m) at which the CH_4 production yield has a maximum. The key experimental data to evaluate the effectiveness of the models are the flux dependence; the general trend of experimental results is that with increasing flux, CH_4 yield increases ($<5\times10^{14}$ H/cm^{2}sec) and becomes plateau and then decreases ($>5\times10^{15}$ H/cm^{2}sec). The present models have limitations for their application to the flux dependence. and thus there is no model to explain the above results as a whole. The data needs of flux dependence are high not only for the elaboration of chemical sputtering theory but also for the practical designing of carbon limiters suffering from high flux irradiation. The data of flux dependence have still some ambiguities. To obtain much more precise data it is necessary to measure them under the same condition as much as possible. It is so far difficult to be performed in a wide range of flux(10^{12}-10^{20} H/cm^{2}sec).

Recently new results have been reported: (1) CD_4 production yield exceeds the physical sputtering yield even at room temperature if the deuteron energy is less than 100 eV[18]; (2) C_2 hydrocarbon production becomes larger in low proton energy region(200-500 eV) than in keV region[17.19]. Information on the chemical sputtering at room temperature is still limited, and some discrepancy exists in both identification of the species of C_2 hydrocarbons and quantitative determination of individual yields[17.19]. Much efforts are required to investigate them in detail although there are experimental difficulties coming from small production yields at room temperature as well as from indirect determination of C_2 hydrocarbon species.

Synergistic effects are of importance on carbon erosion. One of them is enhancement of erosion by simultaneous atomic hydrogen and energetic particle bombardment. and another is radiation-enhanced sublimation at target temperatures >1100 K. While the knowledge of the synergistic effects has been accumulated. the erosion data in the energy range between sub-eV and 100 eV are insufficient. which will give much more insight into radiation effects on chemical reactions. It is still unclear that erosion rates of radiation-enhanced sublimation would be similar to erosion rates at near sublimation temperature estimated from the vapor pressure. It must be clarified because of the importance of estimating high temperature erosion for selecting a carbon material for limiter material suffering from high heat flux. In that respect. the influence of oxygen on erosion should be again emphasized.

Reference

[1] N. Matsunami et. al.. IPPJ-AM-32 report series of the Institute of Plasma Physics, Nagoya. Japan (1983).
[2] J. Bohdansky. Nucl. Fusion, Special Issue (1984) 61.
[3] M. Saidoh, J. Nucl. Mater. 128-129 (1984) 540.
[4] M. Saidoh et. al.. J. Nucl. Mater. 145-147 (1987) 387.
[5] Y. Yamamura et. al.. IPPJ-AM-26 report series of the Institute of Plasma Physics, Nagoya, Japan (1983).
[6] Y. Yamamura, private communication.
[7] J. Roth, in: Sputtering by Particle Bombardment II, Topics in Applied Physics. Vol. 52. Ed. R. Behrisch (Springer-Verlag. New York. 1983) p.21.
[8] J. Roth , in: Physics of Plasma-Wall Interactions in Controlled Fusion. NATO Advanced Science Institutes Series B Physics. Vol.131. Ed. D. E. Post and R. Behrisch

(Plenum Press. New York. 1986) p.389.
[9] J. Roth. Nucl. Fusion, special issue (1984) p.72.
[10] A. A. Haasz et. al.. Rad. Effects 89 (1985) 63.
[11] W. L. Hsu. J. Vac. Sci. Technol. A6 (1988) 1803.
[12] S. K. Erents et. al., J. Nucl. Mater. 63 (1976) 399.
[13] R. Yamada and K. Sone, J. Nucl. Mater. 116 (1983) 200.
[14] A. A. Haasz and J. W. Davis, J. Chem. Phys. 85 (1986) 3293.
[16] N. Itoh and Y. Horino. Nucl. Instr. and Methods B28 (1987) 264.
[17] R. Yamada, J. Nucl. Mater. 145-147 (1987) 359.
[18] J. Roth and J. Bohdansky, Nucl. Inst. and Meth. B23 (1987) 549.
[19] J. W. Davis et. al., J. Nucl. Mater. 155-157 (1988) 234.

Effects of Fluence and Temperature on Sputtering Yield by He-ion bombardment

by

M.Tomita, K.Masumori, M.Takami, H.Akatsuka, T.Nate,
S.Miyagi and M.Sakisaka
Department of Nuclear Engineering,
Kyoto University,
Yoshida Honmachi, Sakyo-ku, Kyoto 606 Japan

In 1960's were carried out a few works on temperature dependence of the metal sputtering by heavy-ion bombardment[1-6]. These revealed that the yield variations were within ±30% in the temperature range of $T/T_m<0.6$, where T_m represents the melting point of respective metals. It has, however, been shown by simulation calculation[7,8] that a large part of sputtered atoms by light-ion bombardment consists of the primary or secondary knocked-on atoms. Furthermore the sputtering yield of metals usually has a maximum at the incident energy of 1-10 keV[9] and are 0.01-0.1 atoms$\cdot$ion^{-1} for light-ion bombardment, whereas those for heavy-ion impact are 1-10 atoms$\cdot$ion^{-1}. This fact implies accumulation of implanted light-ions in a target material and, in connection with the results of simulation calculation, this accumulation would suggest that different trens in temperature dependence could be expected for the sputtering yield by light-ion bombardment.

Variations of sputtering yield with fluence and temperature, T, were measured for metals of Mo[10], W, Nb[11], Zr and V, respectively, by using a flux of $\sim 1\times10^{15}$ cm$^{-2}\cdot$s^{-1} of the 25 keV He-ions, a UHV irradiation chamber (pressure$<5\times10^{-7}$ Pa) and a collector method we developed[10]. The number of collected atoms was determined by a conventional RBS method. Sticking probability of sputtered atoms onto a carbon collector was obtained by the same method described elsewhere[12]. The values obtained for Mo, W, Nb and Zr are 0.82±0.03, 0.97±0.01, 0.97±0.01 and 0.96±0.01, respectively. The experimental arrangement for irradiation is shown schematically in fig.1. We measured the sputtering yield for six steps of fluence, i.e., 0.1, 0.1, 0.2, 0.3, 0.3 and 0.3 C of He^+, by using six sets of a collector array which was composed of eight collectors at 10°-80° with respect to the normal of a target so as to measure the angular yields shown in fig.2-6. Angular distribution changed often drastically its pattern as fluence increased. When we discuss quantitatively on the sputtering yield at corresponding fluence step patterns of angular distribution should be taken into account, because a violent distribution would not result in a correct yield by the present collector method.

The sputtering yield at elevated temperatures for each metal are shown in figs.7(a),(b),(c) and (d) as a function of fluence. The yield observed increases with fluence and reaches a saturation level except Nb(770 K)- and V-data. This tendency seems to be more remarkable as the temperature is raised. An another behavior is seen in fig.7(d) of V, where the yield at 1100 K and 1270 K contrarily decreases with fluence and reaches a level.

The value of saturation level $\overline{Y(T)}$ at T was determined by averaging the ield of 4th to 6th steps of fluence. The saturated yields of four metals except V are shown in figs.8-11 as a function of T. $\overline{Y(T)}$ of Mo, Nb and Zr varied remarkably with temperature, whereas that of W was constant in the temperature range concerned. In particular $\overline{Y(T)}$ of Mo increased exponentially in the range of 300- 1300 K and the value of $Y(1220)/Y(350)$ was 3.1. For Nb and Zr $\overline{Y(T)}$ varied similarly with temperature and had a maximum at about 900 K. The largest change in $\overline{Y(T)}$'s was 50% or more for both metals in the range of 370-1300 K. The error of all experimental data shown in fig.8-11 is as large as a size of each full circle.

Finally we can point out the following remarks:

1) At the energy lower than 25 keV the change greater than 100% can probably be expected in the sputtering yield at high fluence and high temperature. Hence their effects should be examined in a more wide energy range, particularly in the range of 1 keV or lower.

2) In order to investigate the accumulation effect of implanted He atoms on the sputtering yield, an in situ observation of He concentration at the surface layer should be performed by an appropriate method, e.g., Elastic Recoil Detection(ERD) using an energetic heavy-ion beam.

3) Although hydrogen atoms can diffuse into a metal with much larger probability than helium atoms under the adequate thermodynamical conditions, it should be confirmed whether the similar phenomena described in this report are induced or not by the bombardment of hydrogen ions or helium-hydrogen mixed ions.

Figure caption

fig.1	A schematic drawing of irradiation apparatus. On lower half is shown separately a detail of the target-collector assembly.
fig.2	Angular distribution of sputtered Mo-atoms at (a) 350 K and (b) 1070 K. Words 1st, 2nd,- - - mean the order of fluence step.
fig.3	Angular distribution of sputtered W-atoms at 1200 K.
fig.4	Angular distribution of sputtered Nb-atoms at 470 K and 1200 K.
fig.5	Angular distribution of sputtered Zr-atoms at 580 K and 1370 K.
fig.6	Angular distribution of sputtered V-atoms at 600 K and 1100 K.
fig.7	Variations of sputtering yield against He-fluence; (a) Mo, (b) Nb, (c) Zr, (d) V
fig.8	Saturated sputtering yield of Mo against temperature in a linear scale(a) and a semi-logarithmic scale(b). In (a) the solid line represents the best fitted one[10] which was given by the Kelly's formula[13], $Y(T) \propto (T+T_s)^{3/2}\exp[-L/(T+T_s)]$, with a spike temperature T=6800 K. In(b) the best fitted function, $Y(T)=A\exp(-BT)$, is shown by a solid line. The value of coefficient $B=1.33\times10^{-3}\text{K}^{-1}$ has been well reproduced by a lattice vibration model[10] based on the results of Sigmund[14] and Sanders-Fluit[15]
fig.9	Saturated sputtering yield of W against temperature. The solid line denotes the average.
fig.10	Saturated sputtering yiled of Nb against temperature. Three lines represent the calculated ones. Solid: lattice vibration model[10], $B=1.9\times10^{-3}\ \text{K}^{-1}$. Broken: Kelly's formula[13], T_s=7000 K. Dotted: Sigmund-Szimonski's formula[16], $Y(T) \propto (1+T/T_s)^4\exp[-L/(T+T_s)]$, T_s=7000 K.
fig.11	Saturated sputtering yield of Zr against temperature.

References

[1] R.S.Nelson, Phil.Mag. 11(1965)291

[2] C.E.Carlston, G.D.Magnuson, A.Comeaux and P.Mahadevan, Phys.Rev. 138A(1965)A759

[3] O.Almen and G.Bruce, Nucl.Instr. and Meth. 11(1961)257

[4] R.S.Nelson, M.W.Thompson and Montgomery, Phil.Mag. 7(1962)1385

[5] M.W.Thompson and R.S.Nelson, Phil.Mag. 7(1962)2015

[6] J.J.Ph.Elich, H.E.Roosendaal and D.Ondedelinden, Rad.Effects 10(1971)175

[7] R.Behrisch, G.Maderlechner, B.M.U.Scherzer and M.T.Robinson, Appl.Phys 18(1978)381

[8] U.Littmark and S.Fedder, Nucl.Instr. and Meth. 194(1982)607

[9] N.Matsunami, Y.Yamamura, Y.Itikawa, N.Itoh, Y.Kazumata, S.Miyagawa, K.Morita, R.Shimizu and H.Tawara, Atomic Data and Nucl. Data Tables 31(1984)1

[10] M.Tomita, T.Nate, S.Miyagi and M.Sakisaka, J.Nucl.Mater. 138(1986)248

[11] M.Tomita and K.Masumori, to be published

[12] M.Tomita, N.Ikuchi, S.Miyagi and M.Sakisaka, Nucl.Instr. and Meth. 213(1983)469

[13] R.Kelly, Radiat. Eff. 32(1977)91

[14] P.Sigmund, Phys.Rev. 184(1969)383

[15] J.B.Sanders and J.M.Fluit, Physica 30(1964)129

[16] P.Sigmund and M.Szimonski, Appl.Phys. A33(1984)141

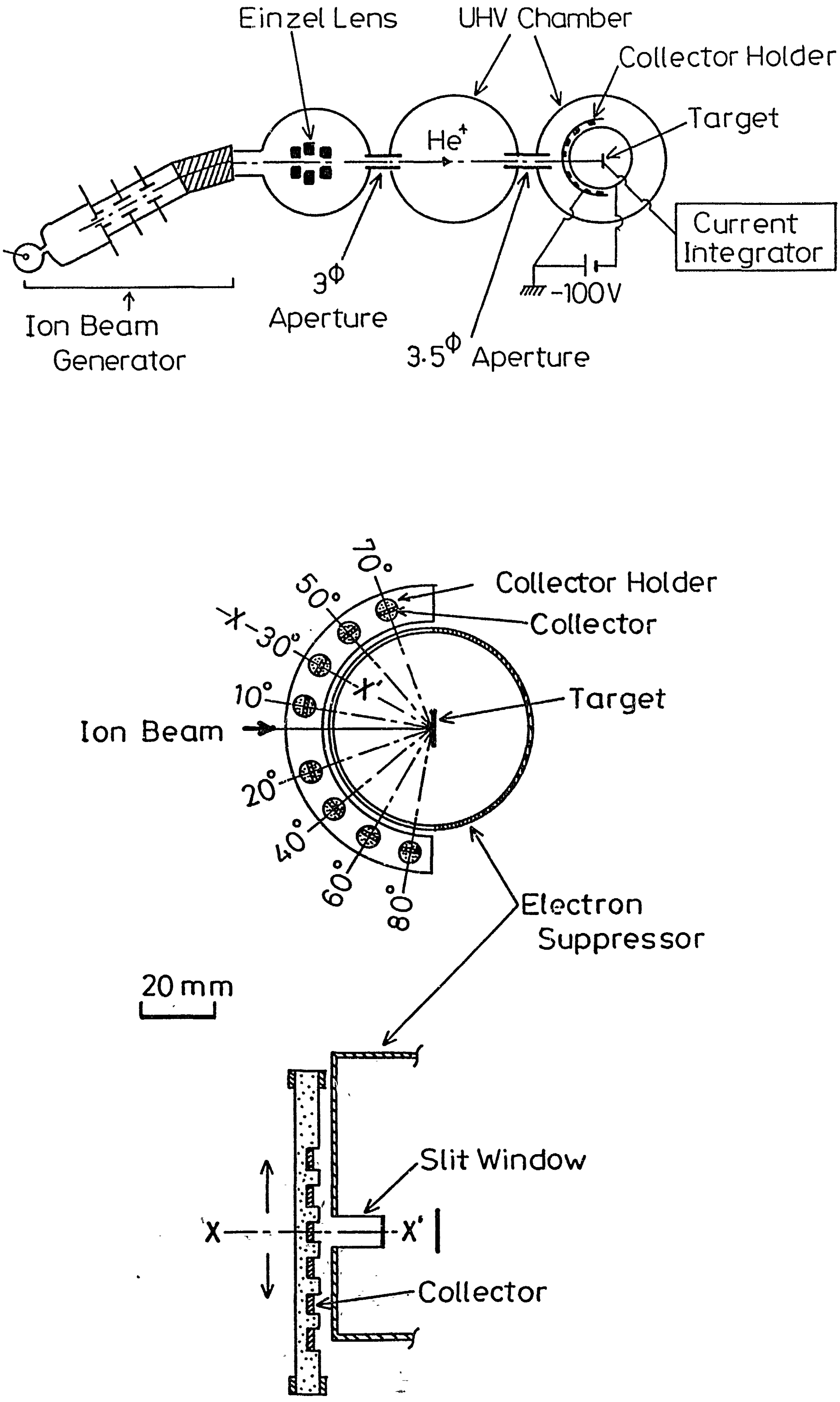
Einzel Lens
UHV Chamber
Collector Holder
Target
He$^+$
Current Integrator
-100V
Ion Beam Generator
3^{Φ} Aperture
3.5^{Φ} Aperture
70°
50°
X
30°
X'
10°
Ion Beam
20°
40°
60°
80°
Collector Holder
Collector
Target
Electron Suppressor
20 mm
Slit Window
X
X'
Collector

fig. 1

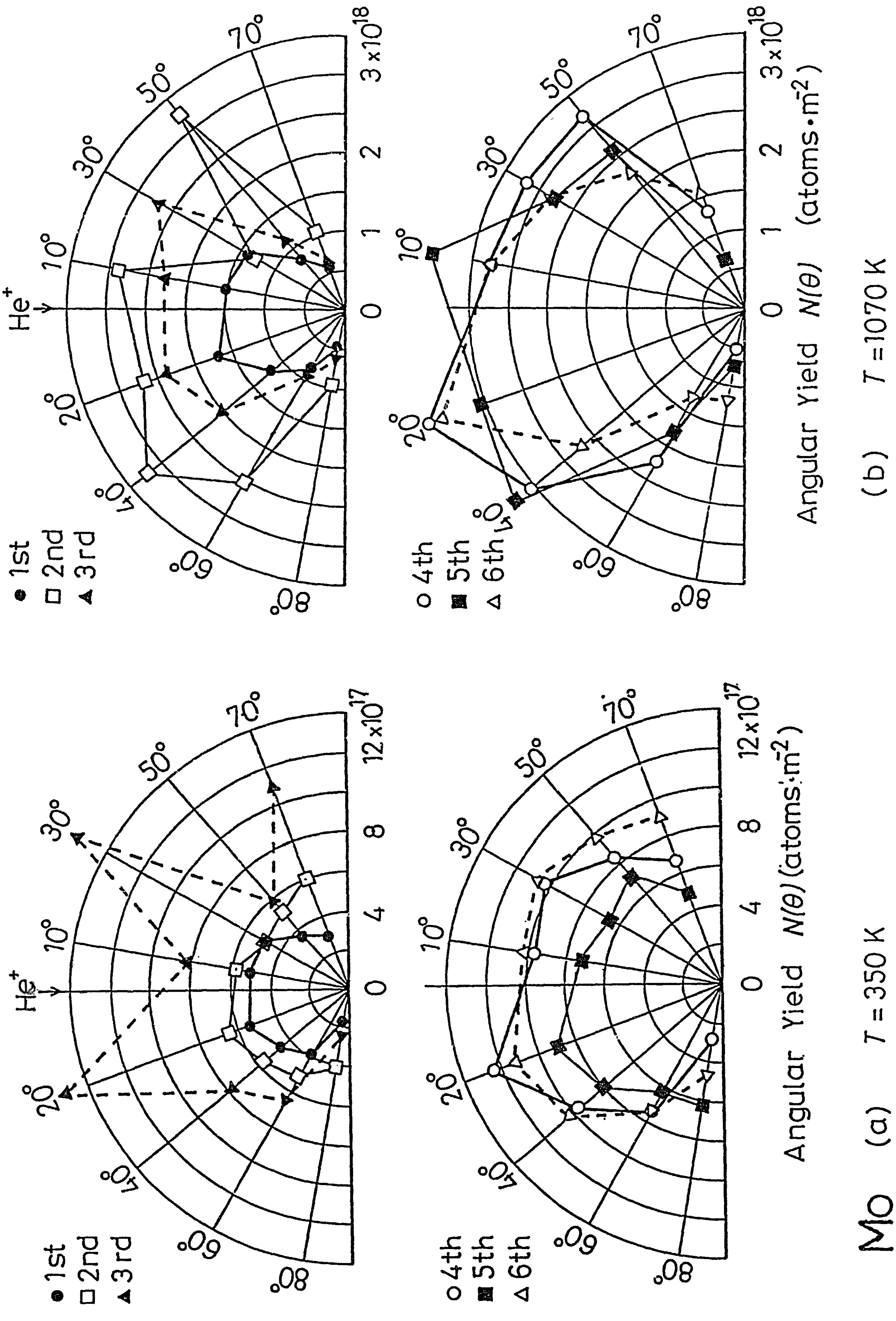
Mo
(a) T = 350 K
(b) T = 1070 K
He+
● 1st
□ 2nd
▲ 3rd
○ 4th
■ 5th
△ 6th
0
4
8
12x10^17
1
2
3x10^18
10°
20°
30°
40°
50°
60°
70°
80°
Angular Yield N(θ) (atoms·m^-2)

fig. 2

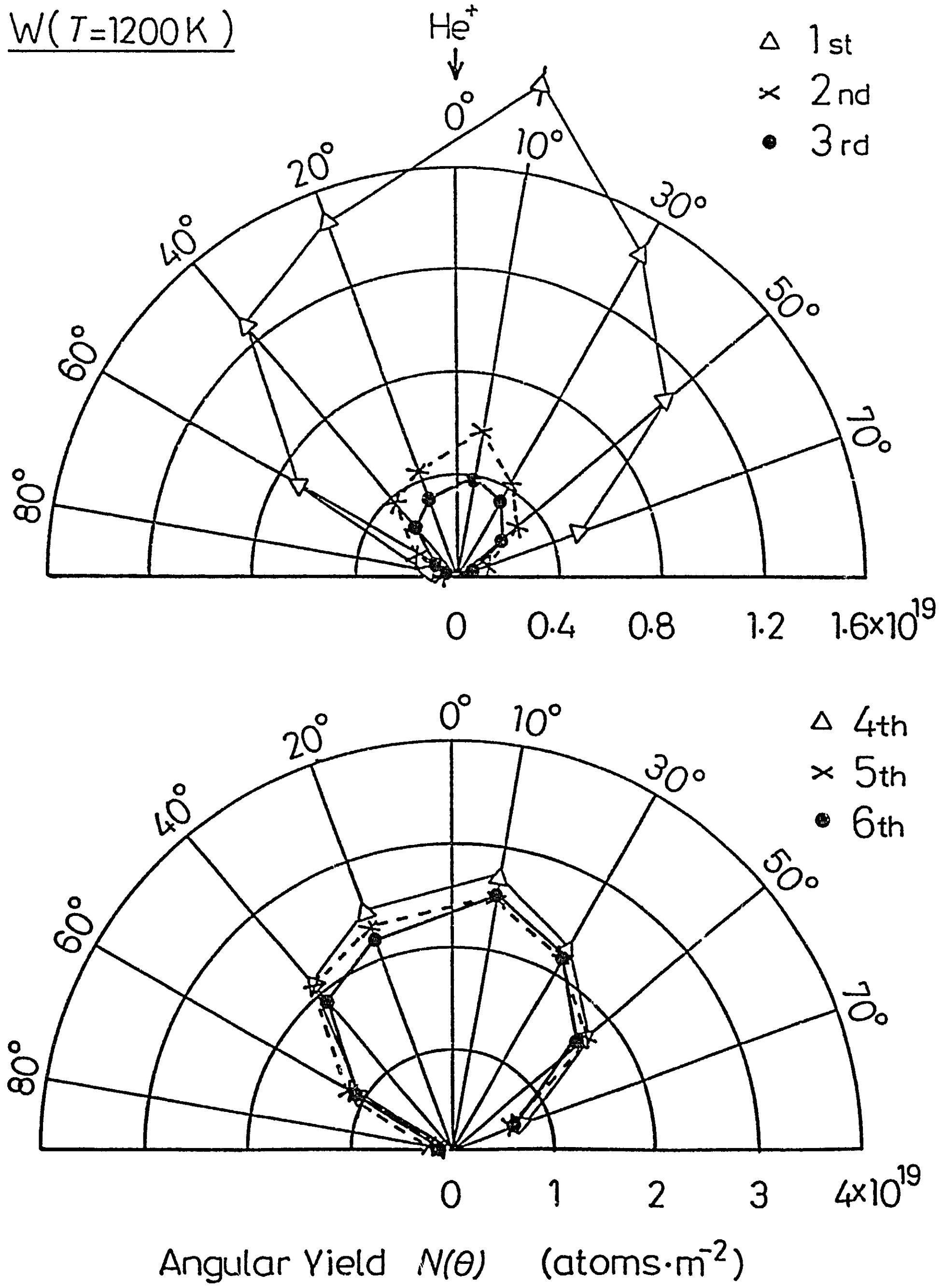
W(T=1200K)
He⁺
0°
10°
20°
30°
40°
50°
60°
70°
80°
△ 1st
× 2nd
● 3rd
0
0.4
0.8
1.2
1.6×10^19
△ 4th
× 5th
● 6th
0
1
2
3
4×10^19
Angular Yield N(θ) (atoms·m⁻²)

fig. 3

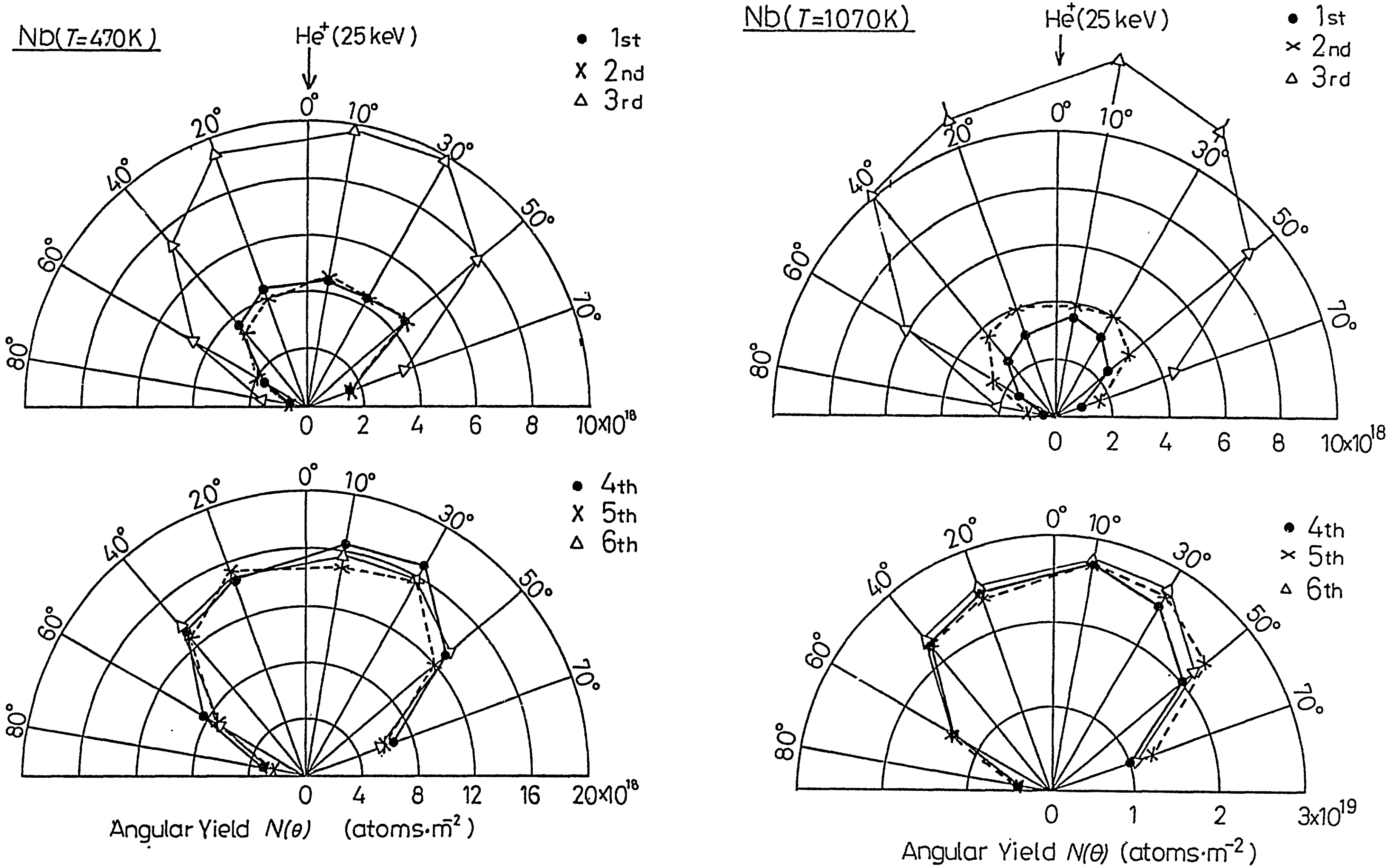
Nb(T=470K)
He⁺(25 keV)
● 1st
X 2nd
Δ 3rd
0° 10° 20° 30° 40° 50° 60° 70° 80°
0 2 4 6 8 10x10^18
● 4th
X 5th
Δ 6th
0 4 8 12 16 20x10^18
Angular Yield N(θ) (atoms·m⁻²)
Nb(T=1070K)
He⁺(25 keV)
● 1st
× 2nd
Δ 3rd
0 2 4 6 8 10x10^18
● 4th
× 5th
Δ 6th
0 1 2 3x10^19
Angular Yield N(θ) (atoms·m⁻²)

fig. 4

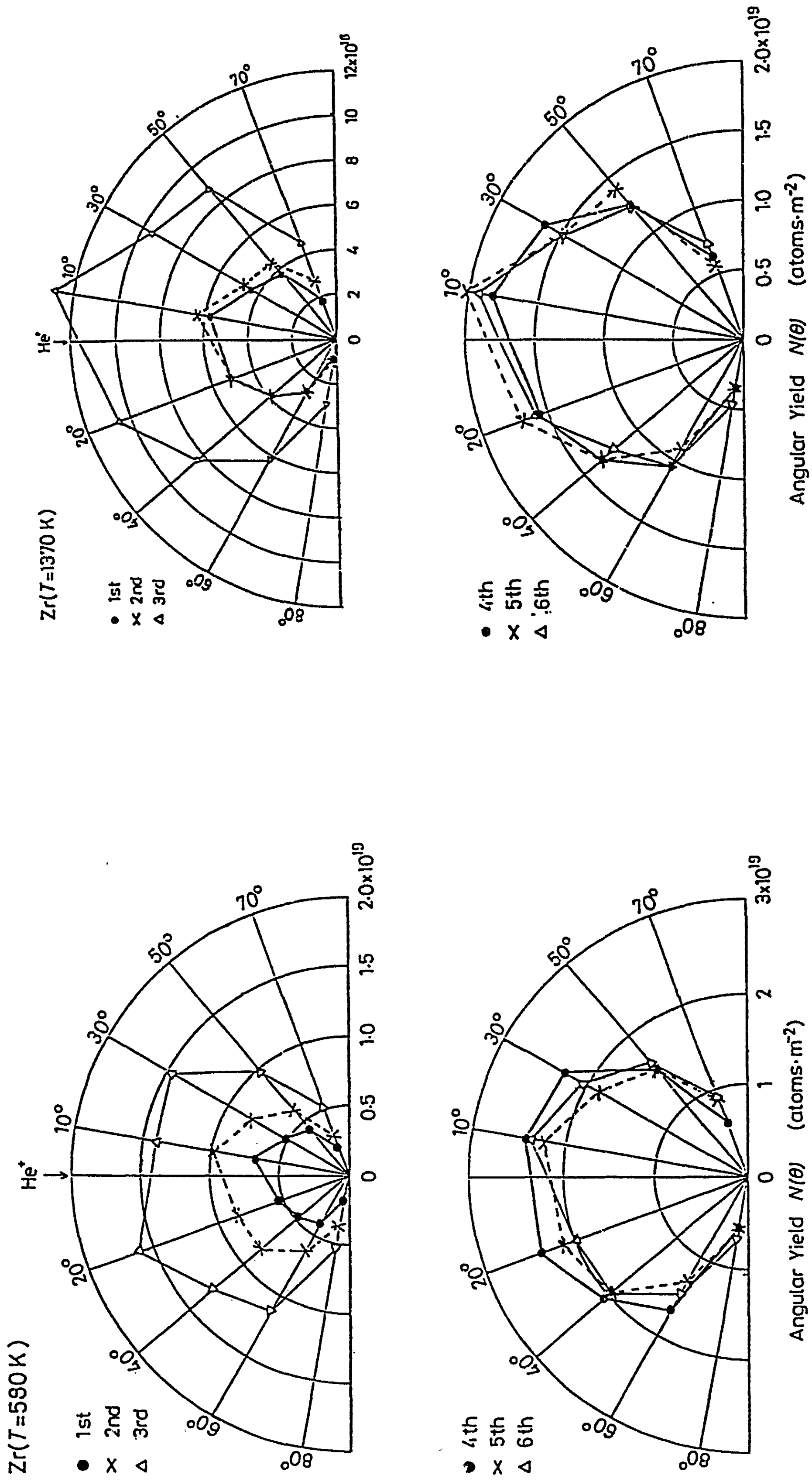
Zr(T=580 K)
● 1st
× 2nd
Δ 3rd
He⁺
10°
20°
30°
40°
50°
60°
70°
80°
0
0.5
1.0
1.5
2.0×10¹⁹
4th
5th
6th
1
2
3×10¹⁹
Angular Yield N(θ) (atoms·m⁻²)
Zr(T=1370 K)
● 1st
× 2nd
Δ 3rd
0
2
4
6
8
10
12×10¹⁸
● 4th
× 5th
Δ 6th
0.5
1.0
1.5
2.0×10¹⁹
Angular Yield N(θ) (atoms·m⁻²)

fig. 5

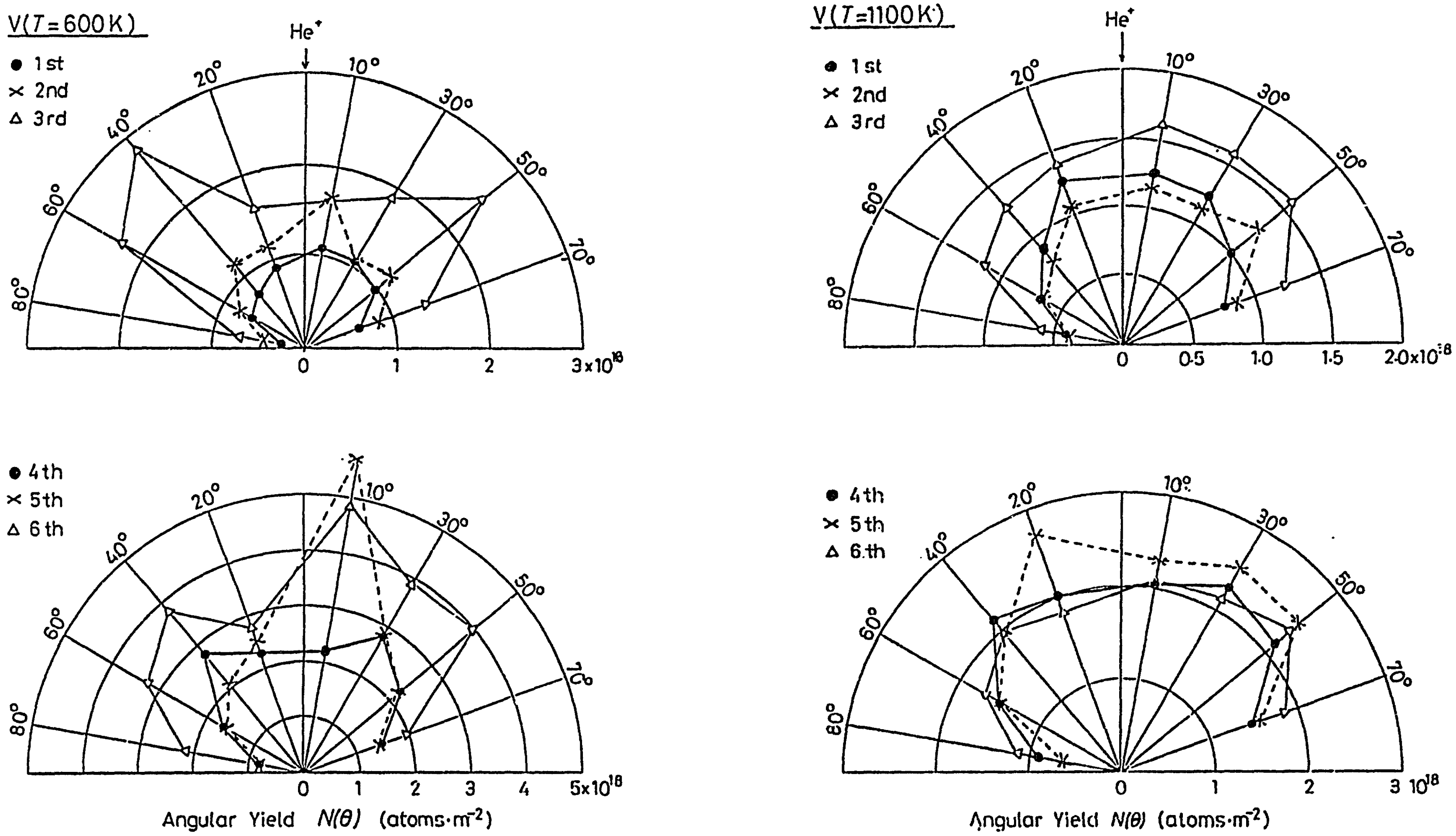
V(T=600K)
● 1st
× 2nd
△ 3rd
He⁺
10°
20°
30°
40°
50°
60°
70°
80°
0
1
2
3×10¹⁸
V(T=1100K)
● 1st
× 2nd
△ 3rd
He⁺
0
0.5
1.0
1.5
2.0×10¹⁸
● 4th
× 5th
△ 6th
0
1
2
3
4
5×10¹⁸
Angular Yield N(θ) (atoms·m⁻²)
● 4th
× 5th
△ 6th
0
1
2
3 10¹⁸
Angular Yield N(θ) (atoms·m⁻²)

fig. 6

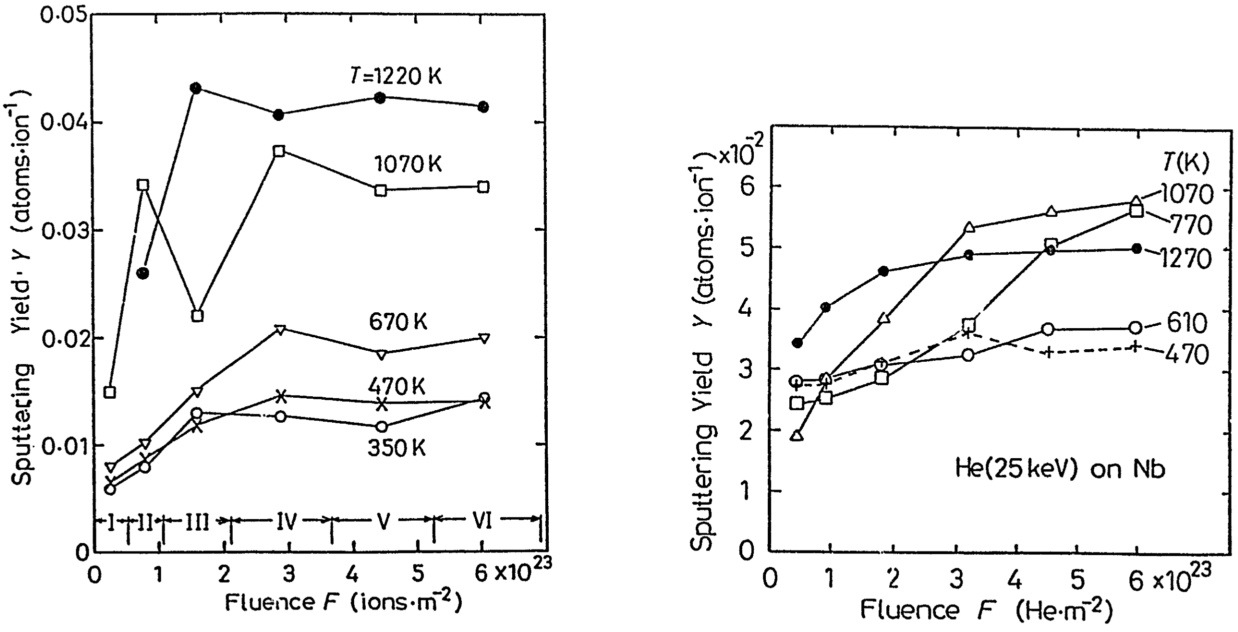

7(a) Mo

7(b) Nb

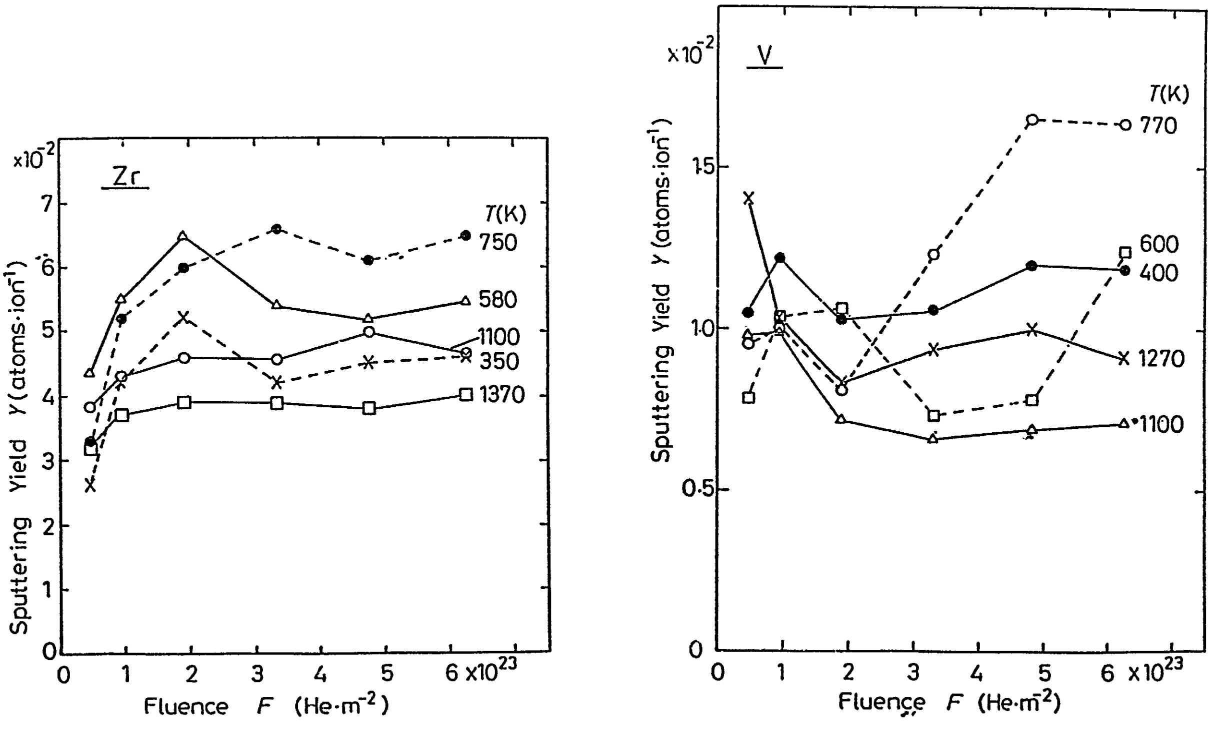

7(c) Zr

7(d) V

fig. 7

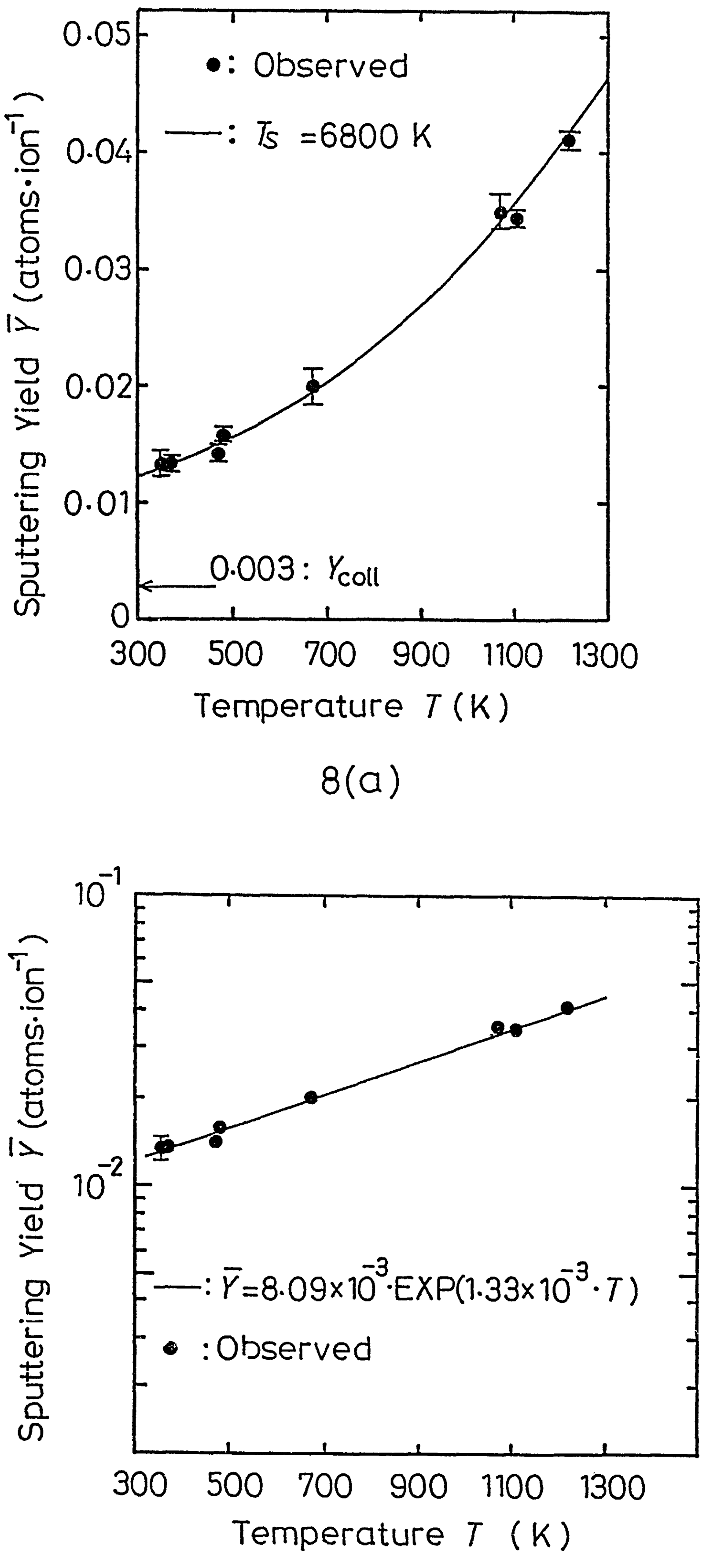
0·05
0·04
0·03
0·02
0·01
0
Sputtering Yield $\overline{Y}$ (atoms·ion^{-1})
●: Observed
——: T_S =6800 K
0·003 : Y_{coll}
300
500
700
900
1100
1300
Temperature T (K)
10^{-1}
10^{-2}
Sputtering Yield $\overline{Y}$ (atoms·ion^{-1})
——: $\overline{Y}$=8·09×10^{-3}·EXP(1·33×10^{-3}·T)
● :Observed
300
500
700
900
1100
1300
Temperature T (K)

8(a)

8(b)

fig. 8

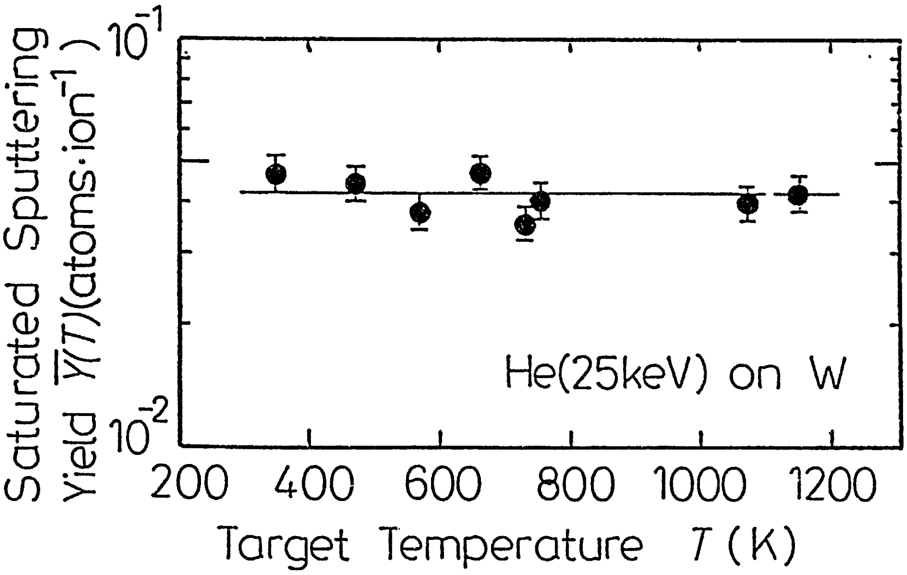

fig. 9

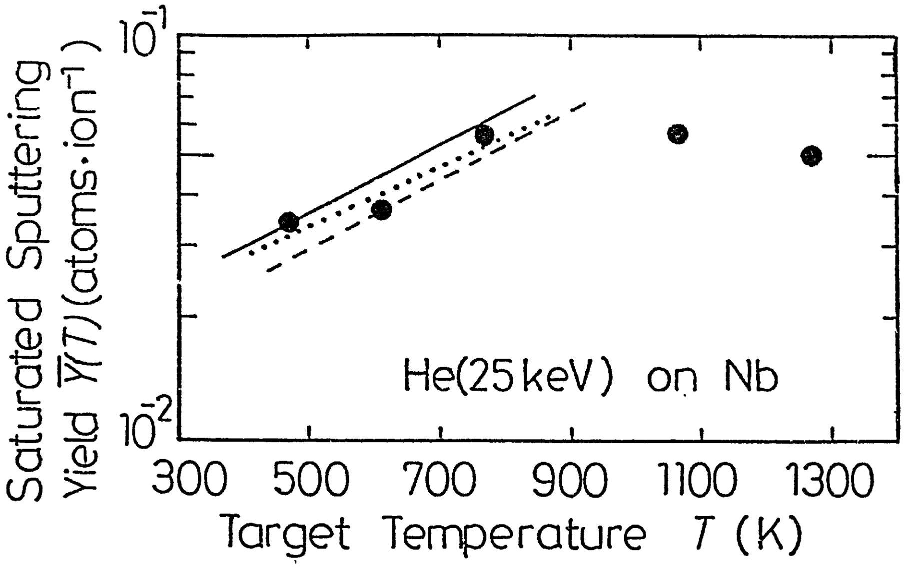

fig. 10

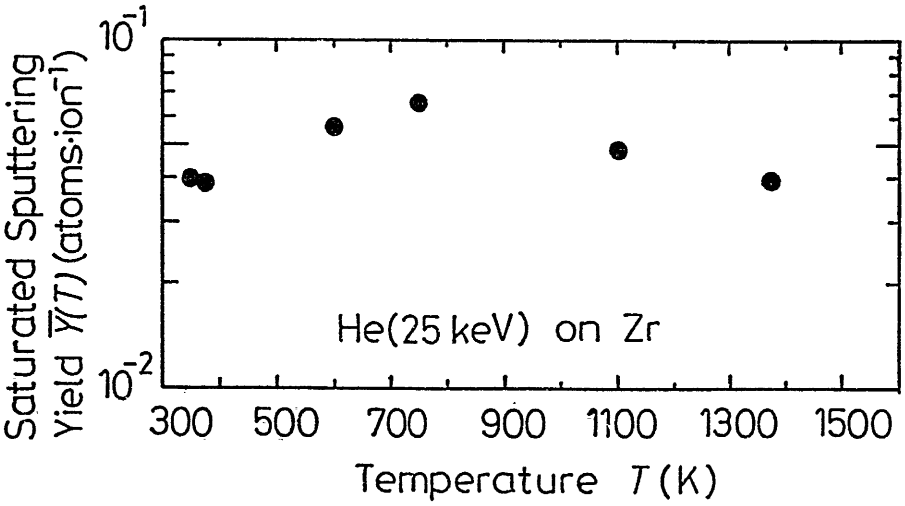

fig. 11

Role of ion radiation-enhanced segregation and diffusion to subsurface composition change of sputtered alloys

T.Koshikawa

Osaka Electro-Communication Univ., 18-8 Hatsu, Neyagawa, Osaka
572, Japan

Surface compositional changes of alloys by ion sputtering have been extensively studied owing to their importance in the field of the plasma-wall interaction in the fusion reactor, thin film preparation with sputtering, surface and interface analysis with ion beam techniques, and so on. Recently ion radiation-enhanced segregation (IRES) or Gibbsian segregation and ion radiation-enhanced diffusion (IRED) were observed to be very important in compositional changes.

We measured the depth profiles of $Au0.56Cu_{0.44}$ alloys sputtered with Ar ions at lower than room temperature, obtained the IRED coefficients. Simulation results including IRES and IRED are also tried to know the role of IRES and IRED to the composition change from the surface to the bulk.

In order to obtain depth profiles of a $Au_{0.56}Cu_{0.44}$ alloy after steady state sputtering with Ar ions for a chosen temperature and ion beam current density, the alloy was cooled to -120° C and sputtered with low current density ions ($0.4\mu A/cm^2$, 2keV). Depth profiles were measured with low (60eV for Cu and 69eV for Au) energy Auger peaks. The composition was corrected with calibration curves obtained from the Au-Cu standard samples made by coevaporation techniques.

Typical experimental results of depth profiles measured with low energy Auger peaks for chosen sample temperatures are shown in Fig.1. Au is enriched at the surface, depleted beneath the surface and then rises gradually to near bulk concentration. Depth of the altered layer depends on the sample tempersture. This shows that segregation and diffusion play an important role on compositional change at the subsurface of alloys sputtered with ions. From these results, the diffusion coefficient and activation energy of IRED were estimated from this results and used in the simulation of sputtering. The composition, which was corrected by a deconvolution method, is shown in Fig.2. The figure shows the corrected composition depth profiles at low temperature. The concentration of Au at the surface is about 60-75 at%, depletes near the surface and increases gradually with depth to the bulk composition. The altered depth strongly depends on sputtering temperature. Corrected composition at the to-surface is influenced by estimation of the depth derived from the sputtering time. In this derivation, we should assume some values, i.e., sputtering yield of an Au-Cu alloy, coincidence of electron beam for Auger analysis with ion beam for sputtering and so on. This error is large, so values of 69-75 at% include some ambiguity.

Fig.3 shows the simulation results of depth profiles. The sputtering times are indicated. The ratio of the partial sputtering yiels is 1:1 (Au:Cu) and the sample temperature is 153K. The ejected depth of the sputtered atoms is 0.2nm. After 150s, the steady state profile is reached. The Au concentration at the top-surface and in the depleted layer are about 68 and 49 at%, respectively. The composition at the top-surface is slightly different from the corrected value in Fig.2, and is whithin the error bars. The value for the depleted layer is similar to that in Fig.2. In general, the simulated results folloe the corrected profiles.

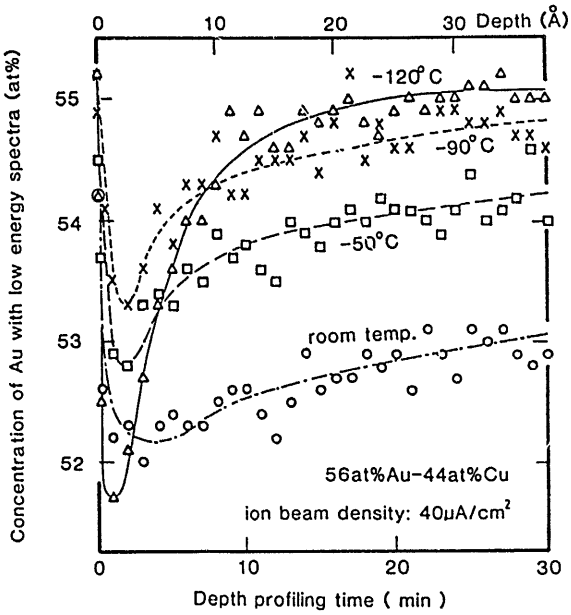

Fig.1 Temperature dependence of the depth profiles of $Au_{0.56}Cu_{0.44}$ sputtered with Ar ions of 2keV and 40uA/cm^2.

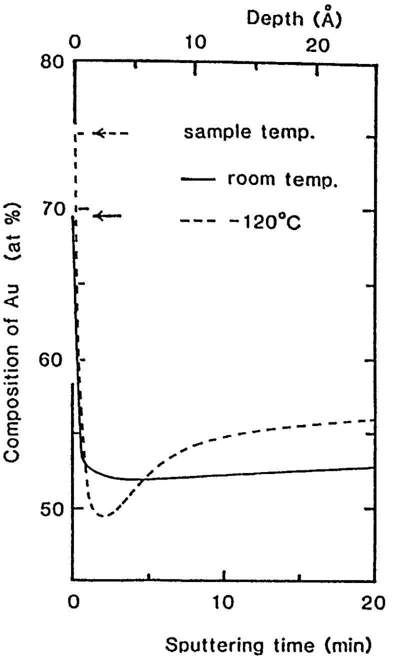

Fig.2 Corrected depth profiles after deconvolution for T=−120 °C and room temperature. Escape of Auger electrons is assumed to be exponential and its mean depth is 0.4nm.

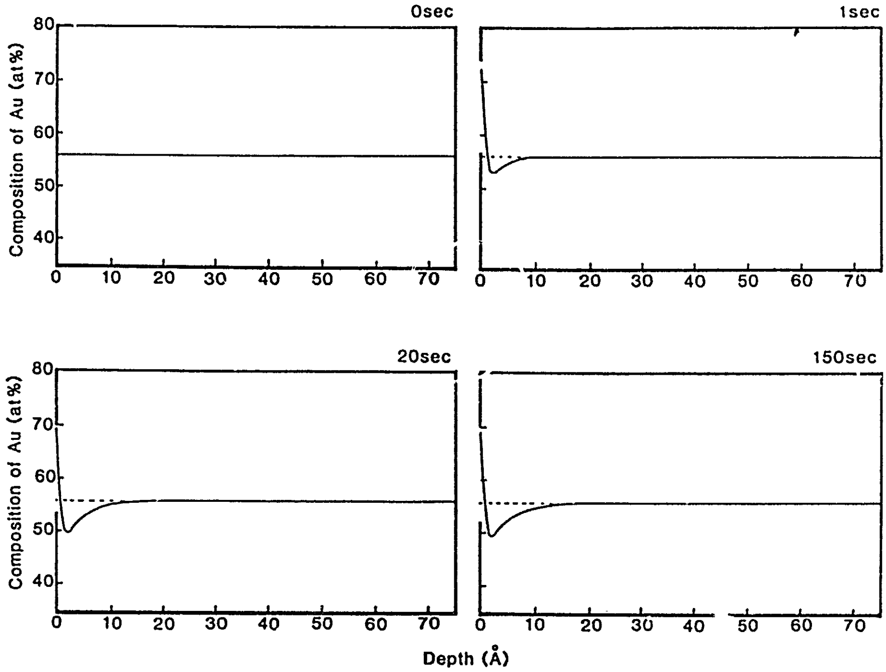

Fig.3 Change of depth profiles of Au simulated in our sputtering model. The temperature is −153K. The ratio of partial sputtering yield is 1:1 (Au:Cu). "Time" shows the sputtering time after ion bombardment. The mean ejected depth of sputtered atoms is 0.2nm.

Present Status of Data Compilation on Ion Backscattering

Tatsuo Tabata and Rinsuke Ito
Osaka Prefectural Radiation Research Institute
Shinke-cho, Sakai, Osaka 593

Recent results are briefly described of the joint work made at the Institute of Plasma Physics, Nagoya University, to compile the data on the backscattering coefficients of ions and to develop empirical formulas for these coefficients. Computer-simulation data on light-ion backscattering at low energies and both experimental and computer-simulation data on heavy-ion backscattering have been added to the compilation. The computer-simulation data for heavy ions have been found to show deviations from a universal curve on to which experimental data are well scaled.

INTRODUCTION

Part of the effort of Plasma-Wall Interaction Working Group at the Institute of Plasma Physics, Nagoya University, has been directed to a joint work to compile data on the number and energy backscattering* coefficients of ions incident on solids. In the joint work, empirical formulas have also been developed to facilitate interpolaion and extrapolation of the data. The latest publication of the work is Ref. 1. The work done after its publication is summarized in the present report.

NEW DATA

The following data have been added to the compilation of the backscattering coefficients†:

(1) Computer-simulation data on light-ion backscattering at low

---

*Backscattering is also called "reflection" especially in the community of thermonuclear-fusion research.

†Numerical data generated in the studies reported in Refs. 2, 3, 11 and 12 have been provided by courtesy of Eckstein.

energies[2,3];
(2) Experimental data on heavy-ion backscattering[4-10];
(3) Computer-simulation data on heavy-ion backscattering.[11,12]
Here we call the ions with mass $M_1>4$ "heavy ions." These data as well as the data compiled earlier are available on the data retrieval and display system[13] of the Institute of Plasma Physics; the name of the database is BACKS. Computer-simulation data[14] on the backscattering of ^{3}He ions are in preparation for inclusion.

All the data described in Ref. 2 are also stored on microfiches at the Institute of Plasma Physics. These data include not only the total backscattering coefficients but also differential distributions of backscattered particles over the energy of the backscattered particles, polar and azimuthal angles, as functions of incident polar angle and energy.

The computer-simulation data for low energies[2,3,11,12] show a trend that the number and energy backscattering coefficients decrease with decreasing energy for energies below a few eV. These data were obtained by assuming a surface binding energy E_s of 1 eV for all the materials.[2] This value of E_s was adopted from the comparison of the results for different values of E_s with the result of the embedded atom-method reported by Baskes.[15] The latter result is available only for hydrogen ions incident on the nickel target. The low-energy data, therefore, have a rather large uncertainty.

EMPIRICAL FORMULAS

Possible Extension down to Low Energies

The empirical formulas for the number and energy backscattering coefficients at normal incidence given in Ref. 1 must be modified to make them applicable down to energies below 1 eV. The modification might be achieved by multiplying them by a function that increases with increasing energy and then reaches a saturation at a few eV (for example, a logistic curve). This modification has not yet been tried because of the uncertainty of the available data.

A Trial for Extension to Heavy Ions

We have compared the empirical formulas in Ref. 1 with the compiled experimental data for heavy ions. The result has shown that the formulas hold rather good for $\delta \leq 0.5$, where δ is the ratio of the mass M_1 of the incident ion to the mass M_2 of the target atom.

To extend the region of applicability of the formulas up to higher values of δ, Ito et al.* have given the following formula for the number backscattering coefficient R_N of ions at normal incidence:

$$R_N \simeq G(\varepsilon)/f_N \ . \qquad (1)$$

Here $G(\varepsilon)$ is "the reduced backscattering coefficient" common to number and energy backscattering, ε is the Thomas-Fermi reduced energy, and f_N is the scaling factor for the number backscattering coefficient. These are given by the following relations:

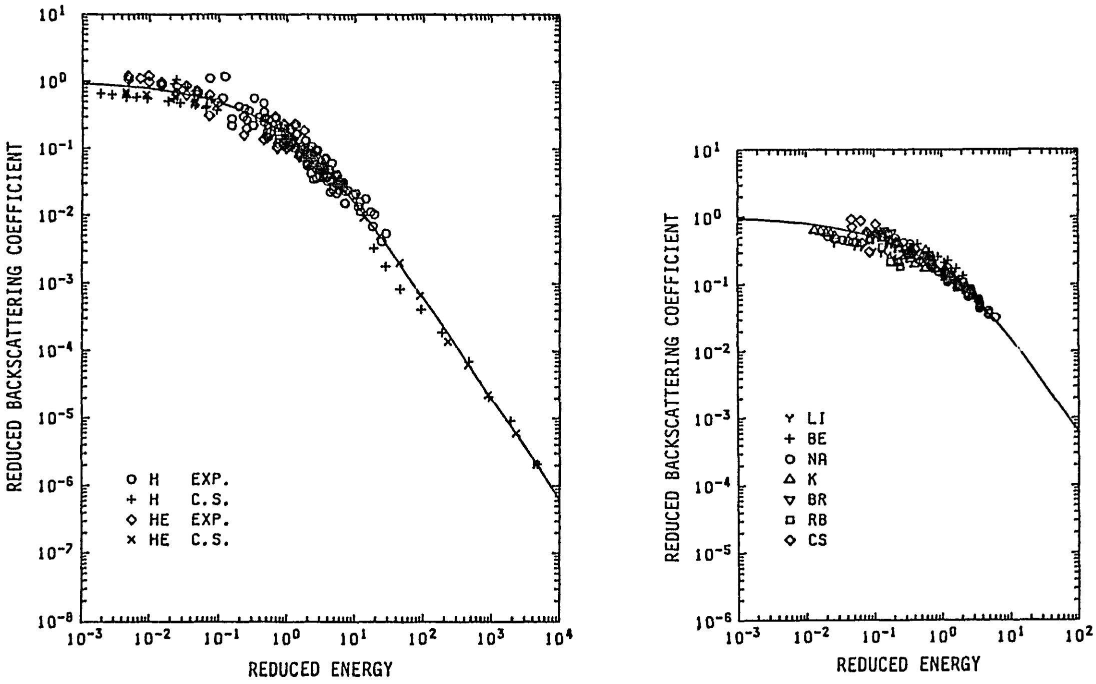

(a) (b)

Fig. 1. Reduced backscattering coefficient as a function of reduced energy. Curve, the function $G(\varepsilon)$ given by Eq. (3); points in (a), experimental and computer-simulation data on the number backscattering coefficient of light ions multiplied by f_N; points in (b), experimental data on the number backscattering coefficient of heavy ions multiplied by f_N (Refs. 4-10; Brunnée's data[9]) at low energies have been excluded because of the dubious dependence on energy).

---

*R. Ito, T. Tabata, K. Morita and H. Tawara, read at the Autumn Meeting of the Physical Society of Japan, Chiba, October, 1985.

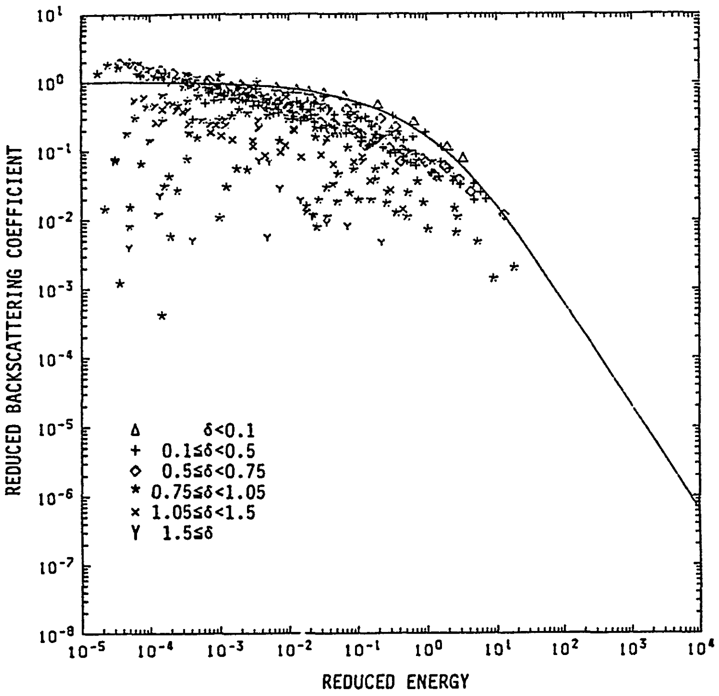

Fig. 2. Reduced backscattering coefficient as a function of reduced energy. Curve, the function G(ε) given by Eq. (3); points, computer-simulation data of Eckstein and Biersack multiplied by f_N.

$$\varepsilon=32.534EM_2/[(M_1+M_2)Z_1Z_2(Z_1^{2/3}+Z_2^{2/3})^{1/2}] \qquad (2)$$

$$G(\varepsilon)=1/[1+(\varepsilon/0.104)^{0.577}+(\varepsilon/0.730)^{1.5}] \qquad (3)$$

$$f_N=Z_1^{2/3}M_1^{-1/2}(\rho_a/\rho_t)\mu^2(1+\mu)^{-2}/\Psi\ . \qquad (4)$$

In Eqs. (2) and (4), Z_1 and Z_2 are the atomic numbers of the incident ion and the target atom; ρ_a/ρ_t is the ratio, as defined in Ref. 1, of an approximate expression to a more accurate expression for the range of the ion in the target material (the former expression assumes the velocity-proportional stopping of the LSS theory for all the energies, which brings about a simple scaling); μ and Ψ are given by

$$\mu=M_2/M_1 \qquad (5)$$

$$\Psi=(1+24.1\mu^{-3.995})/\{\mu/[(1+\mu)(\varepsilon/1.84+1)]$$

$$+(1+\mu)^3\varepsilon/[\mu^3(1-3/2\mu+0.90/\mu^2+1/2\mu^3)(\varepsilon+13.3)]\}\ . \qquad (6)$$

The scaling factor f_N has been determined semiempirically by taking into account Wedell's result of an extended single-collision model[16] to some extent (the definition and the behavior of Ψ at low energies are much different from those of the function ψ_0 given by Wedell). This scaling brings the available experimental data up to δ=4.8 on to a single curve

Table 1. Ion-target combinations of available data on the number backscattering coefficient of heavy ions incident on solid surfaces. c, computer-simulation data available; ¢, computer-simulation data for "self-backscattering" ($\delta=1$) available; e, experimental data available; x, both computer-simulation and experimental data available. For the entries below the symbol ¢, δ is larger than unity.

	Target																
Ion	Li	Be	C	Al	Si	Ti	Ni	Cu	Ge	Zr	Mo	Ag	Sm	W	Au	Hg	U
^{7}Li	¢										e						
^{7}Be		¢										e			e		
^{12}C			¢														
^{16}O											c				[δ<1]		
^{20}Ne		c	c		c	c	c				c						c
^{23}Na											e						
^{24}Na									e			x			e		
^{28}Si					¢												
^{40}Ar					c		c		c		c						c
^{38}K											e						
^{42}K									e			x			e		
^{44}K				e	e			e				e			e		
^{58}Ni							¢										
^{75}Br												e			e		
^{84}Br								e				e			e		
^{84}Kr							c				c		c			c	c
^{81}Rb				e				e				e			e		
^{88}Rb				e				e				e			e		
^{89}Rb				e				e				e			e		
^{98}Mo											¢						
^{132}Xe							c			c	c						c
^{125}Cs				e				e				e			e		
^{130}Cs				e				e				e			e		
^{138}Cs								e				e			e		
^{184}W														¢			
^{222}Rn		[δ>1]									c						c
^{238}U																	¢

(Fig. 1). The computer-simulation data of Eckstein and Biersack are not always scaled on to the same curve by the use of this scaling factor (Fig. 2). (While Fig. 2 includes the data for energies below a few eV, where the backscattering coefficient increases with increasing energy, we do not consider these data here.) The non-scaling described above of the computer-simulation data is difficult to explain, because the values of δ used in the simulation are lower than the maximum value of δ for the available experimental data (see Table 1).

Formulation of the scaling factor for the energy backscattering coefficient similar to Eq. (4) is now in progress.

References

1) R. Ito, T. Tabata, N. Itoh, K. Morita, T. Kato and H. Tawara, Institute of Plasma Physics, Nagoya University, Report IPPJ-AM-41 (1985).

2) W. Eckstein and J. P. Biersack, Appl. Phys. A **38,** 123 (1985).

3) W. Eckstein and D. B. Heifetz, J. Nucl. Mater. **145-147,** 332 (1987).

4) J. Bøttiger and J. A. Davies, Radiat. Eff. **11,** 61 (1971).

5) J. Bøttiger, J. A. Davies, P. Sigmund and K. B. Winterbon, Radiat. Eff. **11,** 69 (1971).

6) J. Bøttiger, H. W. Jørgensen and K. B. Winterbon, Radiat. Eff. **11,** (1971).

7) J. Bøttiger and K. B. Winterbon, Radiat. Eff. **20,** 65 (1973).

8) J. Bøttiger, O. Holck and G. Sidenius, Nucl. Instrum. & Methods **170,** 499 (1980).

9) C. Brunnée, J. Phys. **147,** 161 (1957).

10) D. Hildebrandt and R. Manns, Phys. Status Solidi a **38,** K155 (1976).

11) W. Eckstein and J. P. Biersack, Z. Phys. B **63,** 109 (1986).

12) W. Eckstein and J. P. Biersack, Z. Phys. B **63,** 471 (1986).

13) Thermonuclear Fusion Research Information Center, RIC (Research Information Center Retrieval Display System): Manual for the Use of Numerical Databases (1985) (in Japanese).

14) D. Fink, J. P. Biersack, M. Städele and V. K. Cheng, Radiat. Eff. **104,** 1 (1987).

15) M. I. Baskes, J. Nucl. Mater. **128 & 129,** 676 (1984).

16) R. Wedell, Appl. Phys. A **35,** 91 (1984).

Present Status and Future Requirements of Knowledge of Radiation Effects for Fusion Application

Chiken Kinoshita

Department of Nuclear Engineering, Kyushu University

1. Introduction

An overview is presented of the present status of knowledge of radiation effects for fusion application. Emphasis is placed on fundamental aspects pertinent to reactor requirements, such as the displacement process, the kinetic process, structural properties and electrical properties. Critical problems and expected research works for fusion application are summarized.

2. Displacement process

In the fusion reactor environment, the fast neutron flux produces the majority of radiation damage through the displacement and transmutation processes. Neutron collision will lead to a spectrum of primary knock-on atoms (PKA). The PKA goes on to produce a displacement cascade where a number of Frenkel pairs are included. The number of Frenkel pairs N_d is expressed by the following equation,

$$N_d = 0.8\ k\ (E_p - Q)/2E_d,$$

where E_p is the PKA energy, Q the total energy lost in the cascade by electron excitation, E_d the displacement threshold energy and k the survival probability of Frenkel pairs.

Numerical values are required for E_d, Q and k. Experimental values of E_d for a number of pure metals have been accumulated to understand its physical background and to be used for practical applications. In the case of ceramics, however, experimental needs include more data on E_d including development of new techniques. High voltage electron microscopy is useful for observing the growth rate of dislocation loops which is related to the crystallographic orientation dependence of E_d. The capacitance dilatometer developed by N. Itoh et al. is expected to be used for an average threshold energy through electron irradiation-induced volume change of thick specimens. The value of k is sensitive to irradiation temperature and E_d, and is required for getting N_d. However, cascade structure and its stability are likely to be more important than N_d and they should be understood in terms of the energy density deposited within cascade rather than E_p.

Synergistic effects of knock-on displacement and electron excitation and those of high energy PKA and low energy PKA are very important. Thus bookkeeping on those effects requires more attention and understanding.

3. Kinetic process

Development of microstructures such as defect clusters chemical disordering, precipitation and amorphization in metals and ceramics has been observed with use of electron microscopes during and/or after electron-, ion and neutron-irradiation.

Candidate for fusion reactors such as MgO, TiC_{1-x}, NiO, Al_2O_3,$MgAl_2O_4$, SiC and graphite, as well as metals, are classified into four groups in terms of the characteristics of dislocation loop kinetics under electron irradiation; (1) The dislocation loop kinetics is analogous to that in pure metals where di-interstitials are stable nuclei of loops, and (2) It is controlled by structural vacancies or holes in TiC_{1-x}, NiO, Al_2O_3, FeAl and NiAl. (3) No dislocation loop nucleates in $MgAl_2O_4$, because of large stoichiometric nuclei of dislocation loops, and (4) Amorphization is induced in covalent crystals such as SiC and graphite instead of the nucleation of dislocation loops.

Related phenomena induced by ion- and neutron-irradiation are also examined for the purpose of understanding the development of microstructures under fusion reactor environments, and they are discussed in terms of the crystal structure, the atomic bonding, the structural vacancy, the mass of constituent elements and the impurity. The following conclusive remarks are added to (1)-(4); (5) The structural vacancy is extremely effective to suppress the nucleation and growth of loops in irradiated TiC_{1-x}. (6) Non-stoichiometric interstitial loops such as 1/6 <111> in character are induced in $MgAl_2O_4$ by ion- and neutron irradiations, and are unstable during electron irradiation. These features together with (3) are consistent with the fact that $MgAl_2O_4$ is a radiation resistant material. (7) The amorphization in covalent crystals is due to the stabilization of high defect concentration introduced by repulsive force between the Frenkel pair in those crystals. Further works on the kinetic process are expected for getting the following knowledge, (1) Nucleation and growth kinetics of defect clusters under ion irradiation, (2) Anti-site structure under irradiation, (3) Mechanisms of irradiation induced amorphization, reduction and oxidation, (4) Recombination volume of interstitials and vacancies in ceramics, (5) Role of transmutation elements in the kinetic process, (6) Key issues for radiation-resistant materials, and (7) Others.

4. Structural properties

Structural properties of metals are reviewed by Dr. K. Muroga.

5. Electrical properties

The importance of in-situ measurements of electrical properties with use of well-characterised specimens is stressed by Dr. H. Ohno in the separate review.

COMMENT ON THE RESEARCH STRATEGY OF NEUTRON IRRADIATION EFFECTS ON MATERIALS

T. Muroga
Research Institute for Applied Mechanics, Kyushu University,
Kasuga, Fukuoka 816, Japan

This comment intends to describe the present status and future strategy of the study of neutron irradiaiton effects of fusion reactor materials, near-term issues to be considered in this long-term course of study and some recent experimental results which are suggestive for the future researches.

(I) Strategy of the study of neutron irradiaiton effects

Since no intense fusion neutron source capable of irradiating materials to doses expected in fusion reactors is available, the irradiation study must be carried out with different kinds of irradiaiton particles (simulation irradiation). In the proposal stage of the post-RTNS-II Japan/US cooperation program, we have made a illustration shown in Figure 1 describing the research strategy[1]. The detail of the explanation of this figure will be shown in ref.[2].

On this figure, the following complementary comments will help to explain the present situation and future strategy.

(a) The heavy irradiation effects expected in fusion reactors are, in plinciple, the result of basic processes, some of which were clarified through RTNS-II experiments, and damage accumulation processes. However, the experimenters' experiences have clearly shown that new unexpected materials behavior eventually appears with increasing the irradiation dose. This means that the neutron irradiation experiments at high doses is the top priority in this strategy.

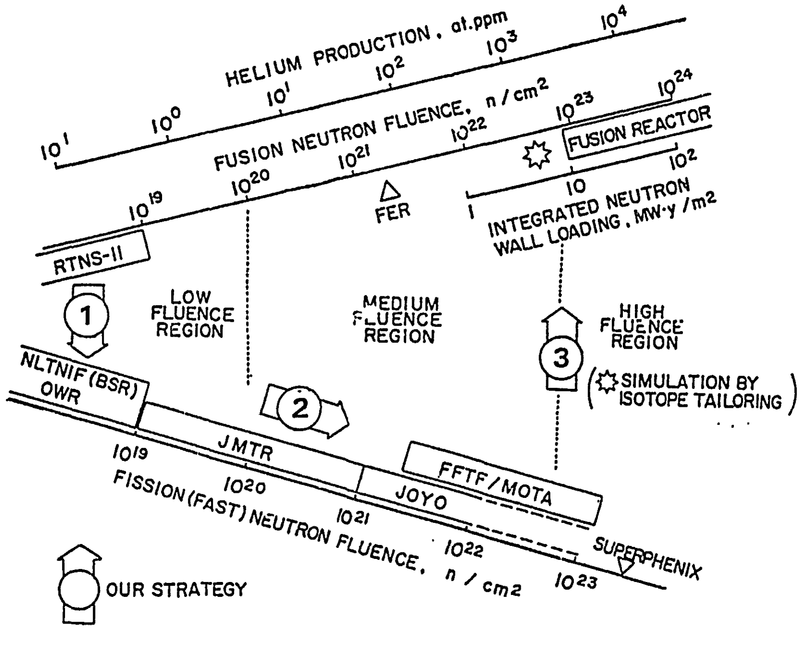

Figure 1. Strategy of the study of fusion neutron irradiation effects using available fission reactors[1,2].

(b) However the estimation of the fusion radiation effects based on available low and high dose data must be careful and logical. Some new ideas to approach the fusion irradiation conditions, e.g. isotopic tailoring, may involve new deviate disturbance in the irradiaiton conditions. This must be considered carefully.
(c) In all prediction stages, fundamental understanding as will be obtained from low dose or simulation irradiation experiments on the materials behavior will aid as base of logics.
(d) High-voltage electron microscopes and heavy ion accelerators have a capability to attain to very high doses. However, these techniques have their unique problems which generally increase with increasing the dose. Thus these technique should be used mainly for the purpose shown in (c).

(II) Near-term issues

There are some critical issues to be solved in the present stage of the long-term strategy shown above. First, through Japan/US cooperation on FFTF/MOTA utilization, which started in FY 1987, some data on high fluence neutron irradiation effects will become availble in near future. Thus it is an immediate requisite to clarify the effect of unique problems of the fast reactor irradiations. The problems expected are,
(a) Unique and not negligible transmutation effects.
(b) Transient or perturbation effects of temperature and neutron flux.
(c) Transient effects of neutron spectrum.
Some of these issues can be studied by the available simulation irradiation techniques and some new designing of the FFTF experiments will also be helpful.

Second, the intense neutron source facilities for the materials irradiation are now at the designing stage. In this stage, answers to some critical problems are required. For example,
(a) What is the acceptable difference in neutron spectrum from that of fusion reactors.
(b) What is the deviation caused by the acceleration of the irradiaiton rate.
(c) What is the acceptable minimum volume of specimen for the property estimation.

(III) Suggestion from the recent experiments

Two examples of the recent experimental information will be shown to demonstrate the needs for the study to solve the issues shown above.

(a) Helium production effects in fast reactor irradiaitons

The mechanism of the effects of nickel content on swelling in austenitic steels is a long standing problem. Concerning this, the effects of nickel to change the properties at void surfaces or the vacancy diffusivities were proposed to account for the decrease in swelling with increasing the nickel content. However, these models cannot explain the increase in swelling after minimum beyond 45% Ni.

Recently the author observed microstructures of a series of Fe-15Cr-XNi specimens and found that the void structure is quite different in high nickel specimens. An example is shown in Figure 2. Figure 2 shows that in the high nickel ternary, small cavities are distributed as well as large voids. This is an evidence of the existense of gaseous impurities in the matrix enhancing the cavity nucleation. The impurities are believed to be helium atoms originated from the transmutative reaction of fast neutrons with nickel.

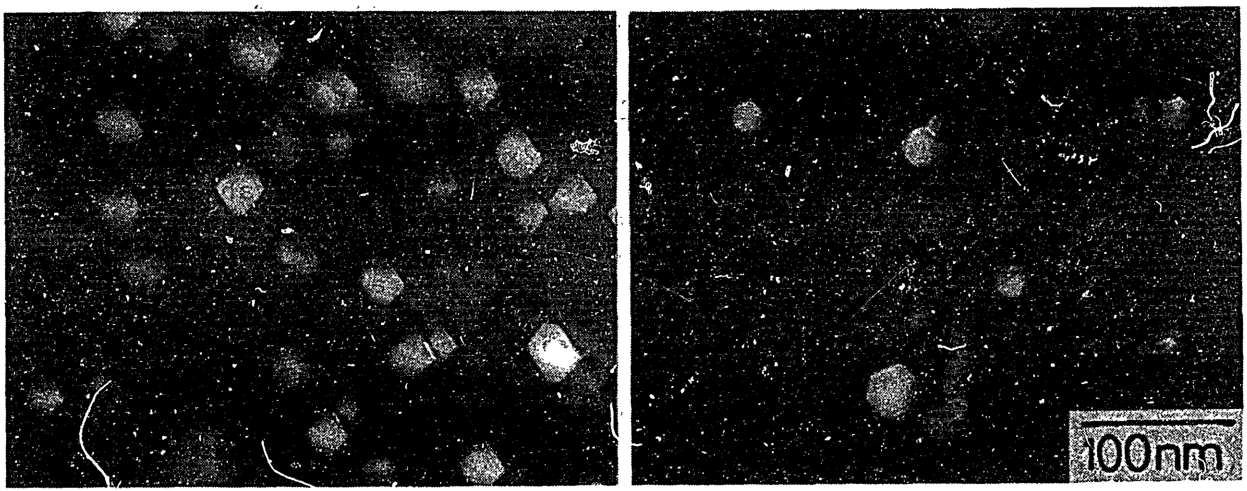

(a) (b)

Figure 2 Microstructures of (a) Fe-15Cr-15Ni and (b) Fe-15Cr-75Ni irradiated in EBR-II at 510°C and $2.6 \times 10^{22} n/m^2$.

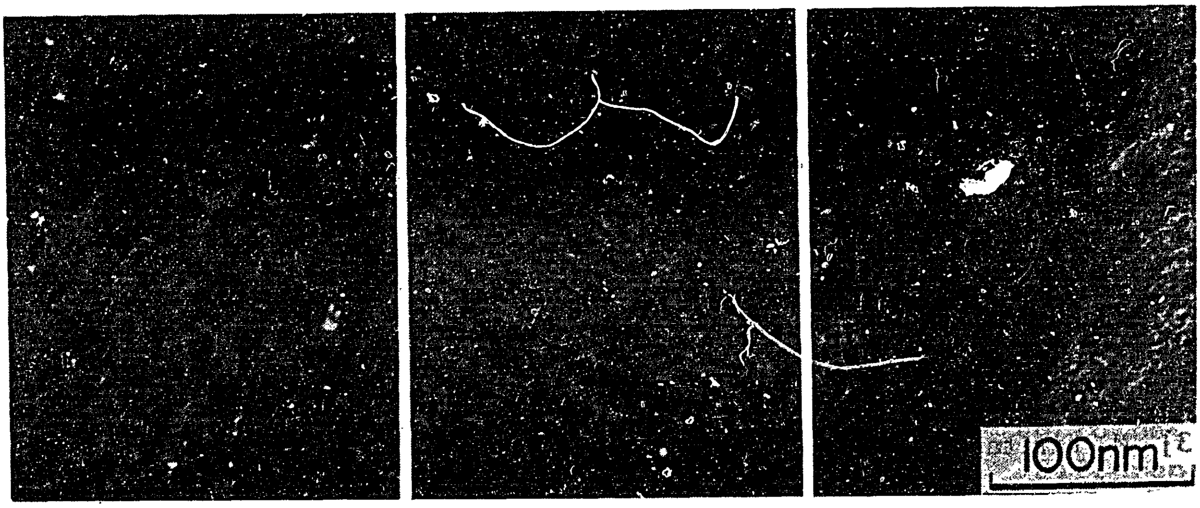

Figure 3 Microstructures of an Fe-15Cr-16Ni irradiated with RTNS-II (a) at 200°C and $1.9 \times 10^{22} n/m^2$, (b) at 200°C and $5.6 \times 10^{21} n/m^2$ followed by irradiation at 350°C and $5.2 \times 10^{21} n/m^2$ and (c) at 350°C and $5.2 \times 10^{21} n/m^2$.

Therefore, the increase in swelling after minimun at high nickel alloys are expected to be, to some extent, due to the increased production of helium. This is a novel information suggesting need for serious consideration of the transmutation effects in fast reactors.

(b) Effects of pre-irradiation at lower temperatures on the defect evolution by irradiaiton at higher temperatures

In the case of fast reactor irradiations the initial transient irradiation at lower temperatures than the designed temperature may have considerable effects on microstructural evolution. This problem is clearly specified in ref. [3]. Under this motivation, a repeated irradiation experiment changing the temperature at the interval from lower to higher was crried out using the RTNS-II. An example demonstrating possible importance of the initial lower temperature irradiation is shown in Figure 3.

The figure compares the microstructures of an Fe-15Cr-16Ni alloy irradiated (a) at 200°C and 1.9x10^{22}n/m^2, (b) at 200°C and 5.6x10^{21}n/m^2 followed by irradiation at 350°C and 5.2x10^{21}n/m^2 and (c) at 350°C and 5.2x10^{21}n/m^2. An irradiaiton at 350°C results in no observable clusters as shown in (c). On the other hand, some defect clusters are observed in the specimen pre-irradiated at 200°C(b). The clusters observed are larger in size than those produced by irradiation at 200°C only(a). Some of the defect clusters in (b) are identified to be voids. This implies that pre-irradiation at 200°C results in the enhancement of void formation during irradiation at 350°C. This suggests the necessity of the consideration of initial transient effects in the analyses of the irradiaiton data from fast reactors.

(IV) Summary

This comment described the present situation and future strategy of the study of neutron irradiation effects for fusion structural materials. This strategy constructed for the structural materials is believed to be applicable also to the development of the plasma-facing materials to be used in the neutron irradiaiton environments.

Contributions by Dr. F.A. Garner of Pacific Northwest Laboratory, Professors N. Yoshida of Kyushu University and M. Kiritani of Nagoya University to the experiments referred in section (III) are acknowledged.

References

[1] Proposal for Post-RTNS-II Project: "US/Japan Planning for the Utilization of Fission Reactors for Fundamental Studies of Irradiation Effects in Fusion Materials", April 1986.
[2] S. Ishino, Proc. of The First Japan/US FFTF/MOTA Experimenters' Workshop, Aug.24-26, 1987 Univ. Tokyo, IPPJ-866, pp. 23.
[3] M. Kiritani, ibid. pp.137.

Radiation effects on electrical properties of ceramics

Hideo Ohno and Yoshio Katano
Material Innovation Laboratory
Japan Atomic Energy Reserch Institute

Ceramics such as alumina(Al_2O_3) and silicon nitride(Si_3N_4) are candidate materials for insulators and rf windows of fusion reactors because of their good mechanical and electrical properties. Many works on radiation effects of Al_2O_3 have been reported. But in the case of electrical properties such as conductivity and dielectric loss, these properties have different tendency if the measurements are done under irradiation or post irradiation. The properties have also been affected by irradiation means(x-ray, electron, γ-ray and neutron),dose rate, fluence and temperature.

Figure 1 shows the radiation-induced conductivity of single crystal Al_2O_3 with 1.5 MeV electron irradiation as a function of dose rate and temperature for Al_2O_3. The electrical conductivity was increased as increasing the dose rate of electron irradiatin. On the other hand the conductivity of Al_2O_3 was decreased with neutron irradiation as shown in fig.2. Radiation-induced rf loss tangent for post-irradiated Al_2O_3 has also been reported to be dependent on neutron energy, fluence and temperature. Different results will be expected in the case of in-situ measurements under irradiation.

Silicon nitride is also a candidate material because of its good mechanical properties. There are few data on radiation effects of electrical properties and we are now planning the in-situ measurements of conductivities under γ-ray irradiation. Figure 3 shows the frequency and temperature dependence of dielectric properties both in innovated Si_3N_4 with additives of MgO and in commercial one with additives of Y_2O_3 and Al_2O_3. Hot pressed Si_3N_4 with additives of 6.6 mol% MgO has good dielectric properties at temperatures below 500° C. The increase of dielectric loss tangent at temperatures above 500° C has correlation with the behavior of glassy phase of grain boundary.

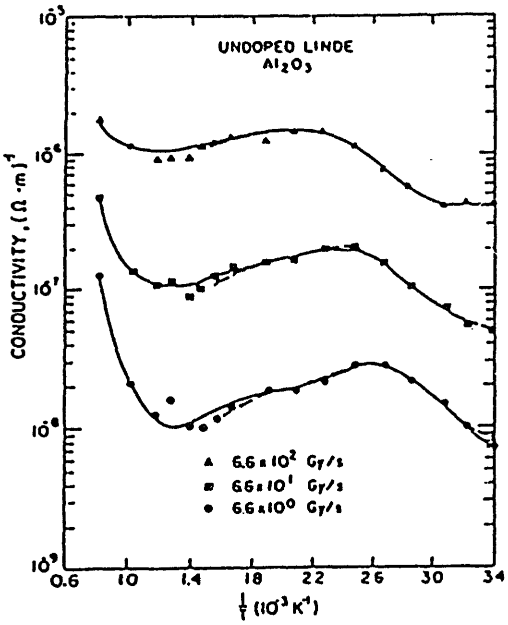

Fig.1 Radiation-induced conductivity of Al_2O_3 with 1.5Mev electron irradiation.
[R.W.Klaffky et al.:Phys.Rev.,B21 (1980)3610]

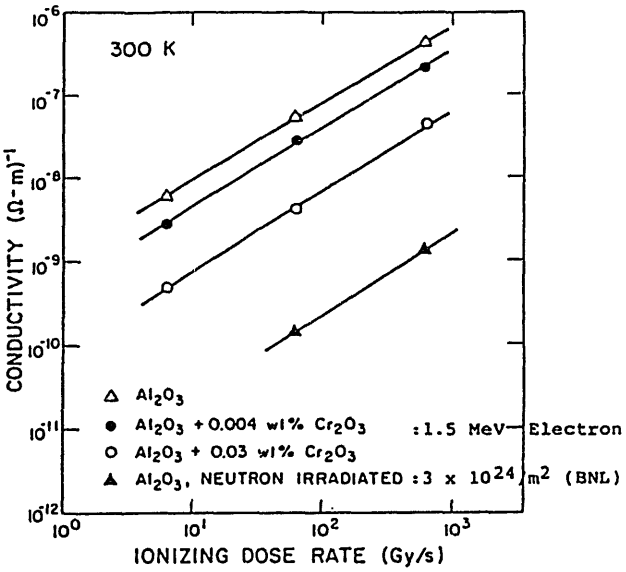

Fig.2 Dose-rate dependence of conductivity of Al_2O_3 with electron and neutron irradiation .
[R.W.Klaffky et al.:Phys.Rev.,B21 (1980)3610 ; F.W.Clinard.Jr.: J. Mater.Eng.System,6(1984)100]

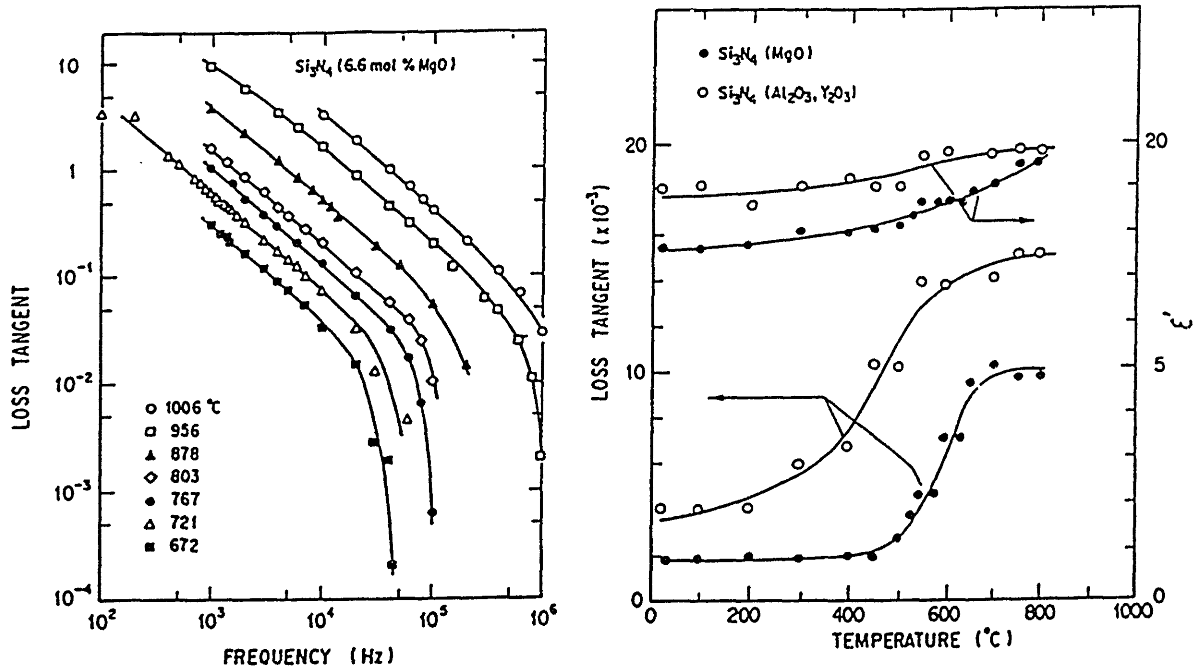

Fig.3 Frequency and temperature dependence of loss tangent of silicon nitride.
[H.Ohno et al.:J.Nucl.Mater.,155-157(1988)372]

LIST OF IPPJ-AM REPORTS

IPPJ-AM-1*	"Cross Sections for Charge Transfer of Hydrogen Beams in Gases and Vapors in the Energy Range 10 eV–10 keV" H. Tawara (1977) [Published in Atomic Data and Nuclear Data Tables 22, 491 (1978)]
IPPJ-AM-2*	"Ionization and Excitation of Ions by Electron Impact –Review of Empirical Formulae–" T. Kato (1977)
IPPJ-AM-3	"Grotrian Diagrams of Highly Ionized Iron FeVIII-FeXXVI" K. Mori, M. Otsuka and T. Kato (1977) [Published in Atomic Data and Nuclear Data Tables 23, 196 (1979)]
IPPJ-AM-4	"Atomic Processes in Hot Plasmas and X-Ray Emission" T. Kato (1978)
IPPJ-AM-5*	"Charge Transfer between a Proton and a Heavy Metal Atom" S. Hiraide, Y. Kigoshi and M. Matsuzawa (1978)
IPPJ-AM-6*	"Free-Free Transition in a Plasma –Review of Cross Sections and Spectra–" T. Kato and H. Narumi (1978)
IPPJ-AM-7*	"Bibliography on Electron Collisions with Atomic Positive Ions: 1940 Through 1977" K. Takayanagi and T. Iwai (1978)
IPPJ-AM-8	"Semi-Empirical Cross Sections and Rate Coefficients for Excitation and Ionization by Electron Collision and Photoionization of Helium" T. Fujimoto (1978)
IPPJ-AM-9	"Charge Changing Cross Sections for Heavy-Particle Collisions in the Energy Range from 0.1 eV to 10 MeV I. Incidence of He, Li, Be, B and Their Ions" Kazuhiko Okuno (1978)
IPPJ-AM-10	"Charge Changing Cross Sections for Heavy-Particle Collisions in the Energy Range from 0.1 eV to 10 MeV II. Incidence of C, N, O and Their Ions" Kazuhiko Okuno (1978)
IPPJ-AM-11	"Charge Changing Cross Sections for Heavy-Particle Collisions in the Energy Range from 0.1 eV to 10 MeV III. Incidence of F, Ne, Na and Their Ions" Kazuhiko Okuno (1978)
IPPJ-AM-12*	"Electron Impact Excitation of Positive Ions Calculated in the Coulomb-Born Approximation –A Data List and Comparative Survey–" S. Nakazaki and T. Hashino (1979)
IPPJ-AM-13	"Atomic Processes in Fusion Plasmas – Proceedings of the Nagoya Seminar on Atomic Processes in Fusion Plasmas Sept. 5-7, 1979" Ed. by Y Itikawa and T. Kato (1979)
IPPJ-AM-14	"Energy Dependence of Sputtering Yields of Monatomic Solids" N. Matsunami, Y. Yamamura, Y. Itikawa, N. Itoh, Y. Kazumata, S. Miyagawa, K. Morita and R. Shimizu (1980)

IPPJ-AM-15	“Cross Sections for Charge Transfer Collisions Involving Hydrogen Atoms” Y. Kaneko, T. Arikawa, Y. Itikawa, T. Iwai, T. Kato, M. Matsuzawa, Y. Nakai, K. Okubo, H. Ryufuku, H. Tawara and T. Watanabe (1980)
IPPJ-AM-16	“Two-Centre Coulomb Phaseshifts and Radial Functions” H. Nakamura and H. Takagi (1980)
IPPJ-AM-17	“Empirical Formulas for Ionization Cross Section of Atomic Ions for Electron Collisions –Critical Review with Compilation of Experimental Data–” Y. Itikawa and T. Kato (1981)
IPPJ-AM-18	“Data on the Backscattering Coefficients of Light Ions from Solids” T. Tabata, R. Ito, Y. Itikawa, N. Itoh and K. Morita (1981) [Published in Atomic Data and Nuclear Data Tables 28, 493 (1983)]
IPPJ-AM-19	“Recommended Values of Transport Cross Sections for Elastic Collision and Total Collision Cross Section for Electrons in Atomic and Molecular Gases” M. Hayashi (1981)
IPPJ-AM-20	“Electron Capture and Loss Cross Sections for Collisions between Heavy Ions and Hydrogen Molecules” Y. Kaneko, Y. Itikawa, T. Iwai, T. Kato, Y. Nakai, K. Okuno and H. Tawara (1981)
IPPJ-AM-21	“Surface Data for Fusion Devices – Proceedings of the U.S–Japan Workshop on Surface Data Review Dec. 14-18, 1981” Ed. by N. Itoh and E.W. Thomas (1982)
IPPJ-AM-22	“Desorption and Related Phenomena Relevant to Fusion Devices” Ed. by A. Koma (1982)
IPPJ-AM-23	“Dielectronic Recombination of Hydrogenic Ions” T. Fujimoto, T. Kato and Y. Nakamura (1982)
IPPJ-AM-24	“Bibliography on Electron Collisions with Atomic Positive Ions: 1978 Through 1982 (Supplement to IPPJ-AM-7)” Y. Itikawa (1982) [Published in Atomic Data and Nuclear Data Tables 31, 215 (1984)]
IPPJ-AM-25	“Bibliography on Ionization and Charge Transfer Processes in Ion-Ion Collision” H. Tawara (1983)
IPPJ-AM-26	“Angular Dependence of Sputtering Yields of Monatomic Solids” Y. Yamamura, Y. Itikawa and N. Itoh (1983)
IPPJ-AM-27	“Recommended Data on Excitation of Carbon and Oxygen Ions by Electron Collisions” Y. Itikawa, S. Hara, T. Kato, S. Nakazaki, M.S. Pindzola and D.H. Crandall (1983) [Published in Atomic Data and Nuclear Data Tables 33, 149 (1985)]
IPPJ-AM-28	“Electron Capture and Loss Cross Sections for Collisions Between Heavy Ions and Hydrogen Molecules (Up-dated version of IPPJ-AM-20) H. Tawara, T. Kato and Y. Nakai (1983) [Published in Atomic Data and Nuclear Data Tables 32, 235 (1985)]

IPPJ-AM-29	"Bibliography on Atomic Processes in Hot Dense Plasmas" T. Kato, J. Hama, T. Kagawa, S. Karashima, N. Miyanaga, H. Tawara, N. Yamaguchi, K. Yamamoto and K. Yonei (1983)
IPPJ-AM-30	"Cross Sections for Charge Transfers of Highly Ionized Ions in Hydrogen Atoms (Up-dated version of IPPJ-AM-15)" H. Tawara, T. Kato and Y. Nakai (1983) [Published in Atomic Data and Nuclear Data Tables 32, 235 (1985)]
IPPJ-AM-31	"Atomic Processes in Hot Dense Plasmas" T. Kagawa, T. Kato, T. Watanabe and S. Karashima (1983)
IPPJ-AM-32	"Energy Dependence of the Yields of Ion-Induced Sputtering of Monatomic Solids" N. Matsunami, Y. Yamamura, Y. Itikawa, N. Itoh, Y. Kazumata, S. Miyagawa, K. Morita, R. Shimizu and H. Tawara (1983) [Published in Atomic Data and Nuclear Data Tables 31, 1 (1984)]
IPPJ-AM-33	"Proceedings on Symposium on Atomic Collision Data for Diagnostics and Modelling of Fusion Plasmas, Aug. 29 – 30, 1983" Ed. by H. Tawara (1983)
IPPJ-AM-34	"Dependence of the Backscattering Coefficients of Light Ions upon Angle of Incidence" T. Tabata, R. Ito, Y. Itikawa, N. Itoh, K. Morita and H. Tawara (1984)
IPPJ-AM-35	"Proceedings of Workshop on Synergistic Effects in Surface Phenomena Related to Plasma-Wall Interactions, May 21 – 23, 1984" Ed. by N. Itoh, K. Kamada and H. Tawara (1984) [Published in Radiation Effects 89, 1 (1985)]
IPPJ-AM-36	"Equilibrium Charge State Distributions of Ions ($Z_1 \geqq 4$) after Passage through Foils – Compilation of Data after 1972" K. Shima, T. Mikumo and H. Tawara (1985) [Published in Atomic Data and Nuclear Data Tables 34, 357 (1986)]
IPPJ-AM-37	"Ionization Cross Sections of Atoms and Ions by Electron Impact" H. Tawara, T. Kato and M. Ohnishi (1985) [Published in Atomic Data and Nuclear Data Tables 36, 167 (1987)]
IPPJ-AM-38	"Rate Coefficients for the Electron-Impact Excitations of C-like Ions" Y. Itikawa (1985)
IPPJ-AM-39	"Proceedings of the Japan-U.S. Workshop on Impurity and Particle Control, Theory and Modeling, Mar. 12 – 16, 1984" Ed. by T. Kawamura (1985)
IPPJ-AM-40	"Low-Energy Sputterings with the Monte Carlo Program ACAT" Y. Yamamura and Y. Mizuno (1985)
IPPJ-AM-41	"Data on the Backscattering Coefficients of Light Ions from Solids (a Revision)" R. Ito, T. Tabata, N. Itoh, K. Morita, T. Kato and H. Tawara (1985)

IPPJ-AM-42	"Stopping Power Theories for Charged Particles in Inertial Confinement Fusion Plasmas (Emphasis on Hot and Dense Matters)" S. Karashima, T. Watanabe, T. Kato and H. Tawara (1985)
IPPJ-AM-43	"The Collected Papers of Nice Project/IPP, Nagoya" Ed. by H. Tawara (1985)
IPPJ-AM-44	"Tokamak Plasma Modelling and Atomic Processes" Ed. by T. Kawamura (1986)
IPPJ-AM-45	Bibliography of Electron Transfer in Ion-Atom Collisions H. Tawara, N. Shimakura, N. Toshima and T. Watanabe (1986)
IPPJ-AM-46	"Atomic Data Involving Hydrogens Relevant to Edge Plasmas" H. Tawara, Y. Itikawa, Y. Itoh, T. Kato, H. Nishimura, S. Ohtani, H. Takagi, K. Takayanagi and M. Yoshino (1986)
IPPJ-AM-47	"Resonance Effects in Electron-Ion Collisions" Ed. by H. Tawara and G. H. Dunn (1986)
IPPJ-AM-48	"Dynamic Processes of Highly Charged Ions (Proceedings)" Ed. by Y. Kanai and S. Ohtani (1986)
IPPJ-AM-49	"Wavelengths of K X-Rays of Iron Ions" T. Kato, S. Morita and H. Tawara (1987)
IPPJ-AM-50	"Proceedings of the Japan-U.S. Workshop P-92 on Plasma Material Interaction/High Heat Flux Data Needs for the Next Step Ignition and Steady State Devices, Jan. 26 – 30, 1987" Ed. by A. Miyahara and K. L. Wilson (1987)
IPPJ-AM-51	"High Heat Flux Experiments on C-C Composite Materials by Hydrogen Beam at the 10MW Neutral Beam Injection Test Stand of the IPP Nagoya" H. Bolt, A. Miyahara, T. Kuroda, O. Kaneko, Y. Kubota, Y. Oka and K. Sakurai (1987)
IPPJ-AM-52	"Energy Dependence of Ion-Induced Sputtering Yields of Monatomic Solids in the Low Energy Region" N. Matsunami, Y. Yamamura, N. Itoh, H. Tawara and T. Kawamura (1987)
IPPJ-AM-53	"Data Base on the High Heat Flux Behaviour of Metals and Carbon Materials for Plasma Facing Components – Experiments at the 10 MW Neutral Beam Injection Test Stand of the IPP Nagoya" H. Bolt, C. D. Croessmann, A. Miyahara, T. Kuroda and Y. Oka (1987)
IPPJ-AM-54	"Final (n, ℓ) State-Resolved Electron Capture by Multiply Charged Ions from Neutral Atoms" N. Shimakura, N. Toshima, T. Watanabe and H. Tawara (1987)
IPPJ-AM-55	"Atomic Data for Hydrogens in Collisions with Electrons – Addenda to IPPJ-AM-46" H. Tawara, Y. Itikawa, H. Nishimura and M. Yoshino (1987)

IPPJ-AM-56	"Total and Partial Cross Sections for Electron Capture for C^{q+} (q= 6–2) and O^{q+} (q=8–2) Ions in Collisions with H, H_2 and He Atoms" H. Tawara (1987)
IPPJ-AM-57	"Atomic Models for Hot Dense Plasmas" K. Fujima (1988)
IPPJ-AM-58	"Recommended Data for Excitation Rate Coefficients of Helium Atoms and Helium-Like Ions by Electron Impact" T. Kato and S. Nakazaki (1988)
IPPJ-AM-59	"Atomic and Molecular Processes in Edge Plasmas Including Hydrocarbon Molecules" Ed. by H. Tawara (1988)
IPPJ-AM-60	"Theory of Threshold Energy of Ion-Induced Desorption by a Few-Collision Model" Y. Yamamura, J. Bohdansky and E. Taglauer (1988)
IPPJ-AM-61	"The Application of Atomic and Molecular Physics in Fusion Plasma Diagnostics" H. W. Drawin (1988)
IPPJ-AM-62	"Low Energy Atomic Collision Research Using Highly Charged Ions from EBIS and Other Ion Sources" H. Tawara (1988)
IPPJ-AM-63	"Partial Electronic Stopping Cross Sections of Atoms for Protons" T. Kaneko (1989)
IPPJ-AM-64	"Future Prospects of Research and Data Activities on Plasma-Wall Interaction in Fusion Devices" Ed. by N. Itoh and T. Kawamura (1989)

Available upon request to Research Information Center, Institute of Plasma Physics, Nagoya University, Nagoya 464, Japan, except for the reports noted with*.